# PROBABILISTIC SEISMIC HAZARD ASSESSMENT FOR EAST ANATOLIAN FAULT ZONE USING PLANAR SOURCE MODELS

A THESIS SUBMITTED TO
THE GRADUATE SCHOOL OF NATURAL AND APPLIED SCIENCES OF
MIDDLE EAST TECHNICAL UNIVERSITY

BY

AKIN MENEKŞE

IN PARTIAL FULFILLMENT OF THE REQUIREMENTS
FOR
THE DEGREE OF THE MASTER OF SCIENCE
IN
CIVIL ENGINEERING

JANUARY 2016

Approval of the thesis:

PROBABILISTIC SEISMIC HAZARD
ASSESSMENT FOR EAST ANATOLIAN FAULT
ZONE USING PLANAR SOURCE MODELS

submitted by **AKIN MENEKŞE** in partial fulfillment of the requirements for the degree of **Master of Science in Civil Engineering Department, Middle East Technical University** by,

Prof. Dr. Gülbin Dural Ünver
Dean, Graduate School of Natural and Applied Sciences _____

Prof. Dr. İsmail Özgür Yaman
Head of Department, Civil Engineering _____

Assoc. Prof. Dr. Zeynep Gülerce
Supervisor, Civil Engineering Dept., METU _____

**Examining Committee Members:**

Prof. Dr. Kemal Önder Çetin
Civil Engineering Dept., METU _____

Assoc. Prof. Dr. Zeynep Gülerce
Civil Engineering Dept., METU _____

Prof. Dr. Nuretdin Kaymakçı
Geological Engineering Dept., METU _____

Assist. Prof. Dr. Atilla Arda Özacar
Geological Engineering Dept., METU _____

Prof. Dr. Bilge Siyahi
Earthquake and Struct. Eng. Dept., GYTE _____

DATE --/--/----

**I hereby declare that all information in this document has been obtained and presented in accordance with academic rules and ethical conduct. I also declare that, as required by these rules and conduct, I have fully cited and referenced all material and results that are not original to this work.**

Name, Last Name: Akın MENEKŞE

Signature :

,

## ABSTRACT

## PROBABILISTIC SEISMIC HAZARD ASSESSMENT FOR EAST ANATOLIAN FAULT ZONE USING PLANAR SOURCE MODELS

Menekşe, Akın

M.Sc., Department of Civil Engineering

Supervisor: Assoc. Prof. Dr. Zeynep Gülerce

January 2016, 112 Pages

The objective of this study is to perform probabilistic seismic hazard assessment (PSHA) using planar seismic source characterization models for East Anatolian Fault Zone (EAFZ) and to update the design ground motions to be used in the region. Development of planar seismic source models requires the definition of source geometry in terms of fault length, fault width, fault plane angles and segmentation points for each segment and associating the observed seismicity with defined fault systems. This complicated task was performed with the help of Updated Active Fault Maps of Turkey (Emre et al., 2012), previously conducted geological site studies in the literature, and Unified Instrumental Earthquake Catalogue of Turkey (Kalafat et al., 2011). The state-of-the-art seismotectonic model developed in this study includes the fault segments, rupture sources, rupture scenarios, and fault rupture models that are combined with composite magnitude distribution model to properly represent the characteristic behavior of faults. This study is also novel in terms of the employed ground motion characterization framework. Recently published global Next Generation Attenuation (NGA-West2) ground motion prediction models (Bozorgnia et al., 2014) and Turkey-Adjusted NGA-West1 models (Gülerce et al., 2015) are used in the ground motion logic tree with equal weights. The results are presented in terms of the hazard curves and deaggregation of the hazard for six selected locations (Bingöl, Elazığ, Kahramanmaraş, Osmaniye, Pütürge, and Hasanbeyli) and compared with the Turkish Earthquake Code (TEC, 2007) requirements. Seismic hazard maps for accepted hazard levels in TEC (2007) for different spectral periods and for

generic rock ($V_{S30}$=760 m/s and $V_{S30}$=1100 m/s) site conditions are also provided. Results of this study will provide an update of the previous seismic hazard maps of EAFZ and design ground motions proposed for the region.

**Keywords:** East Anatolian Fault Zone, probabilistic seismic hazard assessment, planar seismic source models, ground motion prediction equations, hazard maps, Turkish Earthquake Code

# ÖZ

## DÜZLEMSEL KAYNAK MODELLERİ KULLANILARAK DOĞU ANADOLU FAYININ OLASILIKSAL SİSMİK TEHLİKE ANALİZİ

Menekşe, Akın
Yüksek Lisans, İnşaat Mühendisiği Bölümü
Tez Yöneticisi: Doç. Dr. Zeynep Gülerce
Ocak 2016, 112 Sayfa

Bu çalışmanın amacı, Doğu Anadolu Fay Zonu (DAFZ) için düzlemsel sismik kaynak karakteristiği modelinin oluşturulması ve bölgede kullanılacak olan tasarım yer hareketi parametrelerinin olasılıksal sismik tehlike analizi (OSTA) yöntemi kullanılarak güncellenmesidir. Düzlemsel sismik kaynak modellerinin geliştirilmesi, kaynak modelinin fay uzunluğu, fay derinliği, fay yüzey açısı ve segmentasyon noktaları türünden açıklanmasını ve gözlemlenen sismisitenin tanımlanan fay sistemleri ile ilişkilendirilmesini gerektirir. Bu karmaşık süreç güncellenmiş Türkiye Aktif Fay Haritası (Emre ve diğ., 2012), literatürdeki daha önceden yapılmış jeolojik saha çalışmaları ve Türkiye Aletsel Dönem Deprem Kataloğu (Kalafat ve diğ., 2011) yardımıyla yürütülmüştür. Bu çalışmada geliştirilen sismotektonik model, fayların karakteristik davranışlarını uygun bir şekilde yansıtabilmesi için kompozit deprem büyüklüğü dağılımı modeli ile birleştirilmiş fay segmanları, kırılma senaryoları, kırılma kaynakları ve fay kırılma modellerini içermektedir. Yer hareketleri mantık ağacında son dönemde yayımlanan NGA-West2 kuvvetli yer hareketleri denklemleri (Bozorgnia ve diğ., 2014) ve Türkiye'ye uyarlanmış yeni nesil (NGA-West1) (Gülerce ve diğ., 2015) kuvvetli yer hareketi tahmin denklemleri eşit ağırlık verilerek kullanılmıştır. Çalışmanın sonuçları, bölgede seçilmiş altı nokta için (Bingöl, Elazığ, Kahramanmaraş, Osmaniye, Pütürge, Hasanbeyli) önerilen sismik tehlike eğrileri ve tehlike dağılım grafiklerini içerecek şekilde sunulmuş ve bu çıktılar Deprem Bölgelerinde Yapılacak Binalar Hakkında Yönetmelik (TDBYB, 2007) tasarım

değerleri ile karşılaştırılmıştır. Ayrıca çalışma kapsamında TDBYB (2007)'de kabul edilen tehlike seviyelerinde, farklı spektral periyodlar ve jenerik kaya ($V_{S30}$=760 m/s ve $V_{S30}$=1100 m/s) saha koşulları için sismik tehlike haritaları da üretilmiştir. Bu çalışma sonuçlarının, Doğu Anadolu Fayı ve çevresindeki bölgelerde daha önceden yapılmış sismik tehlike haritalarına ve tasarım yer hareketlerine yenilik getireceği düşünülmektedir.

**Anahtar Kelimeler:** Doğu Anadolu Fay Zonu, Olasılıksal Sismik Tehlike Analizi, kuvvetli yer hareketi tahmin denklemleri, sismik tehlike haritaları, Türk Deprem Yönetmeliği

To My Beloved Family

## ACKNOWLEDGEMENTS

I would like to express my sincere thanks and gratitude to my advisor, Assoc. Prof. Dr. Zeynep Gülerce for her guidance, patience and support throughout the preparation of this thesis. Without her continued efforts and support, I would have not been able to bring my work to a successful completion.

I am grateful to Prof. Dr. Kemal Önder Çetin for his suggestions, guidance and understanding during the preparation of this thesis. I would like to thank to Prof. Dr. Nuretdin Kaymakçı and Assist. Prof. Dr. Atilla Arda Özacar for their understanding throughout the preparation of this thesis and their guidance especially for the seismic source characterization efforts.

I would also like to thank Prof. Dr. Norman Abrahamson, for providing the hazard code.

I am very grateful to my friends, Hasan Emre Oktay and Serhat Zencir for their priceless help and support during the preparation of this thesis.

Finally, I would like to thank my father, mother and sister for their love, understanding and encouragement throughout my life and for forgiving me for all the postponed get-togethers with them. I promise to make up for those times after I finish.

## TABLE OF CONTENTS

## LIST OF TABLES

## LIST OF FIGURES

# CHAPTER 1

# INTRODUCTION

The Anatolian plate is shaped by the tectonic movement of Eurasian, Arabian and African plates. The North Anatolian Fault Zone (NAFZ), East Anatolian Fault Zone (EAFZ), West Anatolian Graben Complexes, Aegean Arc, and Bitlis Thrust Zone are the most important fault systems in Turkey. Among these fault systems, NAFZ is the one that produced the largest earthquake ruptures in the last century (e.g. 1939-1943 rupture sequence with four M>6.7 earthquakes, 1999 Kocaeli and Düzce events). Especially after the 1999 Kocaeli and Düzce events, researchers focused on the NAFZ and Marmara Region and published estimates of seismic hazard and risk (e.g. Atakan et al., 2002; Erdik et al., 2004; Crowley and Bommer, 2006; Kalkan et al., 2009; Gülerce and Ocak, 2013). On the other hand, EAFZ has been tectonically quiet relative to the NAFZ in the 21$^{st}$ century and was "neglected" in terms of the probabilistic seismic hazard assessment (PSHA) studies. The previous rupture-cycle for the EAFZ was in between 1800-1900 (1822 Eq., Ms=7.5; 1866 Karlıova Eq., Ms=7.2; 1893 Eq., Ms=7.1; 1874 Eq., Ms=7.1 and 1875 Eq., Ms=6.7) and the next rupture cycle might be in the near future.

In the past, Turkey has suffered great damages due to destructive and large magnitude earthquakes. The probability that the next earthquake along the EAFZ will be destructive is ever increasing because of the increase in the number of critical facilities (such as dams, hydro electrical power plants and pipelines) and population in the region. In order to ensure that adequate and optimal seismic safety requirements are met in the current and planned engineering structures and to reduce the structural damage and loss of human lives, it has become an important task to assess the level of seismic hazard properly and accurately. Unfortunately, only a limited number of seismic hazard studies covering the EAFZ region are currently available and a brief summary of these earlier studies are provided in in this Chapter.

Over the past 5 years, substantial information related to the seismotectonic properties of the EAFZ was published; the active fault maps of Turkey was updated by MTA (Emre et al., 2012), Duman and Emre (2013) documented the geometry and

segmentation characteristics of the EAFZ, measurements of active crustal deformation of the northeastern corner of the Mediterranean Sea from GPS were provided by Mahmoud et al. (2013) and the Integrated Homogeneous Turkish Earthquake Catalog that covers the events between years 1900-2010 was disseminated by Kalafat et al. (2011). Additionally, state-of-the-art global and regionalized ground motion prediction equations (GMPEs) that are applicable to Turkey were developed. These new developments allow the PSHA analyst to properly represent the seismic source and ground motion characteristics for EAFZ and call for the update of the design ground motions based on the PSHA methodology.

### 1.1 Research Statement

The aim of this study is to update the design ground motions and seismic hazard maps around EAFZ using the planar source models that combine the recently published information on source geometry and fault kinematics. For this purpose, seismic source characterization models are developed by defining the geometry of planar fault sources (fault length, width, and segmentation points) with the help of previously conducted site studies and Updated Active Fault Map of Turkey (Emre et al., 2012). The approach proposed by the Working Group of California Earthquake Probabilities (WGCEP, 2003) San Francisco Bay Area Model is adapted along with the composite magnitude distribution model by Youngs and Coppersmith (1985) to determine the magnitude recurrence relations for the fault segments, rupture sources, rupture scenarios, and fault rupture models. Events in the instrumental earthquake catalogue (Kalafat et al., 2011) are associated with the fault rupture models and the scenario weights for rupture scenarios are determined by balancing the accumulated (depending on the associated seismicity) and released (by the proposed rupture model) seismic moments for each rupture system. This study also proposes a substantial change from the other available studies in terms of the ground motion characterization framework. Recently developed NGA-West 2 GMPEs (Bozorgnia et al., 2014) and the Turkey-Adjusted NGA-West 1 (Gülerce et al., 2015) models that were regionalized based on Turkish strong motion database are employed for ground motion estimates and variability.

The results are presented in terms of the hazard curves and deaggregation of the hazard for six selected locations (Bingöl, Elazığ, Kahramanmaraş, Osmaniye,

Pütürge, and Hasanbeyli) and compared with the Turkish Earthquake Code (TEC, 2007) requirements. The seismic hazard maps for peak ground acceleration (PGA), 0.2 and 1 second spectral accelerations are prepared for two different site conditions; $V_{S30}$=760 m/s representing the B/C boundary of NEHRP site classification scheme and $V_{S30}$=1100 m/s to provide the reference rock site conditions that might be used in site-specific response analysis. Proposed design ground motions are compared to the TEC (2007) requirements and the significant differences are thoroughly discussed. The hazard maps presented here will bring in a significant contribution to the ongoing discussions related to the adaptation of current large-scaled PSHA project results in earthquake zoning maps and clearly demonstrate the need of defining planar source zones for accurate estimation of design ground motions, especially in the near-fault areas.

### 1.2 Previous Seismic Studies in the Region

The PSHA studies performed for Turkey are limited, except for the initiative nation-wide works of Erdik et al. (1985, 1999) and Gülkan et al. (1993). During 1980's, **Yarar et al. (1980)** proposed a seismic hazard map for Turkey in terms of the maximum MSK (Medvedev–Sponheuer–Karnik scale) intensity and maximum horizontal peak ground acceleration (HPGA) for the return periods of 200 and 500 years based on a 70-year earthquake catalogue and the neotectonic maps of Turkey. The authors modeled EAFZ by a single source zone and predominantly with the strike slip character. As shown in Figure 1.1, the proposed contours for the 500 year horizontal PGA indicate that the estimated PGA is approximately 300-400 gals (0.3-0.4g) around the EAFZ.

20 years after that, **Erdik et al. (1999)** performed a PSHA study in terms of PGA for all Turkey considering rock site conditions (sites with shear wave propagation velocity greater than 700 m/s) by identifying 37 seismic source zones based on the seismicity profile and the tectonic regime. To use in the seismic source characterization model, instrumental and historical earthquake catalogues were collected and the moment magnitude ($M_w$) values of all the events with different magnitude scales in the compiled catalogues were estimated in order to get a unified magnitude scale. The main strand of EAFZ between Karlıova and Türkoğlu was characterized as one source zone and another zone was defined for the southern extension of EAFZ in the Hatay region. Although the tectonic structures in Karataş-

Osmaniye region were presented; the authors did not use a specific source zone covering these fault segments. For PSHA calculations, Erdik et al. (1999) employed three early-stage ground motion prediction equations (GMPEs) proposed by Campbell (1997), Boore et al. (1997), Sadigh et al. (1997) by assigning equal weights in the logic tree. The iso-horizontal PGA contour map corresponding to 475 year return period presented by the authors is shown in Figure 1.2. The levels of 475-year return period PGA throughout the main strand of EAFZ (between Karlıova and Türkoğlu) and for the southern extension of EAFZ from Türkoğlu are about 0.6g to 0.7g. However in the vicinity of Karataş-Osmaniye Fault, proposed PGA values gradually decrease to 0.2g to 0.3g.

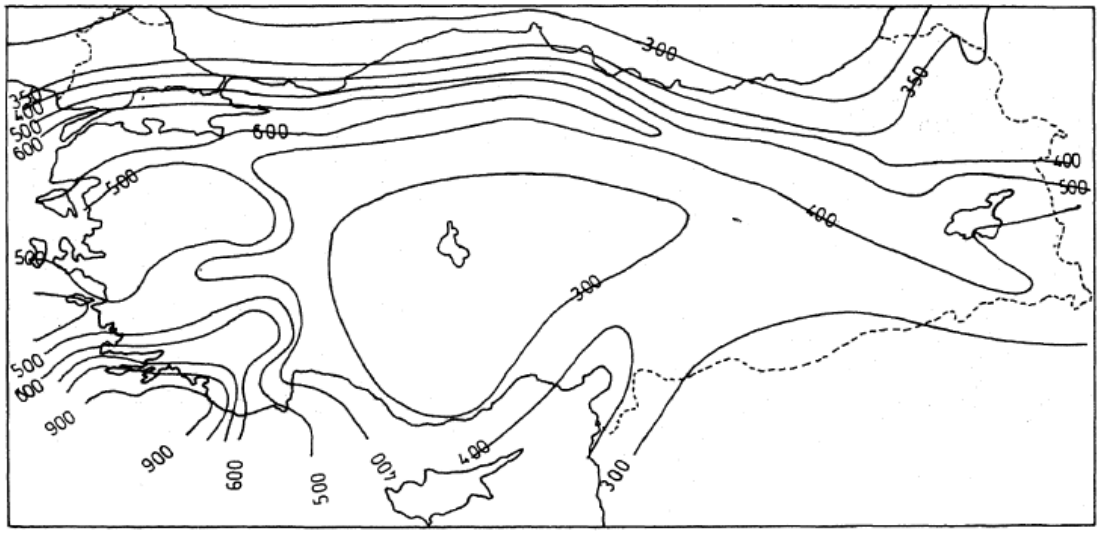


**Figure 1.1: Contour Map of Horizontal Peak Acceleration (expressed in gals) for Rock Site Conditions and for 500 Years Retun Period (after Yarar et al., 1980)**

**Kayabalı (2002)** built a probabilistic seismic hazard map and presented iso-acceleration maps for 100 and 475 years return periods to serve as the basis for the seismic hazard zonation of Turkey. Seismic source characterization was based on the assumption that the earthquakes occur only along faults: the author did not use background (areal) seismic zones because of the uncertain distribution of epicenters of the past earthquakes. Therefore, 14 seismic source zones based primarily on the map of neotectonic elements of Turkey compiled by Yaltirak et al. (1998) and the seismic source zonation map used by Erdik et al. (1985) were used. The minimum

earthquake magnitude was set to 4.0 in the calculations since the events smaller than this value do not have significant contribution to hazard. Maximum earthquake magnitude for each seismic source zone was determined from the relationship between fault rupture length and the earthquake magnitude proposed by Bonilla et al. (1984).

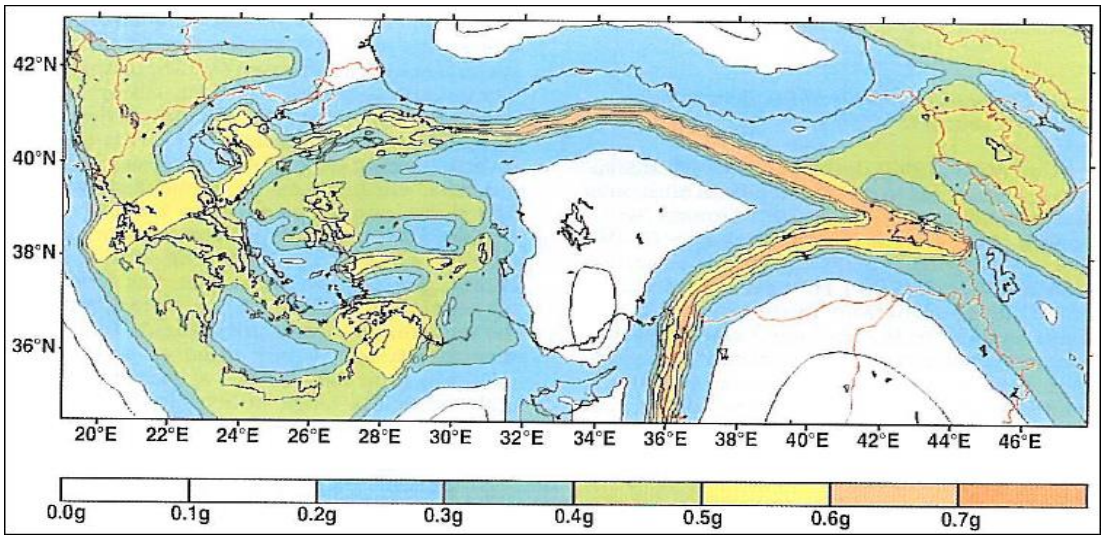


**Figure 1.2: PGA(g) Corresponding to the Return Period of 475 Years (10% probability of exceedance in 50 years) (after Erdik et al., 1999)**

Kayabalı (2002) used the magnitude–frequency parameters proposed by Alptekin (1978) after small modifications. For the source zone that corresponds to EAFZ, the assigned total fault length was 820 km and the maximum magnitude was taken as $M_w$=7.8. In the PSHA calculations, the computer code SISTEHAN II was used and the ground motion prediction model proposed by Joyner and Boore (1988) was employed. The PGA values for the return periods of 100 and 475 years (for bedrock) was computed for 5106 grid points, and iso-acceleration maps were constructed by contouring the acceleration values at each node as shown in Figure 1.3. The 475-years return period iso-acceleration maps show that the PGA values are as high as 0.6g for EAFZ.

Recently, **Bayrak et al. (2014)** investigated the earthquake probabilities around the EAFZ by analyzing the earthquake recurrence parameters for different segments of EAFZ. The authors suggested five seismogenic source zones on the EAFZ based on

the tectonic and seismotectonic regime; estimated the mean return periods for each segment and produced the a- and b-value maps for the EAFZ based on maximum likelihood regression. The earthquake recurrence parameters were determined in terms of the most probable maximum magnitude for 100 year, mean return period for an earthquake occurrence and the probabilities for large earthquakes. Bayrak et al. (2014) estimated the lowest b-value around Bingöl–Karlıova region and concluded that this region has a high stress level due to the tectonic regime. On the other hand, they observed highest b-value around Kırıkhan-Islahiye region and stated that this region has higher geological complexity and the stress in this region decreases over time and can be released by the events that are more frequent but smaller in magnitude. The authors suggested minimum mean return period of 181 years for the earthquakes with magnitude greater than 7.0 for the northern end of the EAFZ (Karlıova) and proposed that the next most significant earthquake will occur in this region. The authors' study does not include any estimates for the design ground motions.

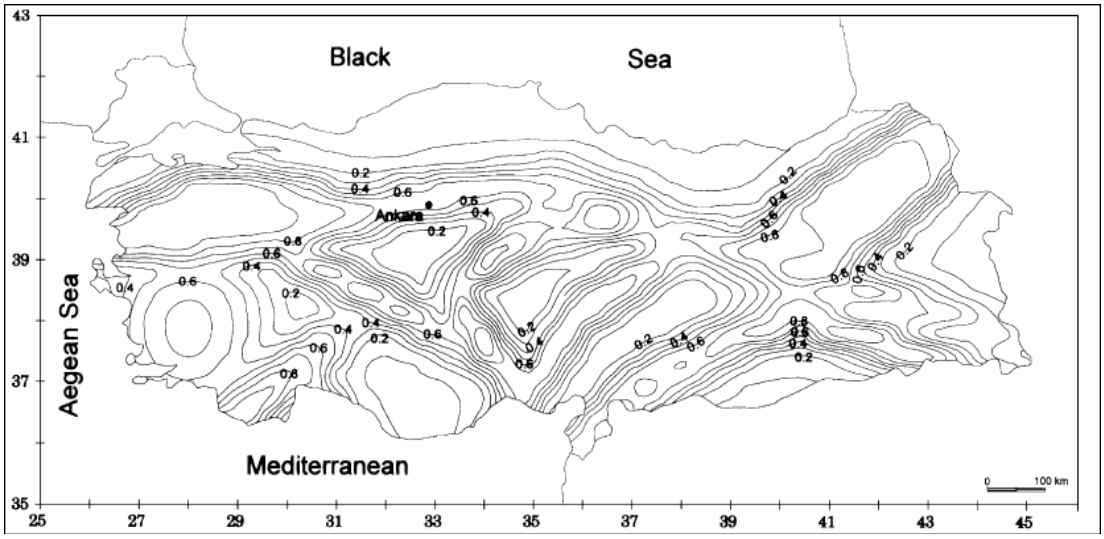


**Figure 1.3: Isoacceleration Contour Map (contour values are in g's) for PGA(g) Corresponding to the Return Period of 475 Years (10% Probability of Exceedance in 50 Years) (after Kayabalı, 2002)**

In addition to the local PSHA efforts mentioned above, the seismo-tectonic models of recent and global PSHA projects partially or fully cover the territory of Turkey. The **SHARE** (Seismic Hazard Harmonization in Europe) project presented the

occurrence of the earthquakes in Euro-Mediteranean region based on three different seismo-tectonic models: zone-based model, the fault-source and background zone model and a kernel-smoothed model that produces earthquake rate forecasts based on fault slip and smoothed seismicity source models. Multiple GMPEs (Akkar and Bommer, 2010 (35%); Cauzzi and Faccioli, 2008 (35%); Zhao et al., 2006 (10%); and Chiou and Youngs, 2008 (20%)) are used in PSHA calculations of SHARE project for shallow crustal and active tectonic regions. The seismic hazard map for Turkey showing 10% exceedance probability in 50 years for PGA (475 years) based on SHARE results is shown in Figure 1.4. This figure indicates that the proposed PGA values through the main strand of EAFZ (between Karlıova and Türkoğlu shown by a green box in Figure 1.4) are about 0.5g, lower than the estimates of Erdik et al. (1999). PGA values (0.3g to 0.4g) smaller than the main strand are proposed for Amanos and Karataş-Osmaniye Regions.

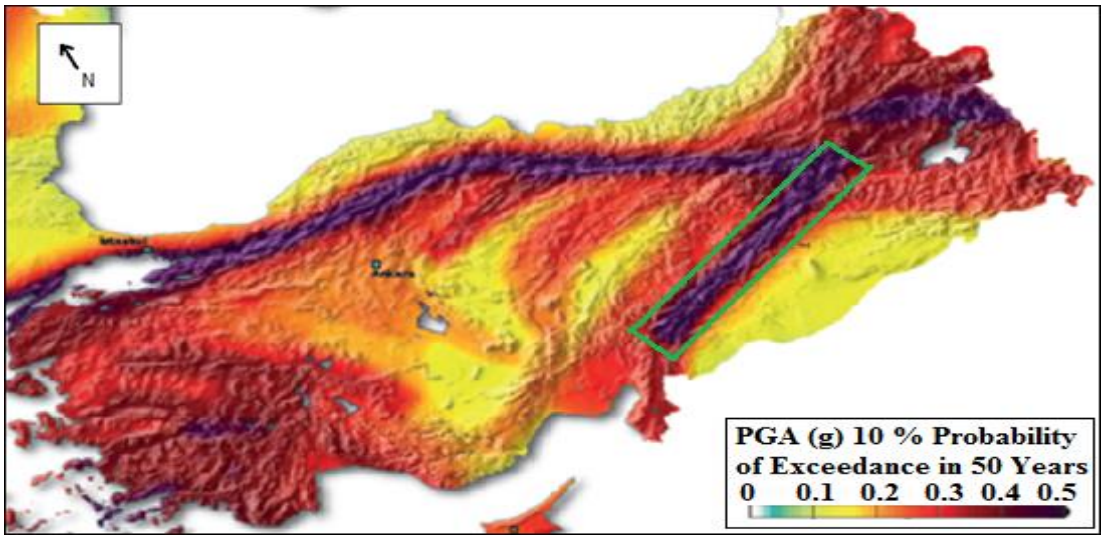


**Figure 1.4: PGA(g) Corresponding to the Return Period of 475 Years (10% Probability of Exceedance in 50 Years) around Turkey (taken from http://www.efehr.org)**

The **EMME** (Earthquake Model of the Middle East) project targeted to evaluate the earthquake hazard, the associated risk on the basis of structural damages, casualties and economic losses as well as the effects of relevant mitigation measures in the Middle East Region. Moment magnitude ($M_w$), body-wave magnitude ($m_b$) and surface-wave magnitude ($M_s$) earthquake catalogs were built based on global

catalogs covering the time period from 1900 to 2010 including 6.102 records (984 records from Turkey). Additionally, country-focused historical earthquake catalogs with more than 2000 records were compiled. Areal source zones based on the collected catalogues and active fault sources were developed in the project. The source zones were defined by tectonic regionalization, maximum magnitude, predominant rupture mechanism, depth distribution and earthquake recurrence parameters. PGA hazard map for 475 years was presented within the EMME project is shown in Figure 1.5. The PGA values throughout the main strand of EAFZ (between Karlıova and Türkoğlu shown by a green box in Figure 1.5) are again around 0.5g. On the other hand, for the southern continuation of EAFZ, the PGA values are a little bit lower (0.4g) than the values estimated for the main strand.

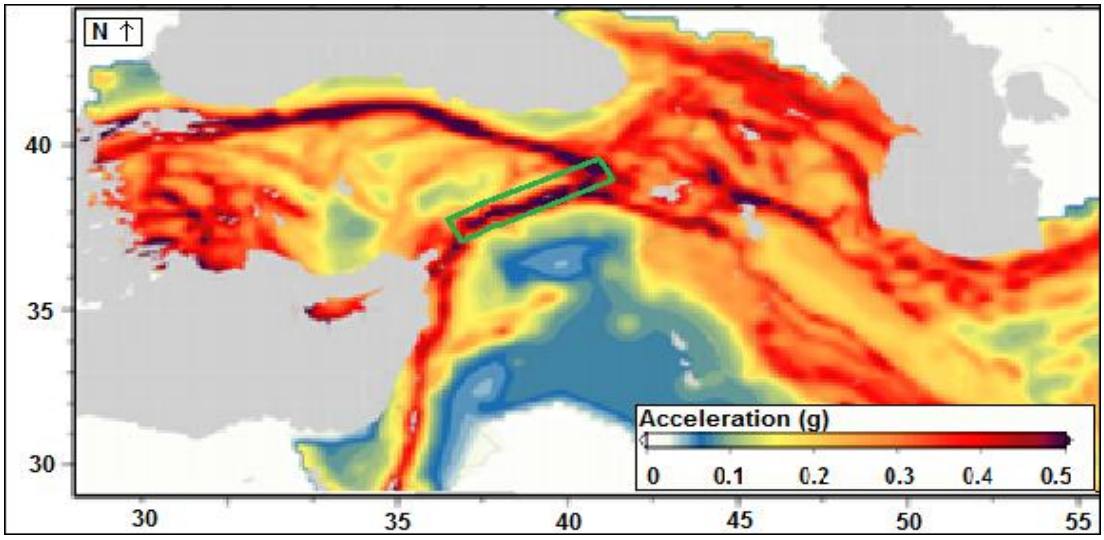


### 1.3 Outline of the Study

The outline of this thesis can be summarized as follows:

In **Chapter 1** the research statement is presented with an emphasis on the previous seismic hazard studies of the region in global and local scales.

In **Chapter 2**, the geological and seismo-tectonic characteristics of the EAFZ are summarized briefly. Seismic source characterization process is discussed in details. The geometry and segmentation points of fault rupture systems; magnitude probability distribution models and model parameters; association of catalogue seismicity with defined rupture systems; magnitude recurrence models, the approach

for balancing the accumulated seismic moment by released seismic moment are presented.

**Chapter 3** briefly introduces the NGA West2 and Turkey-adjusted NGA West1 horizontal GMPE models used in this study. Sensitivity analysis for the selection of most applicable model is also presented in this chapter.

**Chapter 4** includes hazard curves and deaggregation of the hazard for main locations. Hazard maps of the region for different site conditions; comprehensive summary of the study with discussion of the results and recommendations for future works are also given in this chapter.

# CHAPTER 2

# SEISMIC SOURCE CHARACTERIZATION

The East Anatolian Fault Zone (EAFZ) is a northeast-southwest trending, left lateral strike slip fault system starting at Karlıova Triple Junction where it meets the North Anatolian Fault Zone (NAFZ) and continues to Antakya in Eastern Turkey. The transform nature of the EAFZ was first recognized by Arpat and Şaroğlu (1972) and later on the seismotectonic features of this fault zone has been studied by numerous researchers (McKenzie, 1972; Arpat and Şaroğlu, 1975; McKenzie, 1976; McKenzie, 1978; Jackson and McKenzie, 1984; Dewey et al., 1986; Ambraseys, 1988; Taymaz et al., 1991; Westaway and Arger, 1996; Westaway, 2003, 2004; Duman and Emre, 2013). A comprehensive summary of the previous literature on the geological and tectonic characteristics of EAFZ was provided in Duman and Emre (2013) and others; therefore, only the issues that significantly affect the seismic source characterization (SSC) model to be used in PSHA will be elaborated in this section.

## 2.1 Fault Geometry Models

One of the main concerns in SSC modelling is the definition of fault segmentation models for the earthquake rupture forecast. Several studies proposed different segmentation models for EAFZ based on different criteria: Hempton et al. (1981) suggested 5 segments based on the geometrical properties of the fault plane and changes in the fault trend; whereas Barka and Kadinsky-Cade (1988) defined 14 distinct segments based on the discontinuities along the fault plane and the relation between the previous surface ruptures and the earthquake activity. Şaroğlu et al. (1992), divided the EAFZ into 6 segments based on fault step-overs and changes in strike assuming that the segments can move separately along their lengths. A similar approach was adopted in the recent work of Duman and Emre (2013); the authors defined 7 segments with segment lengths varying in between 31-113 km as shown in Figure 2.1. The fault segmentation model proposed by Duman and Emre (2013) was also adopted in the Updated Active Fault Maps of Turkey (Emre et al., 2012).

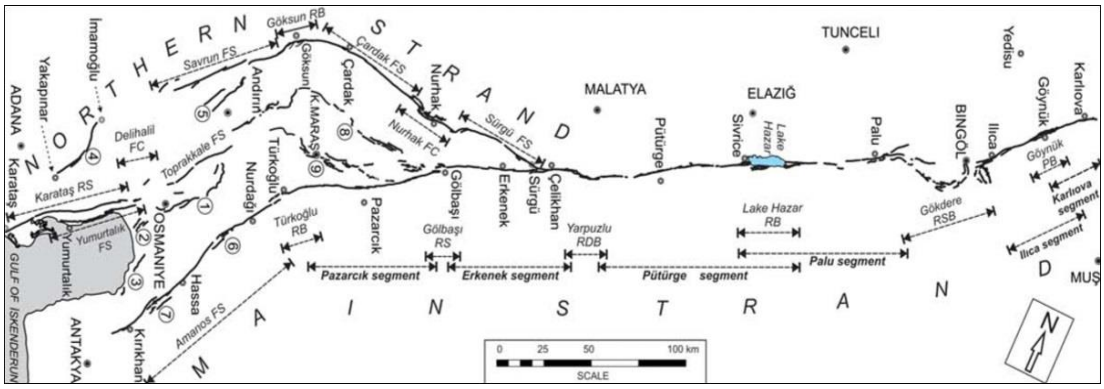


**Figure 2.1: Segmentation Model for the EAFZ Proposed by Duman and Emre (2013)**

Recent large magnitude earthquakes (e.g. 2002 Denali and 2010 El Mayor-Cucapah Earthquakes) showed that the fault ruptures may be complex and span multiple connected fault segments even if the segments are separated by district geological and geomorphological features (Haeussler et al., 2004; Fletcher et al., 2014). To be able to consider multiple-segment ruptures in the rupture forecast, the segmentation model proposed by Duman and Emre (2013) for the main strand of EAFZ is modified by connecting some of the neighboring segments. Specifically, Ilıca and Karlıova Segments are combined into the Ilıca-Karlıova Rupture System (also modified as Gökdere-Ilıca-Karlıova Rupture System as an alternative), Pütürge and Palu Segments are combined as the Pütürge-Palu Rupture System, and Pazarcık and Erkenek Segments are combined to build the Pazarcık-Erkenek Rupture System. These 3 distinct and non-overlapping rupture systems defined in between Karlıova and Türkoğlu are shown in Figure 2.2. Even if the smaller segments are combined into relatively bigger rupture systems, the changes in the fault plane trend, fault jogs and discontinuities are considered by dividing the rupture systems into smaller fault segments and using these segments as basic building blocks for the earthquake rupture forecast. The methodology used in this study was outlined in Working Group on California Earthquake Probabilities (WGCEP-2003) San Francisco Bay Area Model, however, a brief description of the terminology is provided here.

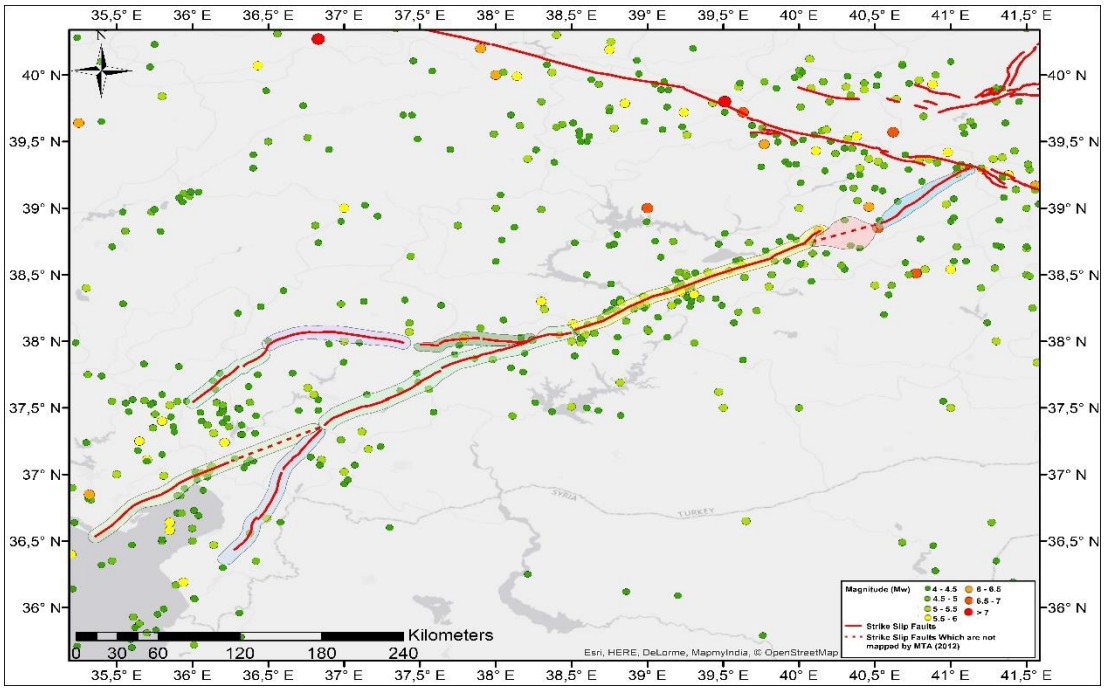


**Figure 2.2: Rupture Systems Defined for EAFZ (majority of the fault lines are digitized from the Updated Active Fault Maps of Turkey published by MTA in 2012)**

In WGCEP-2003, the shortest fault section which is capable of rupturing repeatedly to produce large earthquakes is defined as a **fault segment**. Both kinematic (changes in fault complexity and strike, occurrence of restraining bends, changes in lithology, etc.) and dynamic (timing of events, slip rate, rupture length, and distribution of seismic activity) criteria can be used to delimit the fault segments. The fault segments defined for EAFZ is presented in Table 2.1. The **rupture source** is defined as single or multiple adjacent fault segments that may rupture and produce an earthquake in the future. For example, the Pütürge-Palu Rupture System is composed of 4 fault segments and these segments may be combined into 10 different rupture sources including single or multiple segments as shown in Figure 2.3. Any possible combination of sources that describes a possible failure mode is defined as the **rupture scenario** by WGCEP-2003. According to Figure 2.3, 10 different rupture sources considered for the Pütürge-Palu Rupture System can be combined into 8 different rupture scenarios. The **fault rupture model** includes the weighted combination (weighted average) of all rupture scenarios for the rupture system. The technical basis for choosing the weights of the rupture scenarios by balancing the accumulated and released seismic moment is explained in the next section.

**Table 2.1: The Fault Segments and Rupture Systems Defined for EAFZ. Magnitude of the Characteristic Earthquakes is Calculated Using Wells and Coppersmith (1994) and Hans and Bakun (2014) Rupture Area-Magnitude Relations**

| Segment Name | Length (km) | Width (km) | Slip Rate (mm) | WC94 $M_{char}(M_w)$ | HB14 $M_{char}(M_w)$ |
|---|---|---|---|---|---|
| Gökdere | 66 | 15 | 10 | 7.04 | 7.04 |
| Ilıca | 43 | 15 | 10 | 6.85 | 6.81 |
| Karlıova | 37 | 15 | 10 | 6.78 | 6.73 |
| Pütürge-Palu1 | 39 | 15 | 10 | 6.80 | 6.76 |
| Pütürge-Palu2 | 46 | 15 | 10 | 6.88 | 6.85 |
| Pütürge-Palu3 | 32 | 15 | 10 | 6.71 | 6.66 |
| Pütürge-Palu4 | 34 | 15 | 10 | 6.74 | 6.69 |
| Pazarcık-Erkenek1 | 42 | 15 | 8 | 6.84 | 6.80 |
| Pazarcık-Erkenek2 | 39 | 15 | 8 | 6.80 | 6.76 |
| Pazarcık-Erkenek3 | 35 | 15 | 8 | 6.75 | 6.70 |
| Pazarcık-Erkenek4 | 24 | 15 | 5.9 | 6.59 | 6.54 |
| Karataş-Osmaniye1 | 28 | 15 | 5.9 | 6.66 | 6.60 |
| Karataş-Osmaniye2 | 66 | 15 | 5.9 | 7.04 | 7.04 |
| Karataş-Osmaniye3 | 56 | 15 | 5.9 | 6.96 | 6.96 |
| Amanos1 | 43 | 15 | 2.1 | 6.85 | 6.81 |
| Amanos2 | 41 | 15 | 2.1 | 6.82 | 6.79 |
| Amanos3 | 40 | 15 | 2.1 | 6.81 | 6.77 |
| Sürgü1 | 11 | 15 | 2 | 6.24 | 6.20 |
| Sürgü2 | 25 | 15 | 2 | 6.61 | 6.55 |
| Sürgü3 | 28 | 15 | 2 | 6.66 | 6.60 |
| Çardak1 | 34 | 15 | 2 | 6.74 | 6.69 |
| Çardak2 | 50 | 15 | 2 | 6.91 | 6.89 |
| Savrun1 | 30 | 15 | 2 | 6.69 | 6.63 |
| Savrun2 | 13 | 15 | 2 | 6.32 | 6.27 |
| Savrun3 | 2 | 15 | 2 | 6.51 | 6.46 |

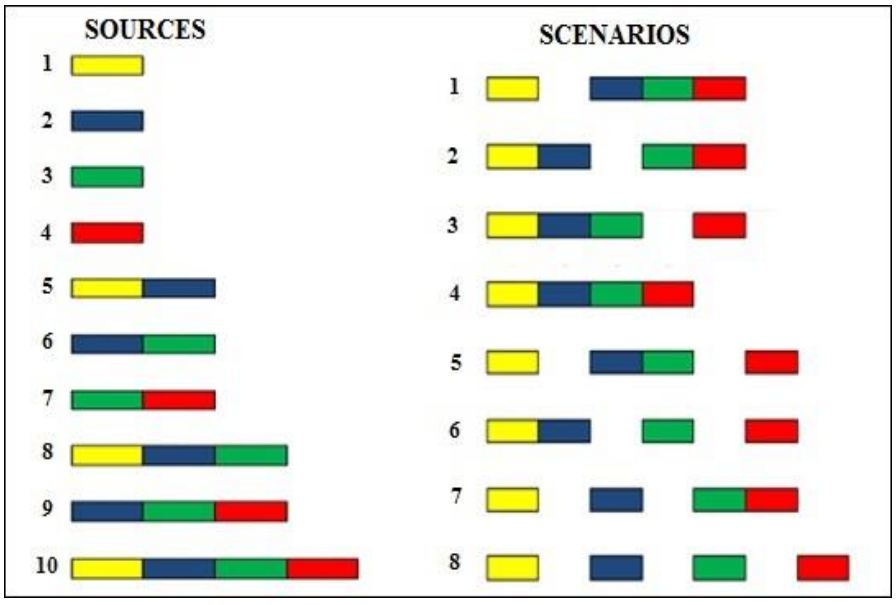


**Figure 2.3: Rupture Source and Full Rupture Scenario Layouts of a Four-Segment Fault (left hand side: 10 rupture sources and right hand side: 8 rupture scenarios)**

### 2.1.1 lıca-Karlıova Rupture System

Ilıca-Karlıova Rupture System originates from the Karlıova Triple Junction and can easily be traced continuously to the east of Bingöl (Şaroğlu and Yılmaz, 1990). This fault system has a total length of 80 km and the general strike of the fault segments is N50E as shown in Figure 2.4. Mahmoud (2012) reported that the morphology of these fault segments is very clear and shows many examples of offsets in rivers and streams. Ilıca-Karlıova Rupture System is characterized by notable seismicity including the 1866 Karlıova Earthquake (Ms=7.0, Ambraseys and Jackson, 1998) and 22 May 1971 (Ms=6.8) Bingöl Earthquake. According to Duman and Emre (2013), the 3.5 m offset that has been recorded on the fault trace by Herece (2008) is an evidence for associating the 1866 Earthquake rupture zone with Ilıca-Karlıova Rupture System.

Karlıova Segment is the north-easternmost part of this rupture system extending in between Göynük and Karlıova regions with a total length of 37 km. This segment has right stepping sections varying in length over the range of 4-12 km (Duman and Emre, 2013). On the other hand, Ilıca Segment has a total length of 43 km and extends between Göynük and Bingöl Plains. 14.5-15 km (Seymen and Aydın, 1972; Herece, 2008) and 17 km (Arpat and Şaroğlu, 1972; Şaroğlu, 1985; Duman and Emre, 2013) maximum fault offsets were documented on the Ilıca Segment based on studies from metamorphic units. Ilıca Segment splits into three branches in the west and terminates in the north of Bingöl Plain (Duman and Emre, 2013). Arpat and Şaroğlu (1972) reported a discontinuous 35 km long surface rupture with a maximum offset of 0.25 m between the Göynük Bend and Bingöl Plain associated with the 1971 Bingöl Earthquake. Later on, Çetin et al. (2003), Herece (2008) and Karabacak et al. (2011) observed surface rupture scars related to the same event along this segment. The fault width for these segments is back-calculated as 15 km based on the surface rupture length of 1971 Bingöl Earthquake using Wells and Coppersmith (1994) rupture area-magnitude relation given in Equation 2.1:

$$M_{char} = 3.98 + 1.02 \log(\mathrm{RA}) \ \ (\pm 0.23) \qquad 2.1$$

where RA is the rupture area (surface rupture length multiplied with fault width).

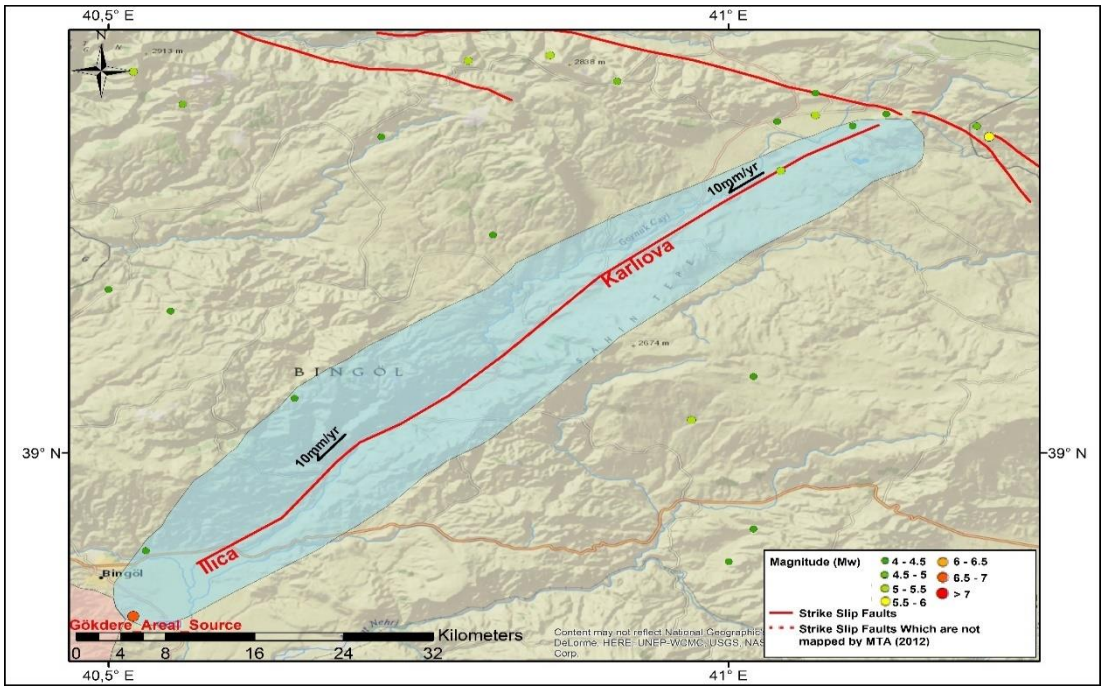


**Figure 2.4: Ilıca-Karlıova Rupture System: The Sub-segments, the Buffer Zone Used for Source to Epicenter Matching, Assigned Slip Rates and Seismicity of the Region**

### 2.1.2 Pütürge-Palu Rupture System

Şaroğlu et al. (1992) defined two separate segments lying in between Palu and Lake Hazar (named as Palu Segment by Duman and Emre, 2013) and Lake Hazar and Sincik (named as Pütürge Segment by Duman and Emre, 2013). The authors proposed that these segments *"can be separated where a pull-apart basin reflected by Lake Hazar is formed, otherwise the two segments are continuous and hence during an earthquake, they may move together"*. A recent structural study of the Hazar Basin constrained by single-channel high-resolution seismic data combined with land-based observations and analysis of sedimentological and geophysical data from Lake Hazar revealed that the main strand of the EAFZ is continuous across the Hazar Basin (Moreno et al., 2009). In the light of above mentioned discussions related to complex and multi-segment ruptures of the recent large events, the spatial distribution of the seismic activity between 1900 and 2014 ($M_w$>1) in the region is evaluted using the data downloaded from http://www.koeri.boun.edu.tr. According to Figure 2.5, the seismicity is continuously scattered in between Çelikhan and Palu including the Lake Hazar Region, indicating that these segments may be combined in the earthquake rupture forecast. Therefore, individual Pütürge and Palu Segments

defined in previous studies are combined as the Pütürge-Palu Rupture System in this study.

The Palu Segment of this rupture system extends in between Lake Hazar and Gökdere Restraining Bend with a total length of 66 km. This segment exhibits a strike slip character with a general strike of N60E. According to Barka and Kadinsky-Cade (1988) and Demirtaş and Yılmaz (1996), Palu Segment is a seismic gap and capable of producing a large earthquake since it has been significantly loaded in the past 200 years (Nalbant et al., 2002).

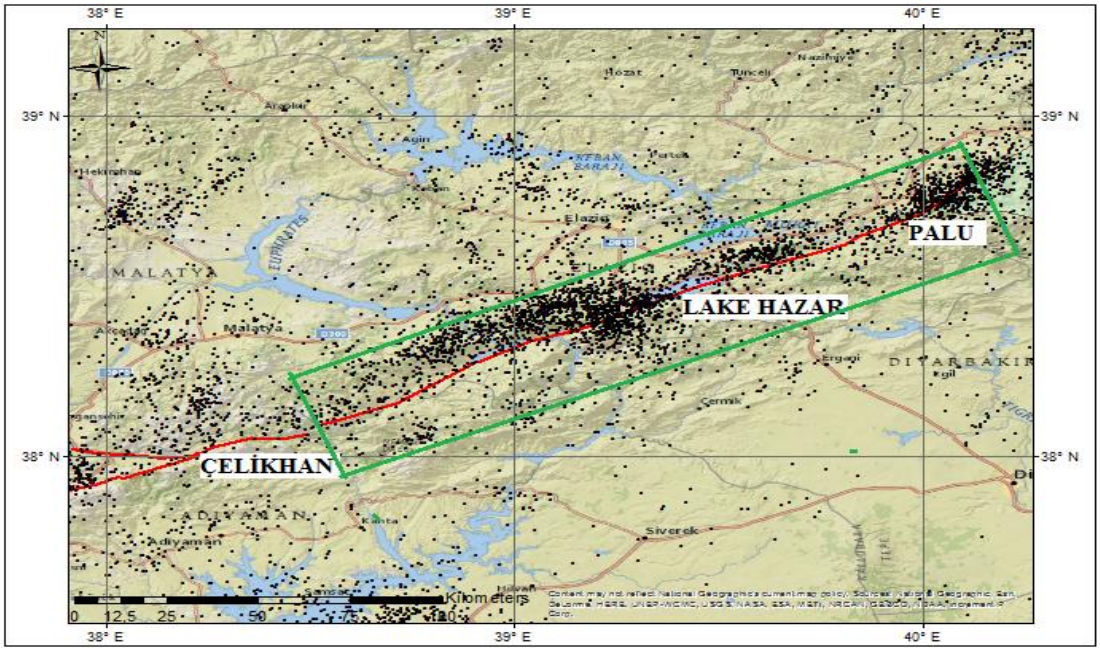


**Figure 2.5: The Spatial Distribution of Catalog Seismicity (1900-2014, Mw>1; downloaded from KOERI web site) in the Vicinity of Lake Hazar Basin**

The latest moderate-to-large magnitude event in the region was occurred on 8 March 2010 Kovancılar Earthquake (Mw=6.1) and the epicenter of the earthquake coincided with the northern branch of Palu Segment (Emre et al. 2010; Tan et al., 2011). Tan et al. (2011) stated that the seismogenic brittle zone depth for the aftershocks of Kovancılar Earthquake is about 15 km which is in good agreement with the fault width value calculated for Ilıca-Karlıova Rupture System. The eastern continuation of the Pütürge-Palu Rupture System (Pütürge Segment) has a slightly sinusoidal shape extending up to the east of Çelikhan with a general strike of N65E and a total

length of about 85 km. 9 to 22 km geological offsets of basement rocks and morphological offsets are measured in the Fırat River Valley (Arpat and Şaroğlu, 1975; Hempton, 1985; Herece and Akay, 1992; Şaroğlu et al., 1992; Westeway and Arger, 2001; Westeway, 2003; Herece, 2008) along this segment. Considering the geometrical discontinuities in the mapped fault plane in the Updated Active Fault Maps of Turkey (Emre et al., 2012), 4 sub-segments are defined for Pütürge-Palu Rupture System as shown Figure 2.6 and Table 2.1. Well-documented paleoseismological evidence is not available for the recurrence interval of the large magnitude earthquakes in the Pütürge-Palu Rupture System. In Ambraseys (1989) and Ambraseys and Jackson (1998), two large magnitude events that occurred in 1874 (Ms= 7.1) and 1875 (Ms= 6.7) were documented around Lake Hazar. Çetin et al. (2003) discussed the possibility of joined rupture of the Palu-Hazar and Hazar-Sincik Segments during the 1874 event. According to Duman and Emre (2013), the 1905 (Ms=6.8) Earthquake may have occurred at the western tip of Pütürge Segment. Assessment of the spatial distribution of seismicity in the region pointed out low seismic activity for this segment; therefore, Bulut et al. (2012) suggested that Pütürge Segment has reached the final phase of seismic cycle due to low seismicity since 1874 Earthquake. In addition to those earthquakes, two other large magnitude historical events have been reported in the area: AD 995 (Ms = 7.0) and AD 1789 (Ms = 7.0) Earthquakes (Moreno et al., 2009).

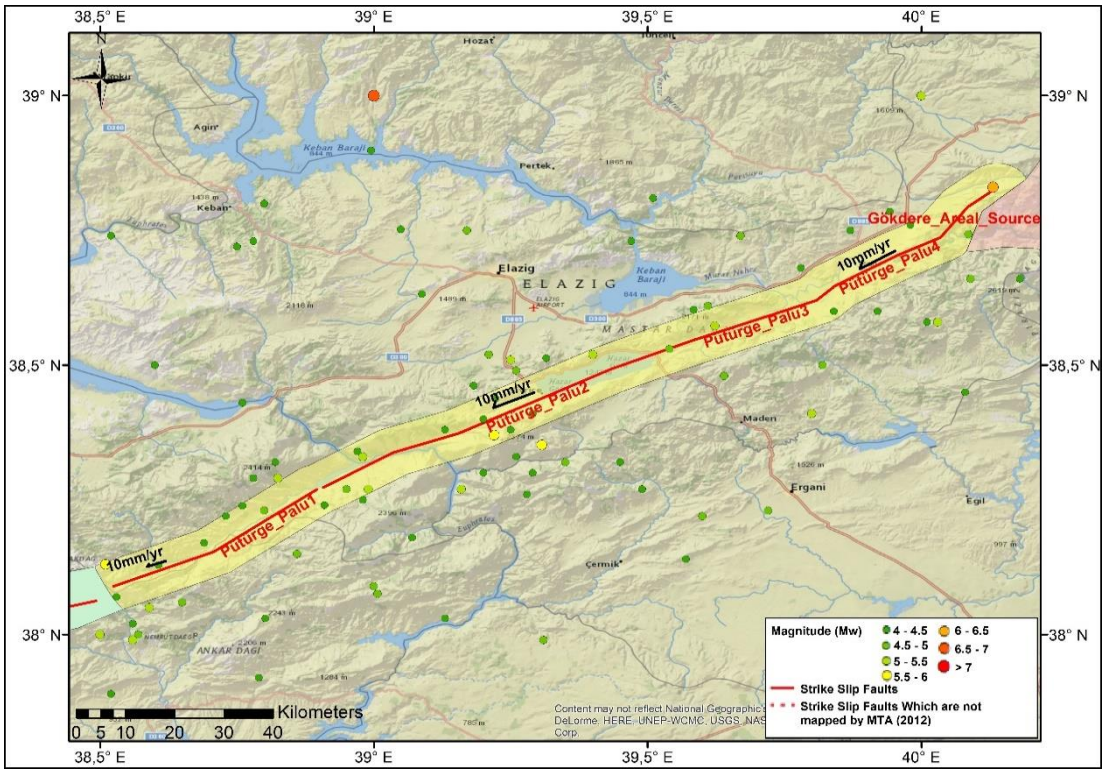


**Figure 2.6: Pütürge-Palu Rupture System: The Sub-segments, the Buffer Zone Used for Source to Epicenter Matching, Assigned Slip Rates and Seismicity of the Region**

### 2.1.3 Pazarcık-Erkenek Rupture System

Pazarcık-Erkenek Rupture System extends in between Türkoğlu and Çelikhan, a region known to be seismically active according to the historical earthquake catalogs (Poirier and Taher, 1980; Ambraseys and Barazangi, 1989; Ambraseys and Melville, 1995). The earthquake records in historical era display that the area has been affected by destructive earthquakes for about 2000 years (Ergin et al. 1967, Ambraseys, 1989; Soysal et al., 1981; Örgülü et al., 2003; Türkelli et al., 2003). According to Ambraseys and Jackson (1998) and Nalbant et al. (2002), Pazarcık-Erkenek Rupture System is associated with the largest of the known historical earthquakes occurred along the EAFZ, such as the 1114 (M > 7.8), 1513 (Ms=7.4), and 1893 (Ms=7.1) Earthquakes. The relation between the Gölbaşı-Türkoğlu (named as Pazarcık Segment by Duman and Emre, 2013) and Çelikhan-Erkenek (named as Erkenek Segment by Duman and Emre, 2013) Segments is a controversial issue. Lovelock (1984), Lyberis et al. (1992), and Chorowicz et al. (1994) argued that no major active strike–slip faults are present in the Gölbaşı Area. On the contrary, McKenzie (1976), Dewey et al. (1986), Perinçek et al. (1987), Barka and Kadinsky-Cade (1988),

Perinçek and Çemen (1990) suggested that the EAFZ is continuous through the Gölbaşı Basin. Interpretations by Biricik (1994), Westaway and Arger (1996), and Güneyli (2008) suggest that the Gölbaşı Basin is a classical pull-apart structure that has been developed between the Çelikhan-Erkenek and Gölbaşı-Türkoğlu Segments. Yılmaz et al. (2006) performed a fault kinematics study along this segment and concluded that the Neocene stress regime in the region shows a distinct strike-slip character with a reverse component and this regime is likely to be continuous as indicated by focal mechanisms of earthquakes in the region. Similar to the Pütürge-Palu Rupture System, the spatial distribution of the seismicity does not reflect any discontinuities along the strike of these segments as shown in Figure 2.7; therefore, Pazarcık and Erkenek Segments are combined to form the Pazarcık-Erkenek Rupture System.

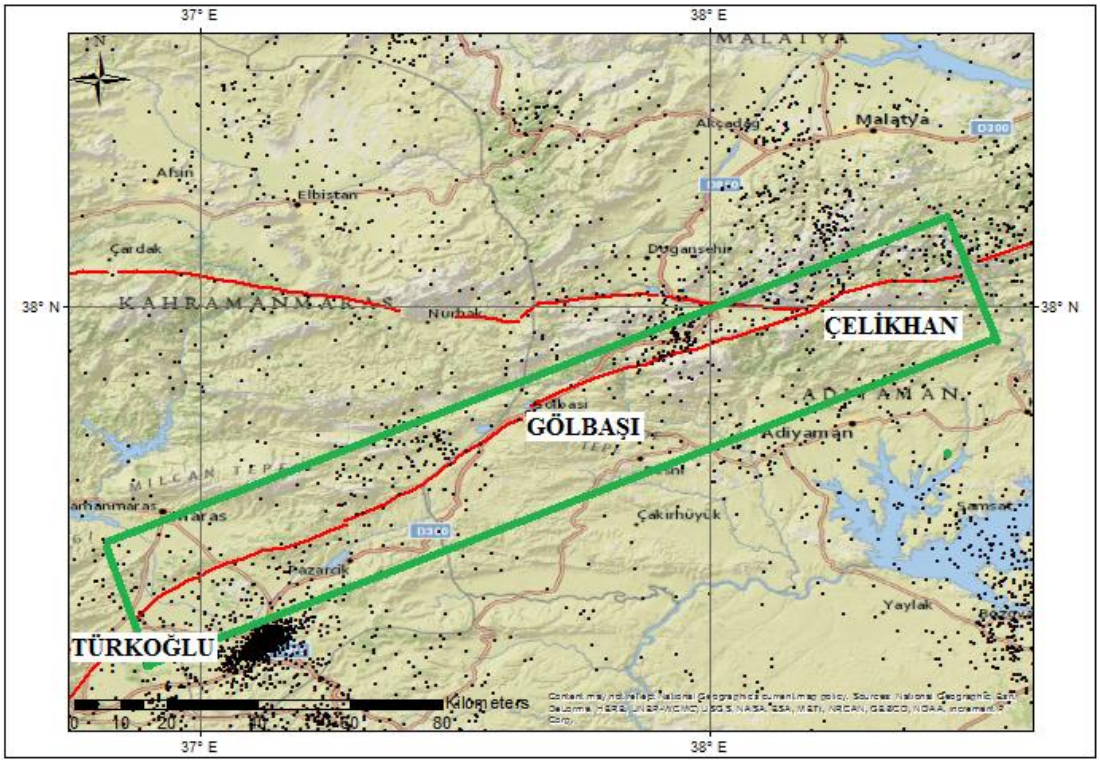


**Figure 2.7: The Spatial Distribution of Catalog Seismicity (1900-2014, Mw>1; downloaded from KOERI web site) in the Vicinity of Gölbaşı Basin**

The northeastern continuation of the Pazarcık-Erkenek Rupture System, the Erkenek Segment, extends from Gölbaşı basin to Yarpuzlu (east of Çelikhan) with a general

strike of N65E with the total length of about 60 km (Figure 2.8) forming 2-15 km long sections that are separated by right and left step-overs, each less than 0.5 km (Duman and Emre, 2013). The western section of Erkenek Segment which follows the southern flank of the Göksu River Valley exhibits a left lateral offset of 13 km (Şaroğlu et al., 1992). Total offsets of 26 and 22.5 km were suggested by (Herece, 2008) based on the geological features for Erkenek Segment. The 80 km long Pazarcık Segment extends between Türkoğlu and Gölbaşı with a general strike of N55E. According to Duman and Emre (2013), Pazarcık Segment has a sinusoidal shape with an echelon pattern in the west (consisting of four sections of about 10 km length) and a more linear geometry between Karaağaç and Gölbaşı Basin in the east. Yalçın (1979), Westeway et al. (2006) and Herece (2008) suggested 19-25 km geological total offsets for this segment. Based on the fault discontinuities mapped in the Updated Active Fault Maps of MTA (Emre et al., 2012), 4 sub-segments are defined for this rupture system as shown in Figure 2.8 and Table 2.1.

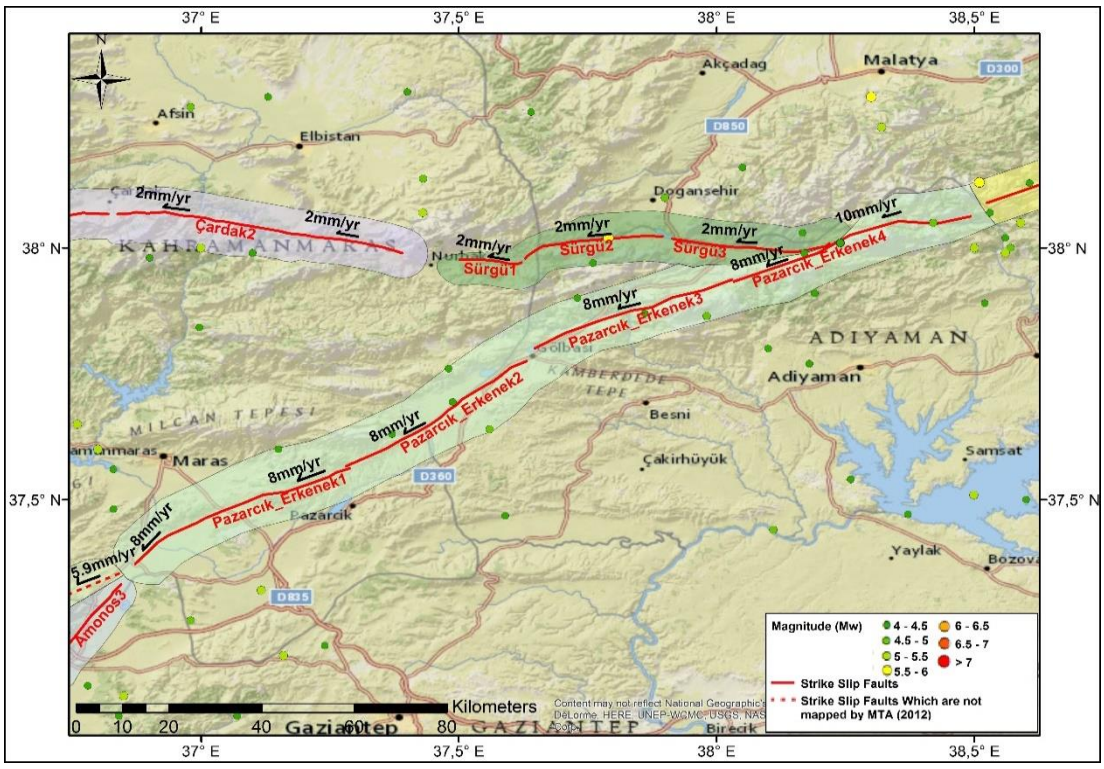


**Figure 2.8: Pazarcık-Erkenek Rupture System: The Sub-segments, the Buffer Zone Used for Source to Epicenter Matching, Assigned Slip Rates and Seismicity of the Region**

Another main concern in developing the SSC models for EAFZ is defining the termination point of EAFZ. Some researchers have suggested that the EAFZ continues westwards from Türkoğlu and connects with Karataş-Osmaniye Fault Zone (McKenzie 1976; Gülen et al. 1987; Karig and Kozlu 1990; Perinçek and Çemen 1990, Westaway and Arger 1996; Westaway 2003). Another interpretation was proposed by Şaroğlu et al. (1992), Herece (2008), Karabacak et al. (2010), and Duman and Emre (2013) claiming that the EAFZ extends southwards from Türkoğlu and reaches Amik Basin through Amanos Fault. Additionally, Meghraoui et al. (2009) proposed that the EAFZ branches into SW-NE trending Karataş-Osmaniye Fault and SSW-NNE trending Karasu Fault based on GPS measurements and the analysis of fault kinematics in Maraş-Antakya region. In this study, both Karataş-Osmaniye and Amanos splays are considered in the earthquake rupture forecast as parallel fault segments that shares the total slip rate in the region as shown in Figure 2.9. The fault lines provided in Updated Active Fault Maps of MTA (2012) are digitized to determine the geometry and segmentation points of the Amanos Rupture System as the Karlıova, Ilıca, Palu, Pütürge, Erkenek and Pazarcık Segments. Since the Karataş-Osmaniye Rupture System was not completely mapped by MTA (Emre et al., 2012), the northern part of the system was extended up to the Türkoğlu Triple Junction using the fault lines provided by McKenzie (1976), Hempton (1987), and Westaway and Arger (1996). It is notable that the Karataş-Osmaniye and Amanos Rupture Systems defined in this study are in close match with the Karataş-Osmaniye and Karasu Faults presented by Westeway (2003) and Meghraoui et al. (2011).

### 2.1.4 Amanos Rupture System

Amanos Fault is the southern strand of the EAFZ splitting from Türkoğlu Triple Junction and extending up to the west of Amik Lake. The fault has a general strike of N30-35E and a total length of about 120 km (Figure 2.9). Duman and Emre (2013) presented three sub-segments (Kırıkhan, Hassa and Nurdağı) for the Amanos Fault following the interpretation of Şaroğlu et al. (1992) with a minor change applied by extending the fault to the south (up to west of Amik Lake) considering the seismicity around the region. These 3 sub-segments are directly adopted from Duman and Emre (2013) to form the Amanos Rupture System.

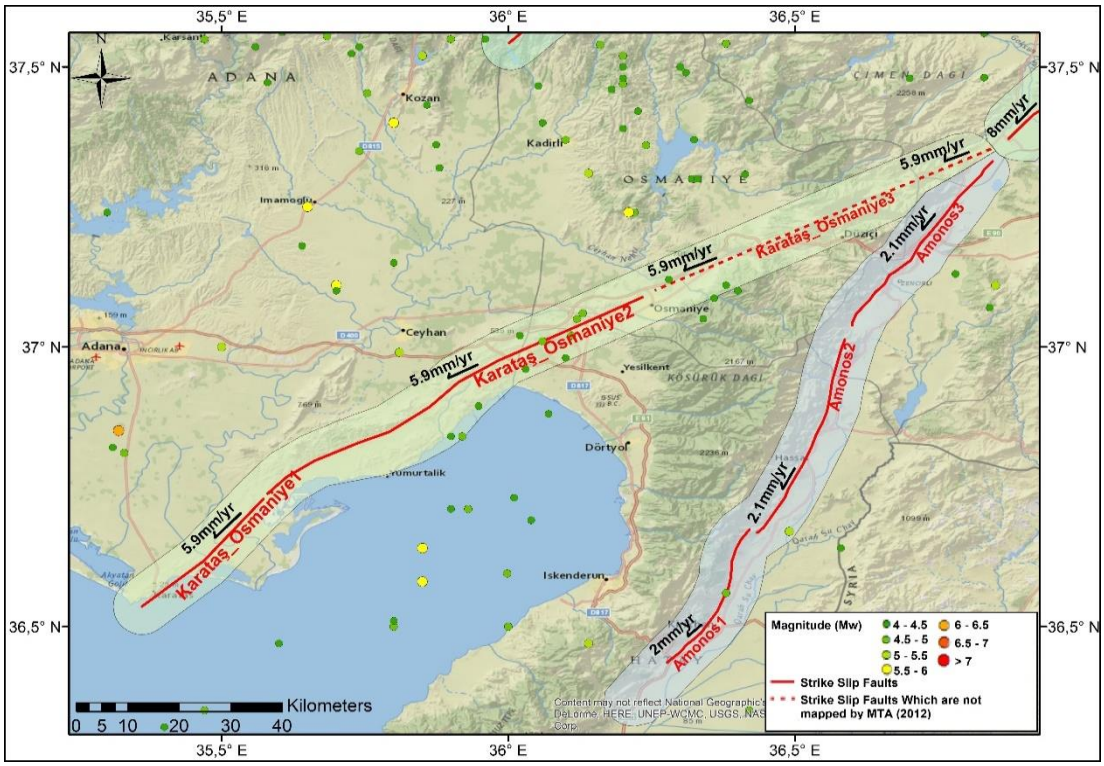


**Figure 2.9: Karataş-Osmaniye and Amanos Rupture Systems: The Sub-segments, the Buffer Zone Used for Source to Epicenter Matching, Assigned Slip Rates and Seismicity of the Region**

The 1822 Antakya Earthquake (Ms=7.2) that produced a 200-km-long surface rupture (Ambraseys and Jackson, 1998 and Seyrek et al., 2007), has been associated with the Amanos Rupture System. Previous studies found no evidence of fresh fault-related topographical feature that have prevailed since this event on this part of EAFZ. If the moment magnitude of the 1822 Event is calculated by the magnitude conversion equations provided in Section 2.2.1 as $M_w$=7.1, then the width of the fault can be back calculated from by Equation 2.1 as 16 km based on this event.

### 2.1.5 Karataş-Osmaniye Rupture System

The western branch of the EAFZ (Karataş-Osmaniye Rupture System) splits from Türkoğlu and extends to Karataş with a general strike of N40-45E and a total length of about 150 km. McKenzie (1976) documented the satellite images of scarps along the line of Yumurtalık and Karataş Faults and inferred these faults as the continuation of the EAFZ from Türkoğlu Triple Junction. Hempton (1987) and Westaway and Arger (1996) argued that the EAFZ should be considered to continue across the Amanos Range to the boundary of the Gulf of Iskenderun along the Karataş-Osmaniye Fault. Several other studies (e.g. Aksu et al., 1992a, 1992b;

Kempler and Garfunkel, 1994) claimed that the left lateral strike-slip earthquake activity continuing off-shore in a zone appears to be linked with the Karataş-Osmaniye Fault and the Girne Mountain range of Northern Cyprus. Yurtmen et al. (2000) stated that the Karataş-Osmaniye Fault Zone forms a part of the modern Turkish-African plate boundary. In the Updated Active Fault Maps of MTA (Emre et al., 2012), Karataş Fault lies in parallel to the Yumurtalık Fault (Figure 2.10a) and these two very close fault segments are represented by the Karataş-Osmaniye-1 and Karataş-Osmaniye-2 Sub-segments that follows the Karataş Fault trace in this rupture forecast. The eastern continuation of this system, the sub-segment named as Karataş-Osmaniye-3, was not mapped by MTA; therefore, the fault geometry is determined based on the distribution of seismicity and fault lines given in McKenzie (1976), Hempton (1987), and Westaway and Arger (1996) (Figure 2.10b).

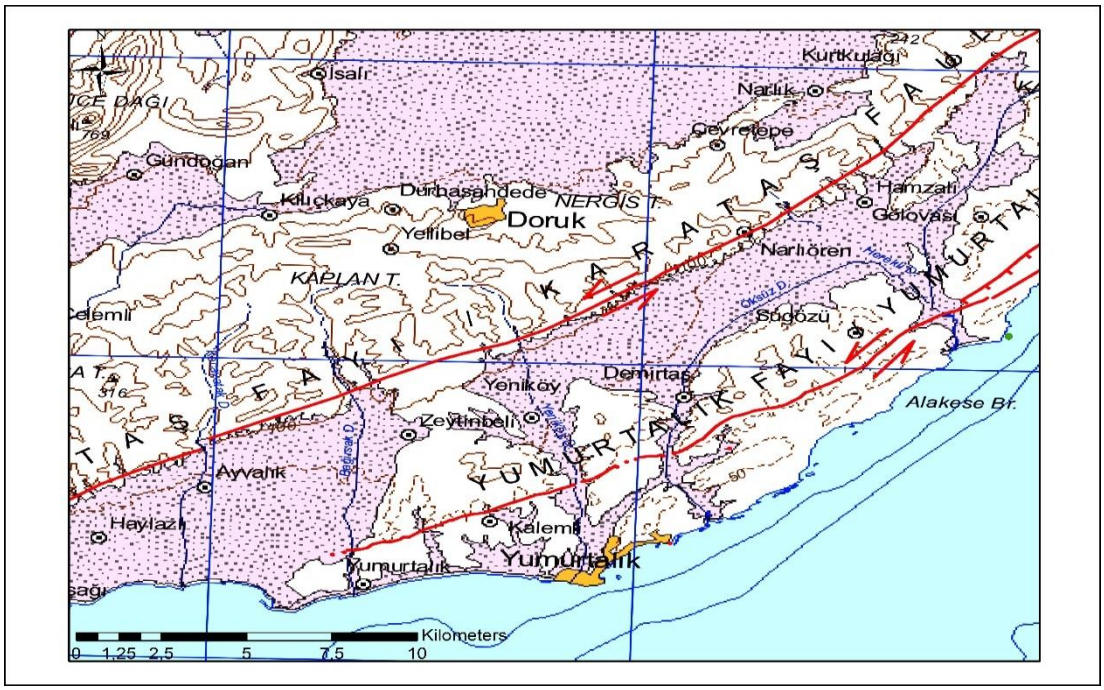


**(a)**

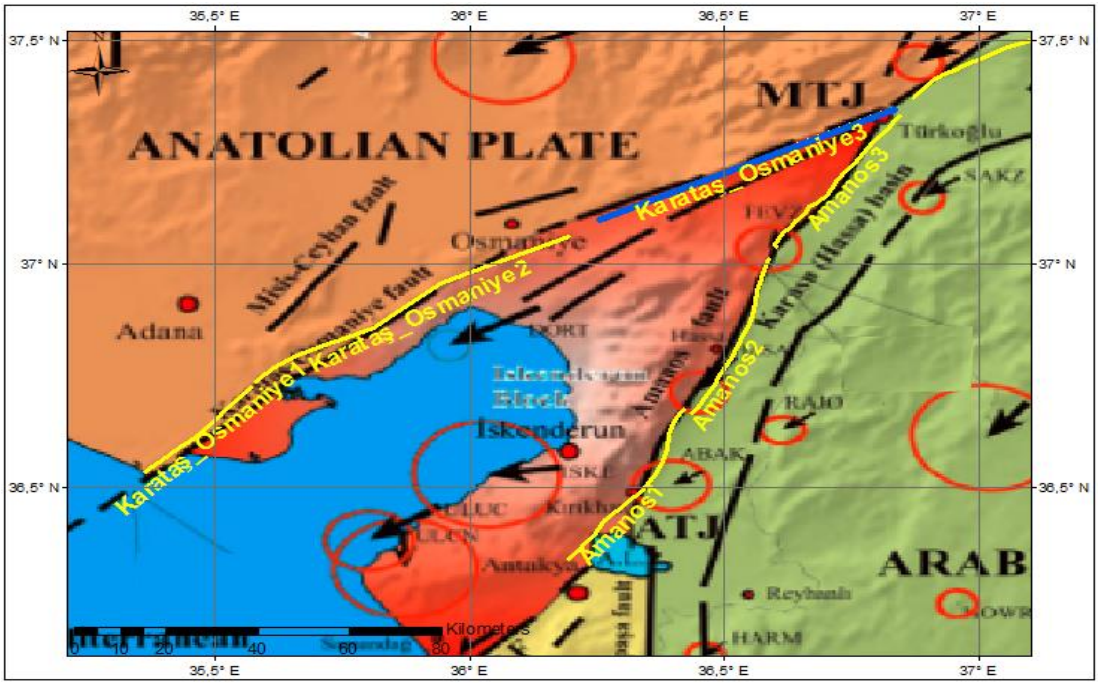


**(b)**

**Figure 2.10: (a) Karataş and Yumurtalık Faults Mapped in Updated Active Fault Maps of MTA (2012), (b) Karataş-Osmaniye and Amanos Fault Systems Suggested by Tari et al. (2013). (Note: yellow lines show Karataş-Osmaniye_1; Karataş-Osmaniye_2; Amanos_1; Amanos_2 and Amanos_3 sub-segments that are digitized from Updated Active Fault Maps of MTA (2012) and the blue line shows the Karataş-Osmaniye_3 segment)**

### 2.1.6 Northern Strand of EAFZ (Sürgü, Çardak and Savrun Rupture Systems)

The main strand of EAFZ shows a narrow deformation zone between Karlıova and Çelikhan; however, starting from the west of Çelikhan a number of splay faults split from the main strand of the EAFZ and transfer the deformation out of the fault zone. SFZ (here referred to as Sürgü and Çardak Rupture Systems) was first introduced as a sinistral strike slip fault by Arpat and Şaroğlu (1975) and the fault plane was later delineated by Perinçek and Kozlu (1984) and Perinçek et al. (1987). Westeway et al. (2006) also mentioned that the SFZ took up the sinistral displacement between the Arabian and Anatolian plates in the Eastern Anatolia during the Pliocene.

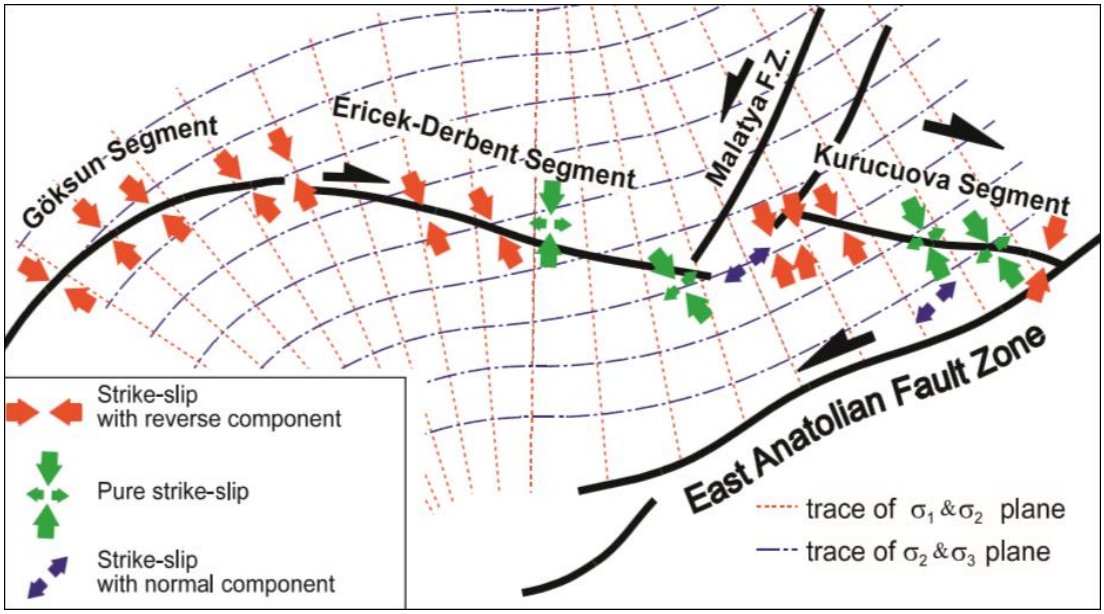


**Figure 2.11: The Spatial Distribution of Horizontal Components of Constructed Palaeostress Configurations and Segments of the SFZ (taken from Koç and Kaymakçı, 2013)**

According to Koç and Kaymakçı (2013), SFZ *has morphotectonic features and kinematic data indicating dextral strike-slip nature with reverse (in the west) and normal (in the east) components; however, it is sub-parallel to the sinistral EAFZ* and *this makes the SFZ an enigmatic structure in having a dextral strike-slip character within a sinistral strike-slip setting*. The authors presented the smoothed trajectories of the principal stress planes based on stress inversion results (Figure 2.11) and proposed that SFZ is a dextral strike-slip fault zone, which has a reverse component in the west especially along the Göksun Segment (here referred to as

Çardak Rupture System); and normal components especially along the Kurucaova Segment (here referred to as Sürgü Rupture System) in the east.

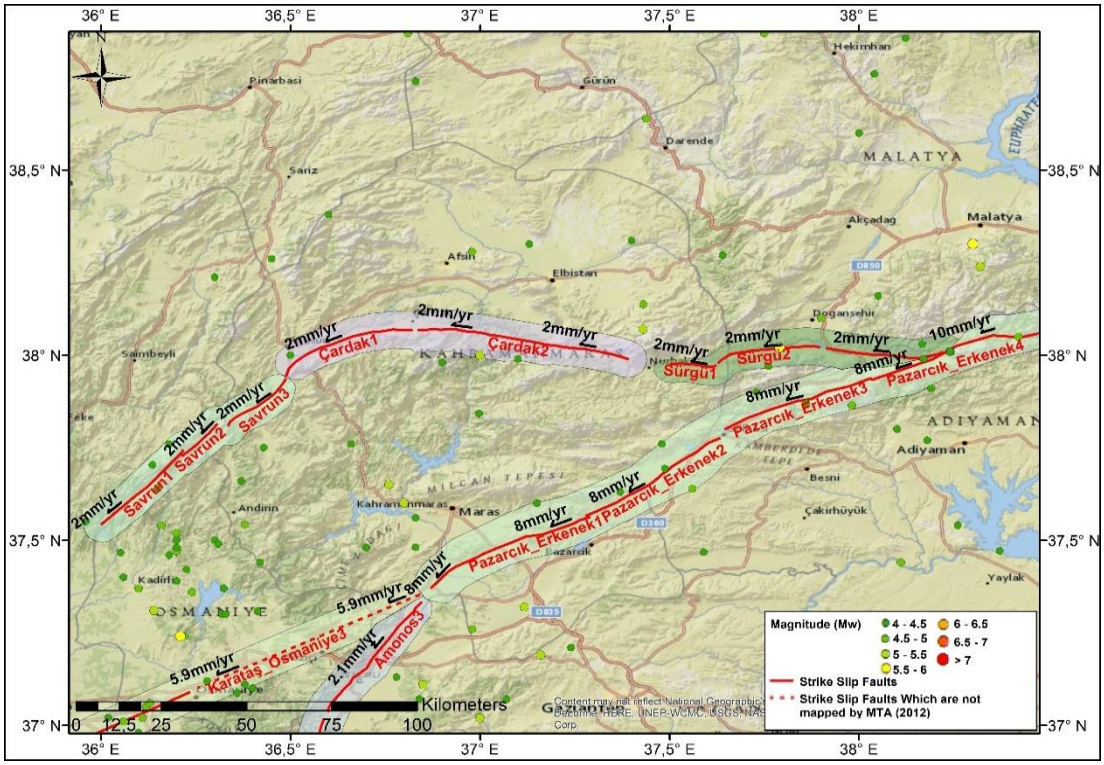


**Figure 2.12: Northern Strand of EAFZ (Sürgü, Çardak and Savrun Rupture Systems): The Sub-segments, the Buffer Zone Used for Source to Epicenter Matching, Assigned Slip Rates and Seismicity of the Region**

Duman and Emre (2013) defined the Sürgü-Misis Fault (SMF) system as the northern strand of the EAFZ and divided the system into two left-lateral strike slip strands separated by Göksun Restraining Bend (please refer to Figure 2.1 for details). The 160 km long eastern strand between Göksun and Çelikhan (here referred to as Sürgü and Çardak Rupture Systems) coincides with the SFZ discussed by Koç and Kaymakçı (2013). Figure 2.12 shows that the seismic activity around the SFZ is very low: only 4 events with Mw>4 can be located in the instrumental catalogue. Koç and Kaymakçı (2013) discussed that the two moderate-magnitude events recorded in 1986 are located at the intersection of the SFZ with the Malatya Fault Zone; therefore, association of these events with SFZ is not very clear. Duman and Emre (2013) showed that the strike of the fault system changes by an average of 45° at the end of Göksun Restraining Bend and then the fault strike generally follows a NE–

SW trend. The authors divided the western strand into several sub-segments which were later grouped into Savrun-Toprakkale Fault System and Yumurtalık-Karataş Fault System. Later fault system is already modeled as the Karataş-Osmaniye Rupture System; therefore, Savrun Rupture System is built by combining the Savrun, Çokak and Toprakkale Sub-segments defined in Duman and Emre (2013) (Figure 2.12).

#### 2.1.6.1 Sürgü Rupture System

The fault segments between Çelikhan and Malatya fault Zone are combined to build the Sürgü Rupture System (Figure 2.13). Sürgü Fault splits from EAFZ around Çelikhan with approximately E–W strike and terminates in the Nurhak Fault Complex. The fault has a sinusoidal shape with total length of about 64 km (Arpat and Saroglu 1975) and the bifurcation angle is about 30° (Koç and Kaymakçı, 2013). In its eastern part, the fault is characterized by a shutter ridge with 17 km long and 1 km wide then traverses westwards for 20 km along the southern flanks of the Sürgü River Valley, where tributaries and intervening ridges are offset systematically. In the west, it is represented by two subparallel faults 5 km apart ending with the Nurhak Area of Fault Complexity (Duman and Emre, 2013). Various kinematic indicators and morphological features related with the activity of Sürgü Fault Zone (SFZ) are observed from the satellite images of the region. The most prominent of these are the linearly arranged pressure ridges formed mainly along the Kurucaova Segment (here reffered to as Sürgü 3 Segment) and step-overs along the main course of the SFZ (Koç and Kaymakçı, 2013). Duman and Emre (2013) stated that an offset of the fault trace across the surface of a Holocene alluvial fan shows Holocene surface faulting occurred along the Sürgü Fault during a large earthquake.

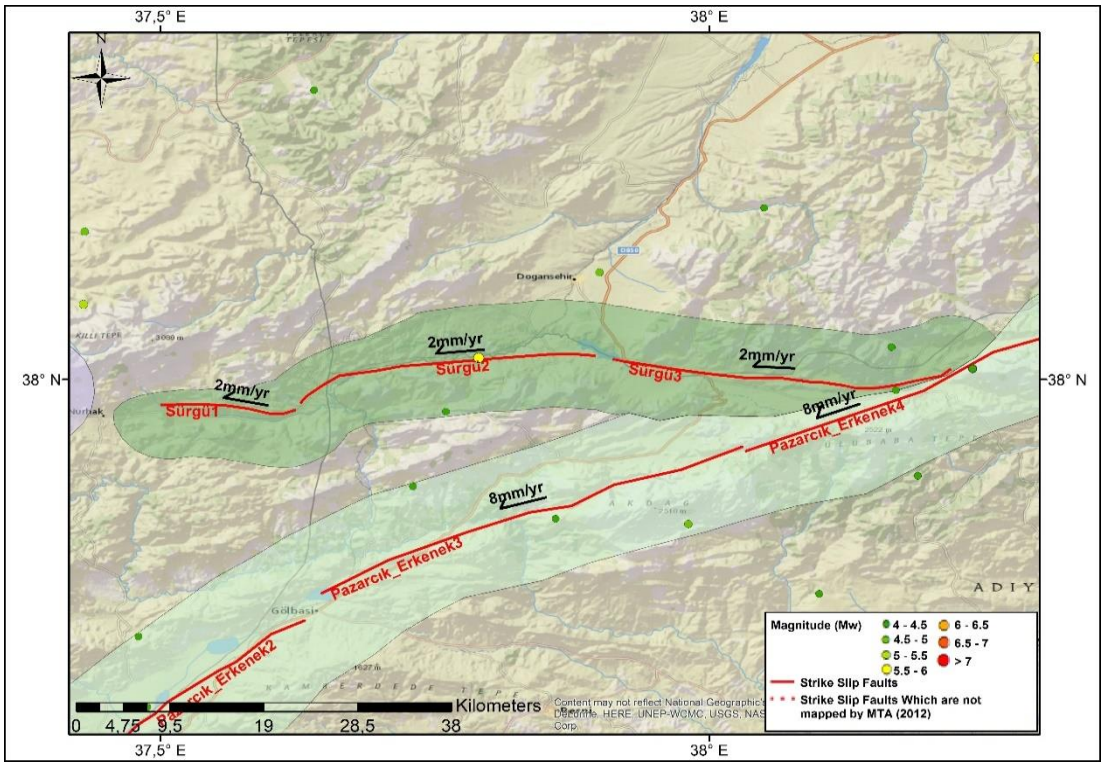


**Figure 2.13: Sürgü Rupture System: The Sub-segments, the Buffer Zone Used for Source to Epicenter Matching, Assigned Slip Rates and Seismicity of the Region**

### 2.1.6.2 Çardak Rupture System

Çardak Fault is a dextral strike-slip fault zone standing between Nurhak in the east and Göksun Restraining Bend in the west. The fault has a total length of about 84 km and it is divided into eastern and western sections separated by a 0.5-km-wide right-stepover (Duman and Emre, 2013). The eastern continuation of the fault is relatively linear with a general strike of N75W and connects with the Nurhak Area. Koç and Kaymakçı (2013) stated that the eastern section (referred to as Çardak 1 Segment) has a reverse component which exhibits a noticeable bending geometry toward the south based on palaeostress configurations. The 50-km-long western section stand side by side with the rock units related to Berit Mountain with a volcanic complex on its northern block. This section includes the Göksun Restraining Bend, which trends N45E at its western tip. As Figure 2.14 shows, two sub-segments defining the eastern and western sections of the Çardak Fault are combined in Çardak Rupture System.

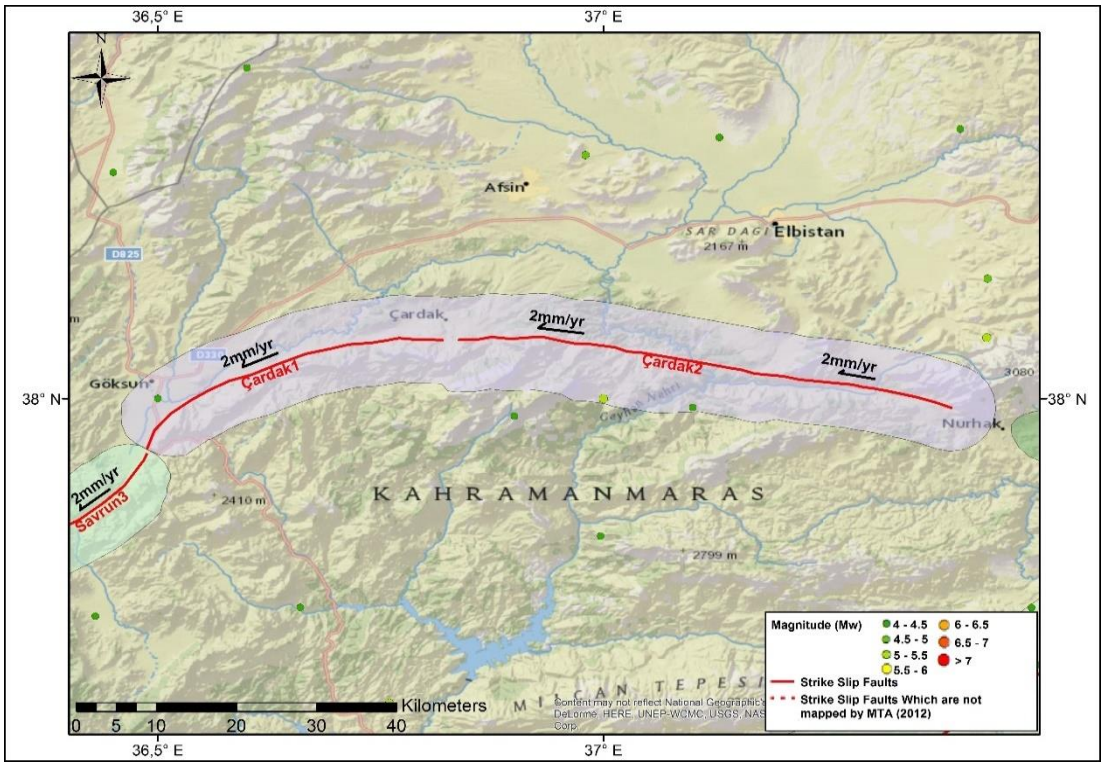


**Figure 2.14: Çardak Rupture System: The Sub-segments, the Buffer Zone Used for Source to Epicenter Matching, Assigned Slip Rates and Seismicity of the Region**

### 2.1.6.3 Savrun Rupture System

Savrun Rupture System is built by combining Savrun, Çokak and Toprakkale Sub-segments defined in Duman and Emre (2013) as shown in Figure 2.15. Fault segments exhibit distinctive active left-lateral fault features such as offset channels, shutter ridges, topographic saddles and fresh fault scarps and they delimit the northern outcrop of the Misis–Andırın Complex (Kozlu, 1987; Perinçek and Kozlu, 1984; Robertson et al., 2004). Savrun Rupture System has a total length of 63 km with a general strike of N40E (Table 2.1). It begins from Göksun Restraining Bend and extends up to Kesiksuyu Dam in north of Sumbas. Since the style of faulting for the Northern Strand of EAFZ is a controversial issue, a set of sensitivity analysis is performed to understand the impact of this parameter on the hazard results.

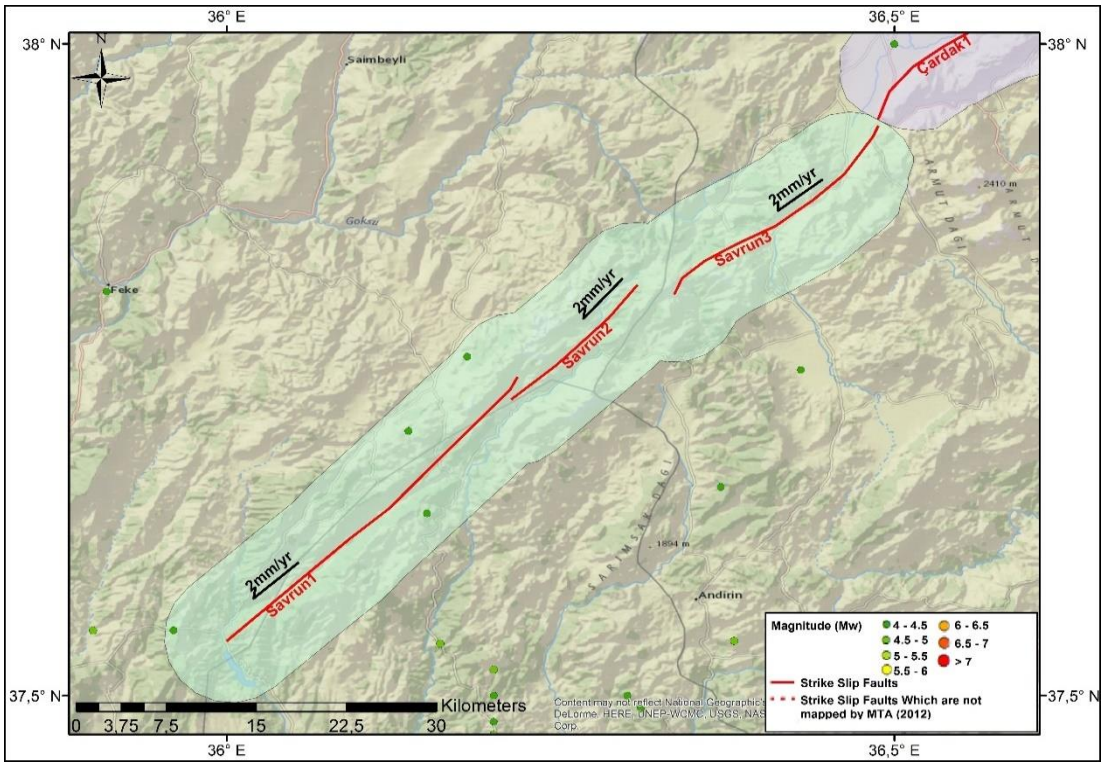


**Figure 2.15: Savrun Rupture System: The Sub-segments, the Buffer Zone Used for Source to Epicenter Matching, Assigned Slip Rates and Seismicity of the Region**

The sensitivity analyses are performed for example near-fault and far field sites (shown in Figure 2.16a) by changing the style of faulting parameter (as strike-slip and reverse) and the dip angle of the fault (90° for SS and 45-65° for RV). Figure 2.16(b) and (c) show the hazard curves for Site 1 and Site 2, respectively (please note that in the sensitivity analysis, all rupture systems defined above are employed). For near fault site, the dip angle and style of faulting (SoF) parameter do not have a significant effect on the hazard results as expected. As the source-to-site distance increases, decreasing the dip angle increases the PGA, especially for higher hazard levels. If the dip angle is selected as 65° to represent the oblique character of SFZ, then the choice of SoF parameter does not change the design PGA values. Based on the analysis results, the SoF parameter is selected to be both SS and RV (with equal weights in the logic tree) and the dip angle is set to 65° in the PSHA runs for the segments of Sürgü and Çardak Rupture Systems

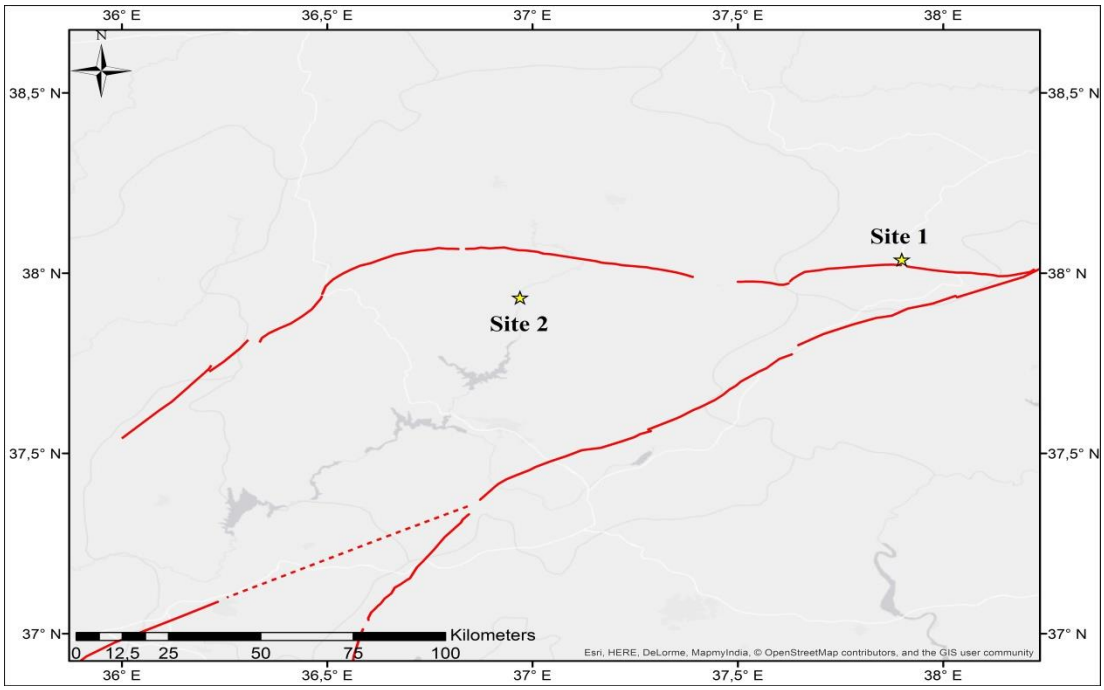


**(a)**

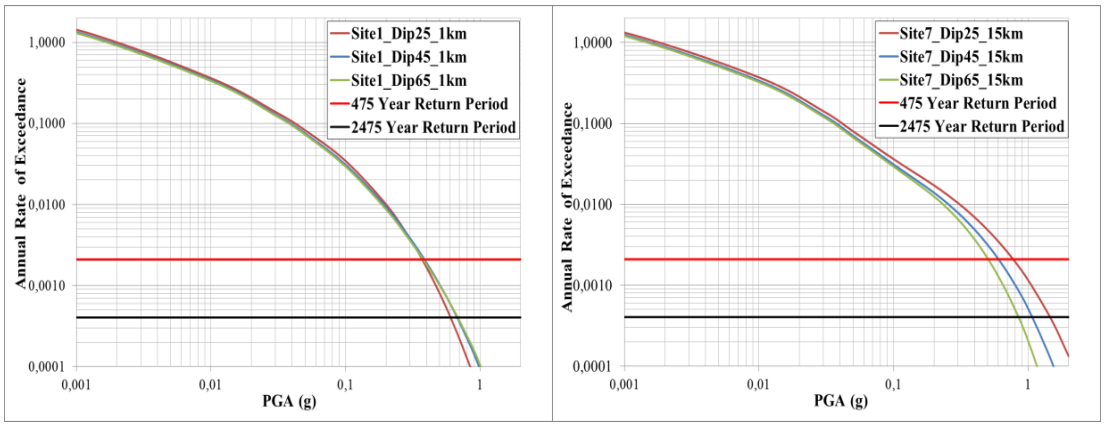


**(a)** **(b)**

**Figure 2.16: Sensitivity Analysis for Source Mechanism of Sürgü and Çardak Rupture Systems (a) Location of Selected Example Sites, (b) Alternative Hazard Curves for Site 1 and (c) Alternative Hazard Curves for Site 7**

### 2.1.7 Gökdere Restraining Bend

Gökdere Restraining Bend stands between east of Palu and Bingöl Basin. According to Duman and Emre (2013) Gökdere Restraining Bend is about 50 km long by 25 km wide and changes the general strike of the EAFZ around 17°. The authors observed folds, thrusts and strike slip faults in eastern and western parts of the bend. The

southern edge of the bend is bounded by the Murat River, which was tectonically incised to a depth of 700 - 1000 m during Quaternary time (Şaroğlu et al., 1992). Herece (2008) measured approximately 600 m uplift based on elevated terrace deposits during the same period. In the east, the bend is bounded by the Bingöl Pull-apart Basin. The northwest and southeast flanks of the bend are delimited by strike-slip faults. In the northwest, faults related to a continuation of the Palu Segment merge with the bend and are transformed into thrust faults or anticlinal axes (Duman and Emre, 2013). Arpat (1971) and Arpat and Şaroğlu (1972) reported up to 1.8-km-long surface ruptures related to the 1971 Bingöl Earthquake in the region. Geometry of the faults modeled in Ilıca-Karlıova and Pütürge-Palu Rupture Systems are discontinuous near the Gökdere Restraining Bend. On the other hand, Mw>4 events were observed in this region during the instrumental period (Figure 2.17). To model this seismicity, two alternative source zone models are defined. **Alternative 1** is an areal source zone that connects the neighboring Ilıca-Karlıova and Pütürge-Palu Rupture Systems as shown in Figure 2.17(a). For the areal source zone, the truncated exponential magnitude distribution model was used with a maximum magnitude value of Mw=6.9 based on the length of faults that defines the boundaries of the bend. The fault mechanism of the areal source was selected as reverse fault in order to be on the safe side. The parameters of the truncated exponential model are not calculated using the seismicity within the zone since the limited data may lead to statistically unstable results. Instead, the a- and b-values calculated for the EAFZ are used to constrain the zone-specific a- and b-values by directly adopting the b-value (slope) and normalizing the activity rate (a-value) by the area ratio. **Alternative 2** is defined by adding the Gökdere Segment (46 km) to the Ilıca-Karlıova Rupture System between the east of Palu and Bingöl Basin as shown in Figure 2.17(b). In this alternative model, a planar fault for western continuation of Ilıca-Karlıova Rupture System was considered although it was not mapped in the Updated Active Fault Maps of MTA (Emre et al., 2012). In order to be consistent with adjacent faults' source model parameters, 15 km width and 10 mm/yr slip rate is assigned to the Gökdere Segment.

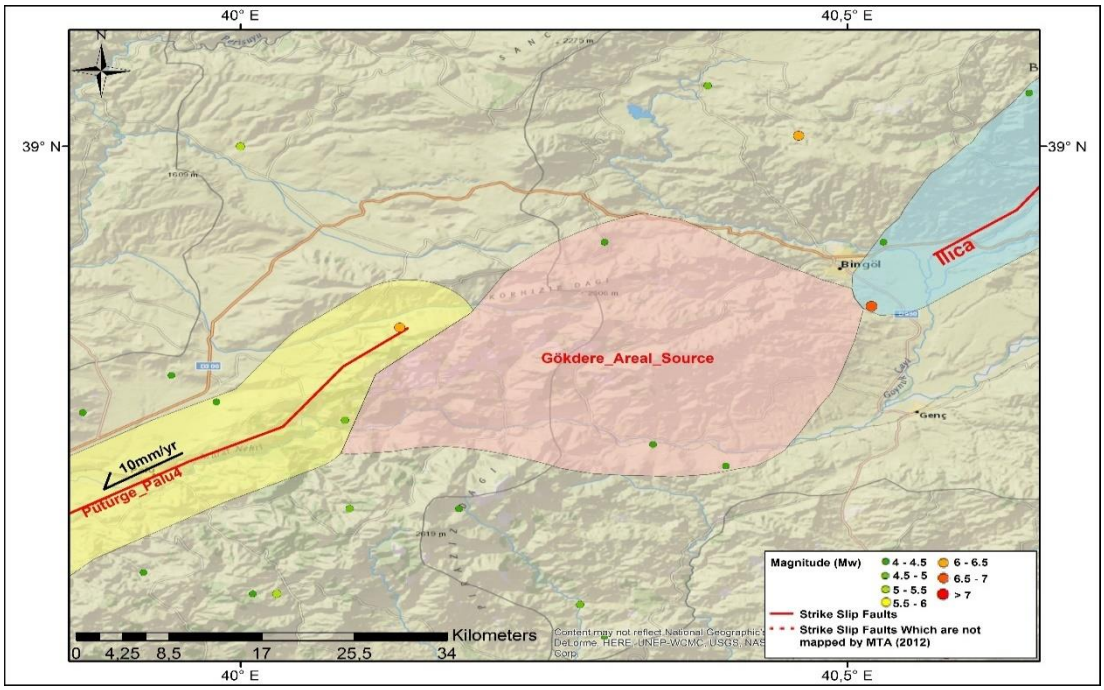


**(a)**

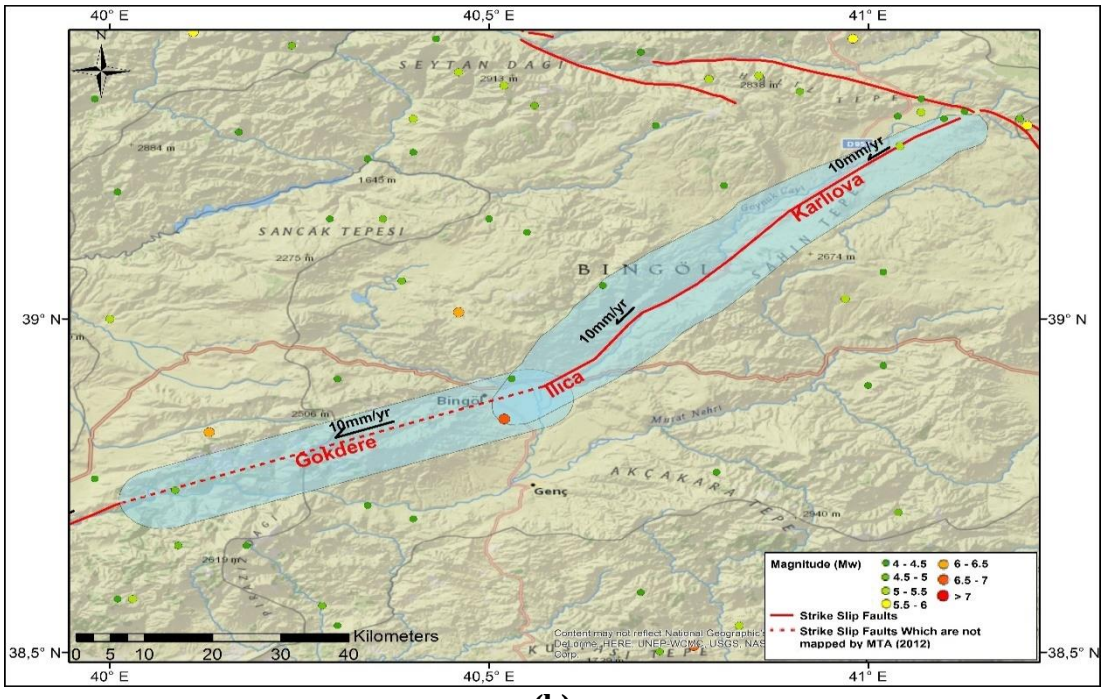


**(b)**

**Figure 2.17: (a) Alternative 1: Geometry of the Gökdere Areal Source and Associated Seismicity, (b) Alternative 2: Modified Gökdere-Ilıca-Karlıova Rupture System: The Sub-Segments (Gökdere, Ilıca and Kalıova Segments), the Buffer Zone Used for Source to Epicenter Matching, Assigned Slip Rates and Seismicity of the Region**

## 2.2 Rupture Models and Moment Balancing Procedure

After the fault geometry models are defined, the rupture models are built by following these steps: i) selection of the proper magnitude probability distribution functions (PDFs) and defining the model parameters, ii) association of the catalog seismicity with the defined rupture systems, iii) modeling the accumulated seismic moment using the annual slip rate and selected magnitude PDF to form the magnitude recurrence model, and iv) balancing the accumulated seismic moment with the released seismic moment based on the associated seismicity.

### 2.2.1 Magnitude Probability Distribution Models and Model Parameters

Seismic sources generate different sizes of earthquakes and magnitude distribution models describe the relative rate of these small, moderate and large earthquakes. Typical magnitude distributions functions that are used in PSHA are shown in Figure 2.18.

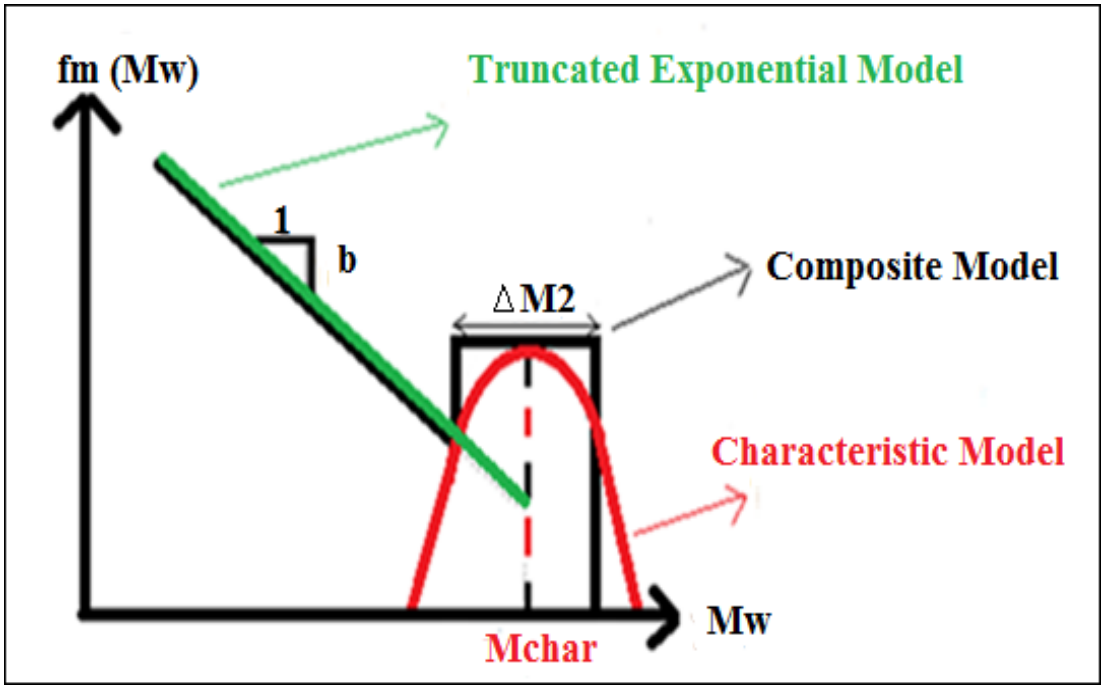


**Figure 2.18: Magnitude Distribution Functions Used in PSHA**

The exponential model proposed by Gutenberg and Richter (1944) is the most common magnitude recurrence relation:

$$Log_{10}N = a - bM \quad (2.2)$$

In Equation 2.2, M is magnitude; N is cumulative number of events larger than M; a is activity rate and b is the relative rate of different magnitude events. This equation is truncated for minimum and maximum magnitudes because there is a certain limited magnitude that a source can produce and there is a certain minimum magnitude that is considered in engineering applications.

After being truncated from both ends the function takes the following form as shown in Equation 2.3 and 2.4:

$$f_m^{TE}(M) = \frac{\beta \exp\left(-\beta(M - M_{min})\right)}{1 - \exp\left(-\beta(M_{max} - M_{min})\right)} \quad (2.3)$$

$$\beta = ln(10) \times b \quad (2.4)$$

where $M_{min}$ is the minimum magnitude and $M_{max}$ is the maximum magnitude. Youngs and Coppersmith (1985) suggested truncated exponential model for large regions and regions with multiple faults. According to authors this model in general is not suitable for individual faults which may tend to rupture as "characteristic" size events. The alternative magnitude model for this case is the "characteristic model" proposed by Schwartz and Coppersmith (1984) (red line in Figure 2.18). In characteristic PDF, once a fault begins to rupture in large earthquakes, it is likely to rupture the whole fault segment and generate similar size earthquakes. In characteristic model, small-to-moderate magnitude events on a fault are not considered.

In 1985, Youngs and Coppersmith proposed composite model that combines the characteristic magnitude model (black line in Figure 2.18) and truncated exponential model. Both seismological and geological properties are considered in this new model. Large magnitude events are represented with the characteristic earthquake magnitude and small to moderate magnitude events are represented by exponential model. The key feature of the composite model is the relative size of the released seismic moments for small to moderate and large magnitude earthquakes. In this model, 94% of the accumulated seismic moment is released by the characteristic earthquakes and 6% of the accumulated seismic moment is released by small-to-moderate earthquakes. The equations that define the composite magnitude PDF is given below:

$$f_m^{YC}(M)=\begin{cases}\frac{1}{1+c_2}\times\frac{\beta\exp\left(-\beta(\bar{M}_{char}-M_{min}-1.25)\right)}{1-\exp\left(-\beta(\bar{M}_{char}-M_{min}-0.25)\right)} & \text{for } \bar{M}_{char}-0.25<M\leq\bar{M}_{char}+0.25\\ \frac{1}{1+c_2}\times\frac{\beta\exp\left(-\beta(M-M_{min})\right)}{1-\exp\left(-\beta(\bar{M}_{char}-M_{min}-0.25)\right)} & \text{for } M_{min}<M\leq\bar{M}_{char}-0.25\end{cases} \quad 2.5$$

where,

$$c_2=\frac{0.5\beta\exp(-\beta(\bar{M}_{char}-M_{\min}-1.25))}{1-\exp(-\beta(M_{char}-M_{min}-0.25))} \quad 2.6$$

and $M_{char}$ is the characteristic earthquake magnitude.

Gülerce and Vakilinezhad (2015) showed that coupling the truncated exponential magnitude PDF with seismic sources defined by planar fault geometries results in unrealistically high rates for small-to-moderate magnitude events. Therefore, the composite magnitude PDF proposed by Youngs and Coppersmith (1985) is preferred to represent the relative rates of small, moderate and large magnitude earthquakes related to the rupture systems defined in Section 2.1. Only for the Gökdere Areal Source (Alternative 1), the truncated exponential magnitude PDF is employed (please refer to Section 2.1.7 for model parameters). The minimum magnitude ($M_{min}$) is set to $M_w$=4.0 for all seismic sources. Characteristic magnitudes for each segment are calculated by the relationships proposed by Wells and Coppersmith (WC94, 1994) and Hans and Bakun (HB14, 2014) for strike-slip faults and are listed in Table 2.1. As shown in Figure 2.19, the difference in the estimated $M_{char}$ values using WC94 and HB14 equations is not very significant (less than 0.1 magnitude unit for all magnitudes) and the values estimated by WC94 equations are systematically larger than the values estimated using HB14 equations. The more conservative $M_{char}$ values based on WC94 equations are preferred and used in the developed SSC model. The upper bounds for the magnitude distribution functions ($M_{max}$) are determined by adding 0.25 magnitude units to the characteristic magnitude for each source.

The Integrated and Homogeneous Turkish Earthquake Catalog (Kalafat et al., 2011) published by KOERI including the events with $M_w$>4 that occurred between 1900 and 2010 is utilized to represent the instrumental seismicity in the region. This catalog is enriched by the $M_w$>4 events that occurred in between 2011 and 2014 (downloaded from http://www.koeri.boun.edu.tr/sismo/2/earthquake-catalog/). The

$M_w$ values for 41 events that occurred in between 2011 and 2014 were not available; therefore, magnitude conversion equations proposed by Akkar et al. (2010) (given in Equations 2.7 and 2.8) are used to calculate these missing $M_w$ values.

$$M_w=1.104M_b-0.194, \quad 3.5 \leq M_b \leq 6.3 \qquad 2.7$$

$$M_w=0.953M_L+0.422, \quad 3.9 \leq M_L \leq 6.8 \qquad 2.8$$

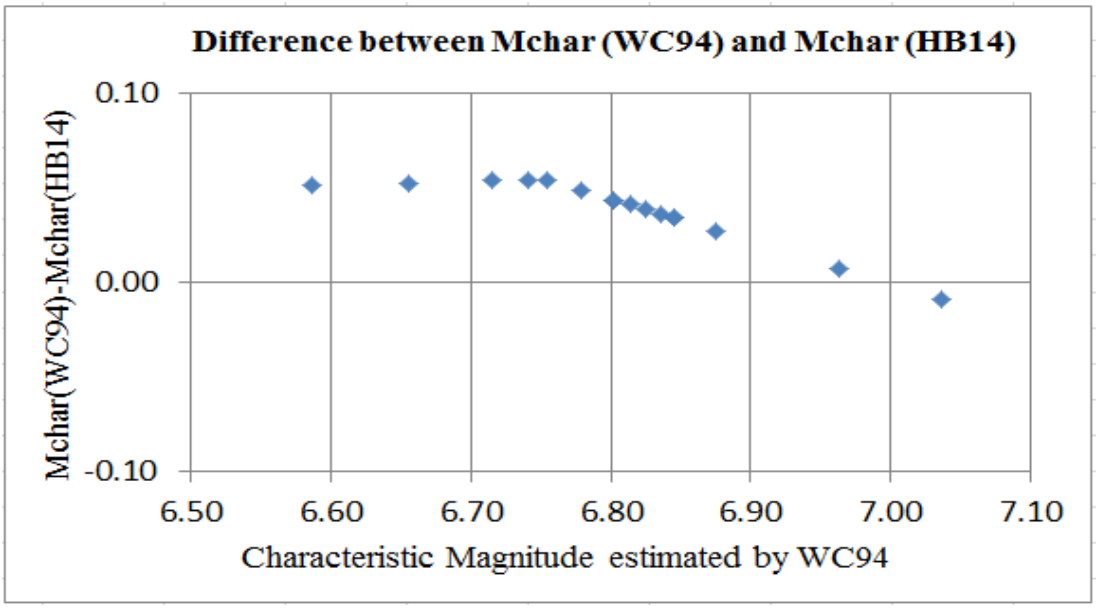


**Figure 2.19: The Difference Between Characteristic Magnitude Values Estimated by WC94 and HB14 Equations**

After the magnitude scales are unified, aftershocks and foreshocks are eliminated based on the method proposed by Reasenberg (1985) using the ZMAP software package (Wiemer, 2001). Reasenberg (1985) algorithm assumes a dynamically modeled (spatial and temporal) interaction zone centered on each earthquake. The events which occur in the zone of previous earthquakes are defined as aftershocks. The b-values for each zone shown in Figure 2.20 are calculated using the maximum likelihood method provided in ZMAP software package and presented in Figure 2.21. Figures 2.21 (a-e) show the completeness magnitudes and the b-values for Ilıca-Karlıova, Pütürge-Palu, Pazarcık-Erkenek, Karataş-Osmaniye, and Amanos Rupture Systems. The completeness magnitude and the b-value calculated for the whole EAFZ shown in Figure 2.21(f). Analysis results show that the b-value varies in between 0.64 and 0.90 for different rupture systems defined along EAFZ, whereas

the b-value for the whole system is equal to 0.84. A recent study on the earthquake probabilities around EAFZ by Bayrak et al. (2014) proposed quite similar b-values for approximately the same rupture systems as shown in Figure 2.22. Both in this study and in Bayrak et al. (2014), the lowest b-value is obtained for Ilıca-Karlıova Rupture System indicating that the Ilıca-Karlıova region has higher stress levels when compared to the others. Both the rupture system specific b-values (shown in Figures 2.21 (a-e)) and the b-value calculated for the EAFZ (0.84 according to Figure 2.21(f)) are employed in the PSHA with equal weights assigned in the SSC logic tree. Since the seismicity within the buffer zones around the Sürgü, Çardak and Savrun Rupture System is limited, only the b-value calculated for the EAFZ (0.84) is used for these rupture systems.

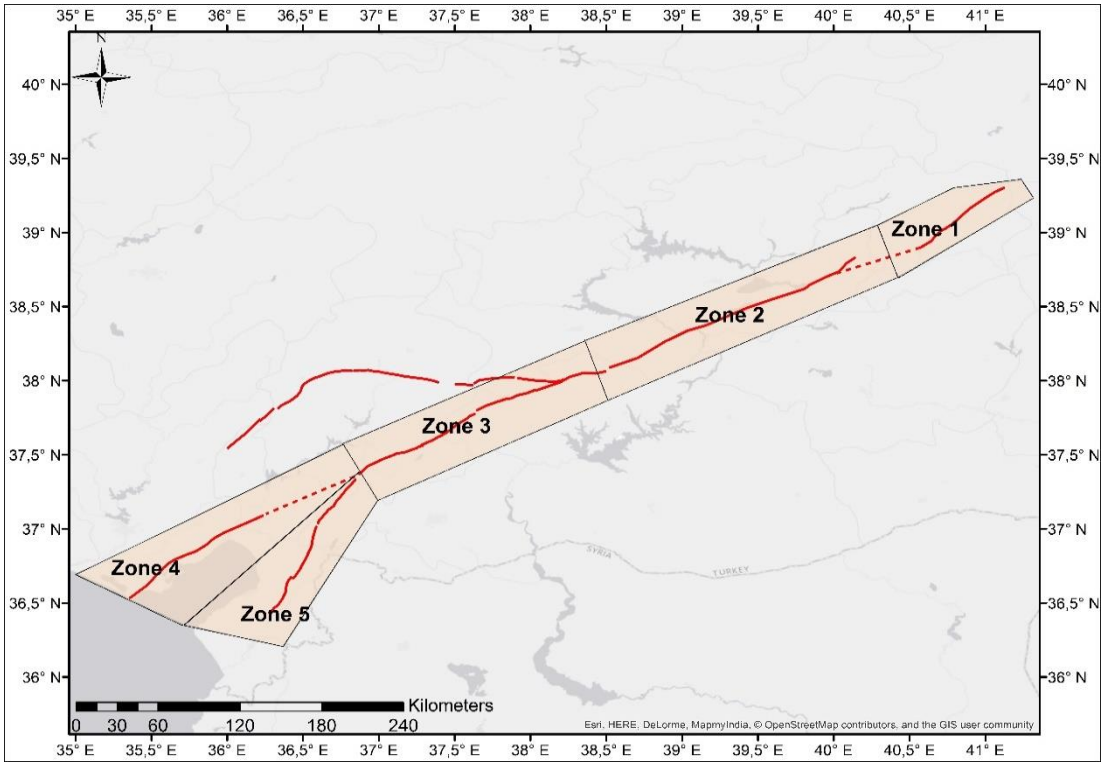


**Figure 2.20: Zones Defined Around the Rupture Systems to Calculate the b-Values**

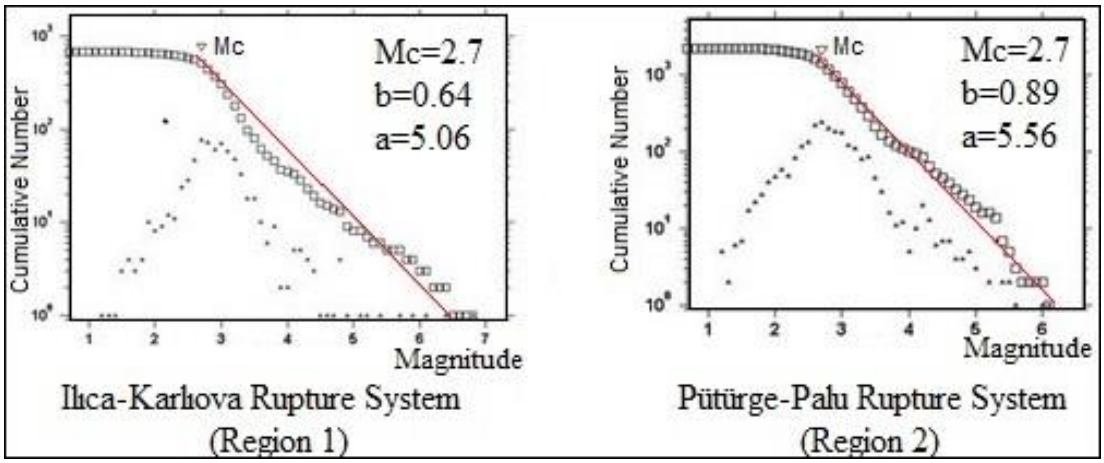


**(a)** **(b)**

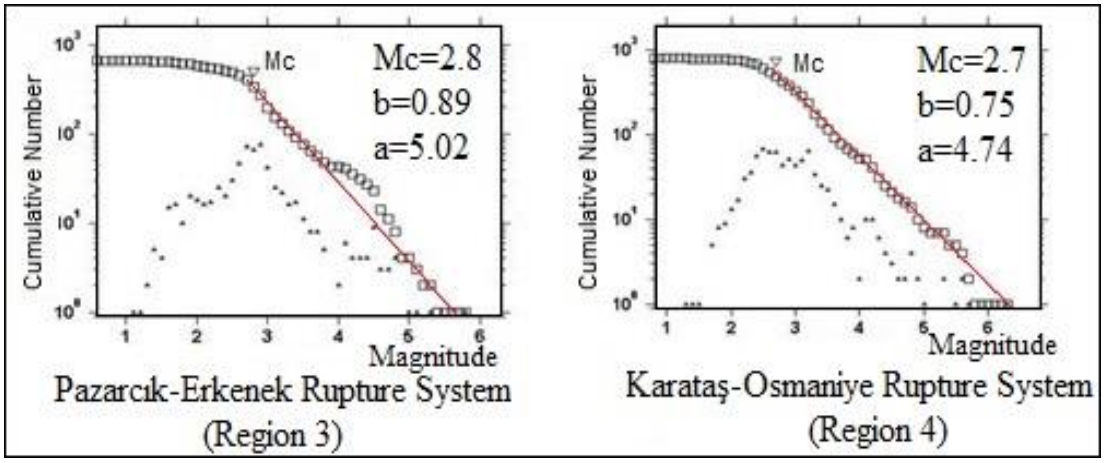


**(c)** **(d)**

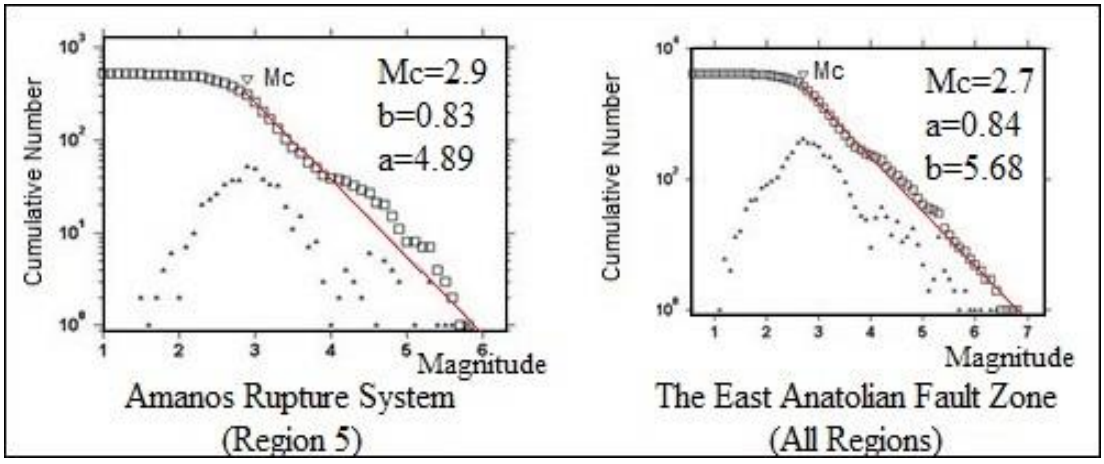


**(e)** **(f)**

**Figure 2.21: Magnitude–Cumulative Number Graphs from Gutenberg–Richter Relation for Ilıca-Karlıova, Pütürge-Palu, Pazarcık-Erkenek and Karataş-Osmaniye, Amanos Rupture Systems and the whole EAFZ**

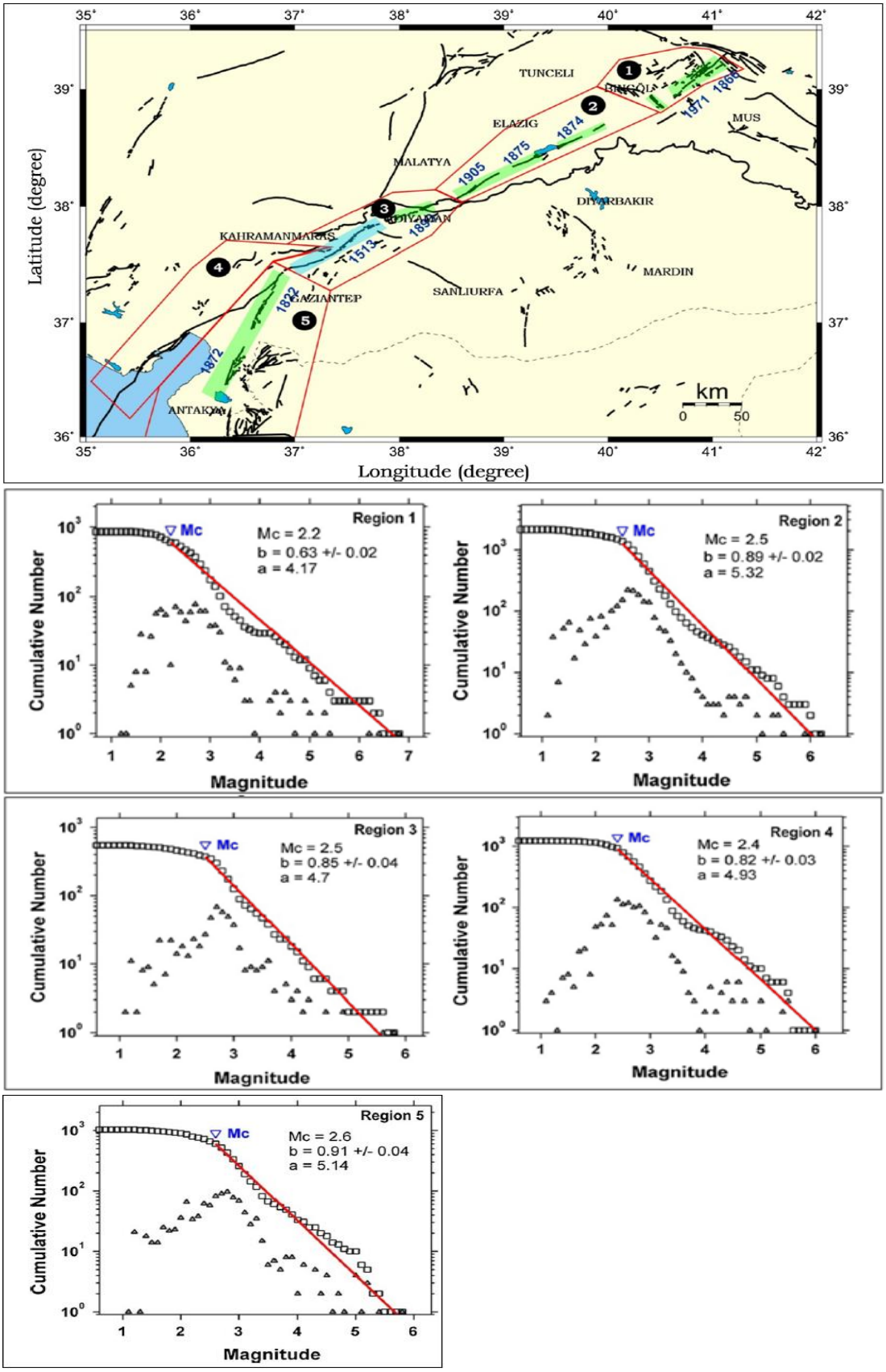


**Figure 2.22: Seismogenic Zones along the EAFZ and the Calculated b-values for Each Seismogenic Source by Bayrak et al. (2014)**

### 2.2.2 Association of Catalog Seismicity with Defined Rupture Systems

Associating the catalog seismicity with defined rupture systems might be challenging, especially when the distance between the parallel fault strands is relatively small. To perform source-to-epicenter matching, buffer zones are created around the rupture systems and the epicenters located within the buffer zone are assumed to be the earthquakes originated from that particular rupture system. The buffer zones created around Ilıca-Karlıova, Pütürge-Palu, Pazarcık-Erkenek, Karataş-Osmaniye, Amanos and Sürgü-Çardak-Savrun Rupture Systems are shown in Figures 2.4, 2.6, 2.8, 2.9, 2.13, 2.14 and 2.15 respectively. Bulut et al. (2012) stated the seismicity around the region generally follows the trend of the EAFZ along a 20 km wide stripe except for the Celikhan Area where off-fault distances of seismicity clusters are larger. We used buffer zones that are 10 km wide (5 km in each side of the fault) around Ilıca-Karlıova, Pütürge-Palu, Karataş-Osmaniye, Amanos and Savrun Rupture Systems. For Pazarcık-Erkenek Rupture System, the buffer zone is slightly widened to 12 km (6 km in each side of the fault) to be able to capture the seismicity in the region. Since the EAFZ splits into two branches at Türkoğlu and Çelikhan, small modifications are made on the buffer zones around Karataş-Osmaniye, Amanos; and Sürgü, Pazarcık-Erkenek Rupture Systems as shown in Figure 2.9 and 2.13.

### 2.2.3 Accumulated Seismic Moment and Magnitude Recurrence Models

Magnitude PDF only represents the relative rate of different magnitude events. In order to determine the absolute rate of events, the rate of events above the minimum magnitude, which is termed as the activity rate $N(M_{min})$, should be used. The activity rate of areal sources may be calculated based on the seismicity within the defined area. However in order to calculate the activity rate of fault sources, the accumulated (Equation 2.9) and released (Equation 2.10) seismic moments are balanced (Equation 2.11)

$$M_0=\mu AD \tag{2.9}$$

$$\log_{10}M_0=1.5M+16.05 \tag{2.10}$$

$$N(M_{min})=\frac{\mu AS}{\int_{M_{min}}^{M_{max}} f_m(M_w)10^{1.5M_w+16.05}dm} \tag{2.11}$$

The activity rate and the magnitude distribution are used to calculate the magnitude recurrence relation, N(M), as shown in Equation 2.12.

$$N(M) = N(M_{min}) \int_{M_{min}}^{M_{max}} f_m(M_w)\, d_M \qquad 2.12$$

### 2.2.4 Annual Slip Rate

Equations 2.9-2.12 indicate that the annual slip rate is one of the most important parameters of the magnitude recurrence model. McClusky et al. (2000) and Reilenger et al. (2006) proposed a 10 mm/yr slip rate for the northeastern part of the EAFZ (between Çelikhan and Karlıova) based on GPS measurements (Figure 2.23). This well-established value for the annual slip rate is adopted for Ilıca-Karlıova and Pütürge-Palu Rupture Systems. On the other hand, various interpretations on the annual slip rate are available for the region between Türkoğlu and Çelikhan (corresponds to the Pazarcık-Erkenek Rupture System defined in this study) in the current literature. Figure 2.23 shows the decrease in the annual slip rate associated with the EAFZ from north to the southern end of the fault zone. Meghraoui et al. (2006) and Karabacak et al. (2011) suggested the 9 mm/yr Holocene slip rate based on palaeoseismological investigations for Pazarcık-Erkenek region. Mahmoud (2012) also proposed a similar value for the annual slip rate based on GPS measurements for the east of Türkoğlu. However, Herece (2009) argued that the total slip in the region is shared by the Erkenek and Gölbaşı segments of EAFZ, the Düziçi Fault and smaller unmapped faults, and ductile deformation and/or thrusting-folding; therefore suggested a reduced slip rate of 7.9±0.3 mm/yr for these segments of EAFZ. Similarly, Duman and Emre (2013) anticipated 6.5-7.0 mm/yr slip rate for the Pazarcık and Erkenek Segments based on the comparisons of fault geometry and geodetic data. In this study, 8 mm/yr slip rate is assigned to Pazarcık-Erkenek Rupture System considering that the total slip rate is shared by the parallel Savrun Rupture System based on the interpretations of Herece (2009) and Duman and Emre (2013).

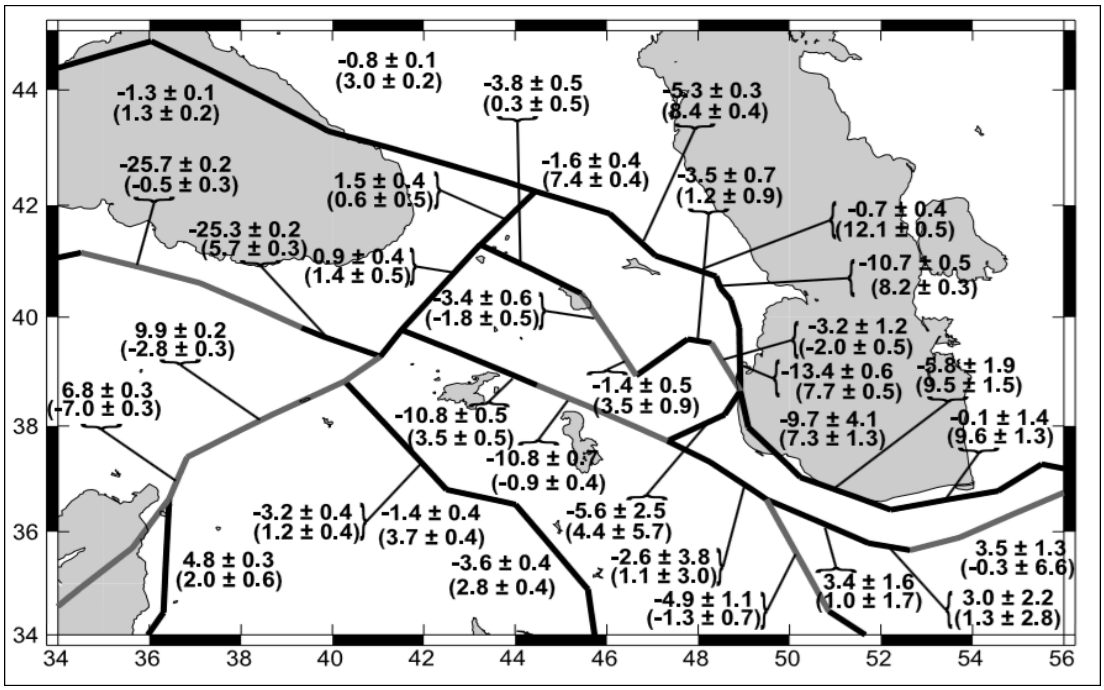


**Figure 2.23: Annual Slip Rates Based on the Block Model Proposed by Reilinger et al. (2006)**

The Karataş-Osmaniye and Amanos Rupture Systems are considered in the earthquake rupture forecast as parallel fault segments that share the total slip rate in the region. Arger et al. (1996) recorded 3.5 ± 0.5 km offsets in 0.6 ± 0.1 Ma years on Karataş-Osmaniye Rupture System, which corresponds to a slip rate of 5.8±1.5mm/yr based on potassium-argon dating technique on quaternary basalts of the region. Meghraoui et al. (2009) investigated the kinematics of Maras-Antakya Triple Junction and proposed a block model based on repeated GPS surveys between 1991 and 2004 that analyze the horizontal velocities at 22 stations located across the EAFZ the Dead Sea Fault Zone (DSFZ). Based on these measurements, 6.3±1.5 mm/yr slip rate across the Karataş-Osmaniye Fault (KOF) and 2.7±1.9 mm/yr across the Karasu Fault (KF) was suggested in the offered block model. In 2011, the authors modified the slip rates proposed in 2009 based on repeated GPS surveys with 32 (observed and predicted) GPS vectors using a simulated annealing algorithm with a downhill simplex method: the slip rate on the Karataş-Osmaniye Fault was reduced to 5.6±1.7 mm/yr and 3.8±2 mm/yr slip rate was allocated to the southern branch (where Yesemek and Amanos Faults stand) by Meghraoui et al. (2011).

In 2012, four alternative block models for the fault segments on the south of Türkoğlu juncture was proposed by Mahmoud (2012) as shown in Figure 2.24.

Except for Model A, all models predict similar slip rates for the main strand of East Anatolian Fault (9 mm/year), a value comperable with the previous estimates based on geodedic measurements and long term geological estimates. In Model A, the Karataş-Osmaniye Rupture System was neglected whereas in Model D, two microplates between KOF and KF was defined; therefore, only Models B and C are consistent with the fault model defined in this study. The fault slip rates predicted by each alternative block model proposed by Mahmoud (2012) is given in Figure 2.25.

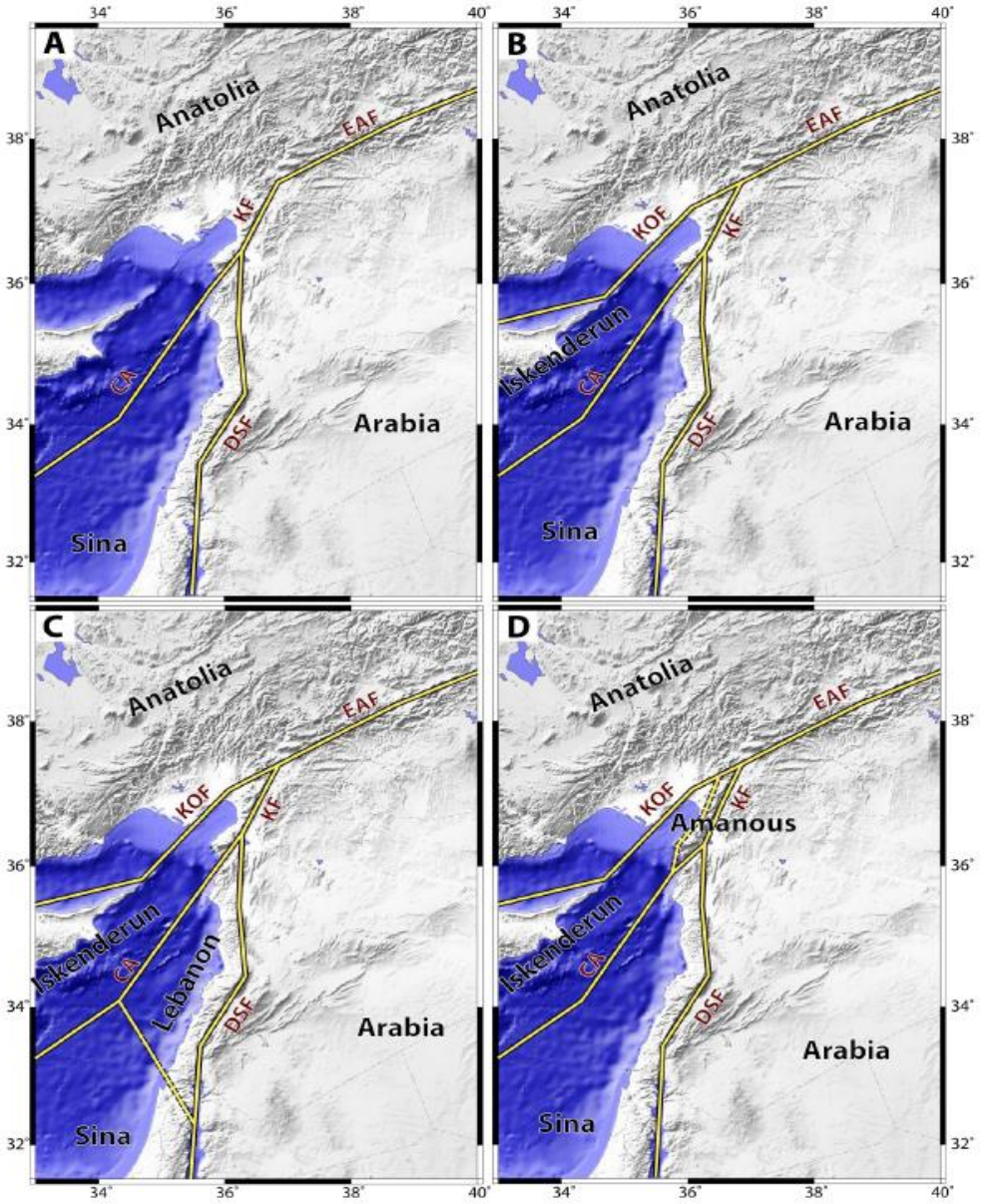


**Figure 2.24: Block models tested for the Türkoğlu Triple Junction by Mahmoud (2012)**

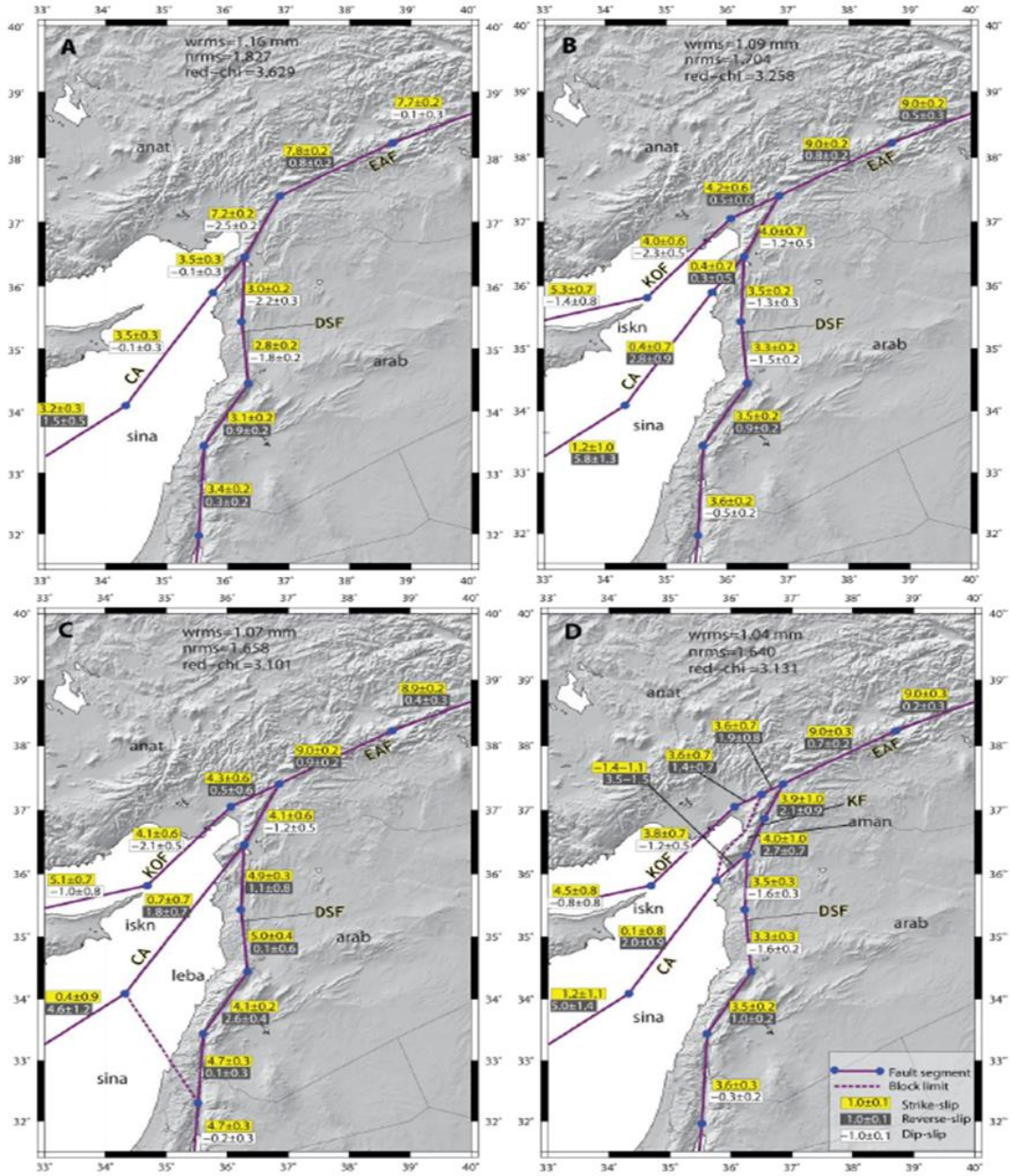


**Figure 2.25: Fault slip rates predicted by the block models prosed by Mahmoud (2012)**

According to Figure 2.25, the slip rate partitioning between KOF and KF is not significantly affected by the block defined on the south of Hatay. The annual slip rate on the Karataş-Osmaniye Rupture System was estimated as 4.2±0.6mm/yr by Model B and 4.3±0.6mm/yr by Model C. It is notable that these estimates are not really consistent with the previous annual slip rates proposed by Meghraoui et al. (2009, 2011) but close to the slip rate values proposed by Rojay (2001). Rojay et al. (2001) proposed that the Karasu Fault Zone is a linkage zone between DSFZ and EAFZ and this fault zone has a left lateral slip rate of 4.1 mm/yr based on the calculations from

displaced lavas. On the other hand, Seyrek et al. (2007) suggested a 2.8 mm/yr slip rate for Amanos Fault based on radiometric dating study on quaternary volcanism and the slip rate of 2.68 mm/yr was given for the Yesemek Fault based on a measurement of 10 km offset of ophiolites from the southern section of the fault by Westeway (2003). Bertrand et al. (2006) suggested 1.5 to 2.3 mm/yr slip rate for Amanos Fault based on GPS studies. In the light of above discussions; 2.1 mm/yr slip rate is assigned for Amanos Fault and 5.9 mm/yr slip rate is assigned for Karataş-Osmaniye Fault considering the total slip rate of 8mm/yr for the east of Türkoğlu along the main strand of the EAFZ. The impact of this assumption on the proposed hazard maps is thoroughly discussed in the last Chapter.

### 2.2.5 Balancing the Accumulated Seismic Moment by Released Seismic Moment

The magnitude probability density function and model parameters (b-value or maximum magnitude) shall be tested before implementing them in a PSHA study (Gülerce and Vakilinezhad, 2015). A weight is given to each rupture scenario and the cumulative rates of events related with that particular rupture system are plotted along with the weighted average of the rupture scenarios to balance the assigned weights and to evaluate the balance of the accumulated and released seismic moment. The "*moment-balancing*" graphs for Ilıca-Karlıova (Ilıca-Karlıova-Gökdere), Pütürge-Palu, Pazarcık-Erkenek, Karataş-Osmaniye, Amanos, Sürgü, Çardak, and Savrun Rupture Systems are provided in Figures 2.26-2.33, respectively. In these plots, the black dots represent the cumulative annual rates of earthquakes and the error bars stand for the uncertainty due to unequal periods of observation for various magnitudes (Weichert, 1980). The best fit between the cumulative annual rate of events and the weighted average of rupture scenarios (red broken lines) is established by modifying the weights of the rupture scenarios.

In Figures 2.26-2.33, the scenarios that are separated by plus signs in the legend are the scenarios with multiple rupture sources. When multiple segments rupture together, these scenarios are separated by a comma sign in the legend. For example, the I+K line in Figure 2.26(a) represents the scenario where Ilıca and Karlıova segments are ruptured individually. This scenario brings in relatively higher rates for small-to-moderate earthquakes when compared to the I,K scenario which represents the rupture of these two segments together to produce a larger event. In each "*moment balancing*" plot, relatively higher weights are assigned to the rupture

scenarios that combine the individual (single-segment) rupture sources based on the assumption that single-segment ruptures are more likely than multiple-segment ruptures. The weights assigned to each rupture scenario are shown in parenthesis in Figures 2.26-2.33 and these values are adopted in the logic tree. Please note that none of the scenarios are discarded by assigning an insignificant (or zero) weight in the moment-balancing procedure. For some rupture systems, such as the Pütürge-Palu Rupture System shown in Figure 2.27, number of associated events is large enough to constrain the scenario weights assigned to each scenario. For Amanos and Savrun Rupture Systems, the number of associated earthquakes is very small, indicating that the assigned scenarios weights are not statistically stable. For these rupture systems, extreme combinations of scenario-weights are avoided. It is notable that for all rupture systems, the rate of large-magnitude events is overestimated by the proposed recurrence models (within the limits of the error bands in positive side). Since the catalogue used in this study is limited to the time range of 1900-2010 and all large magnitude events on EAFZ was occurred before that time span, this overestimation is misleading. Proposed recurrence model would be better-constrained in the large magnitude range if these historical earthquakes were included.

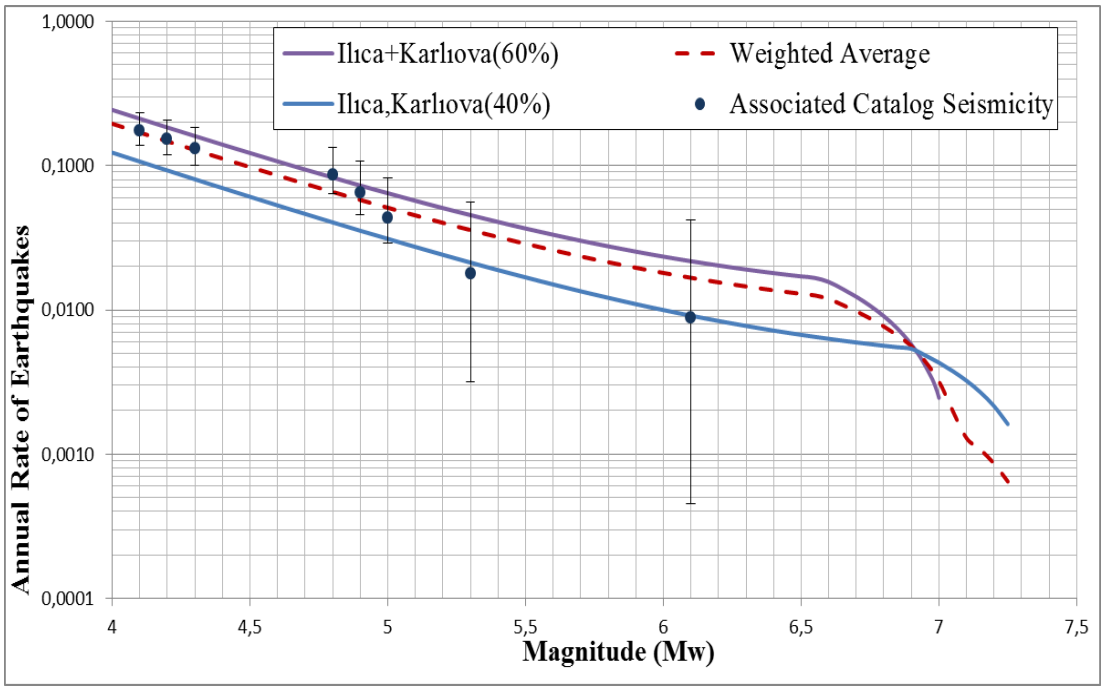


**(a)**

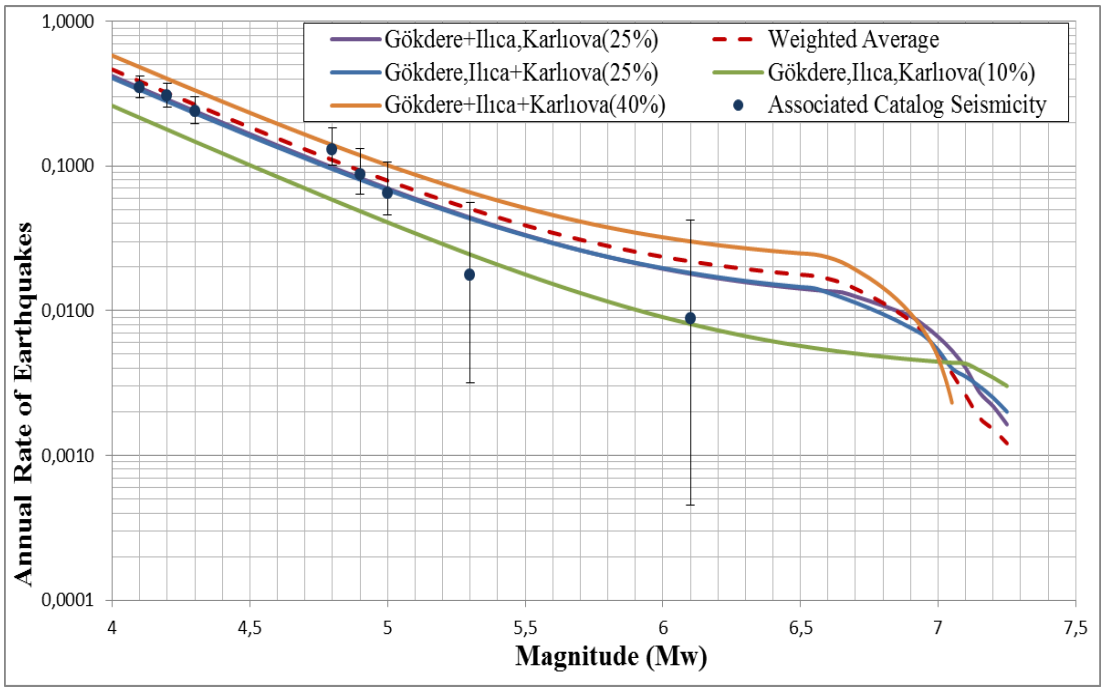


**(b)**

**Figure 2.26: (a) Cumulative Rates of Catalog Events for Ilıca-Karlıova Rupture System and Proposed Magnitude Recurrence Model, (b) Cumulative Rates of Catalog Events for Ilıca-Karlıova-Gokdere Rupture System and Proposed Magnitude Recurrence Model**

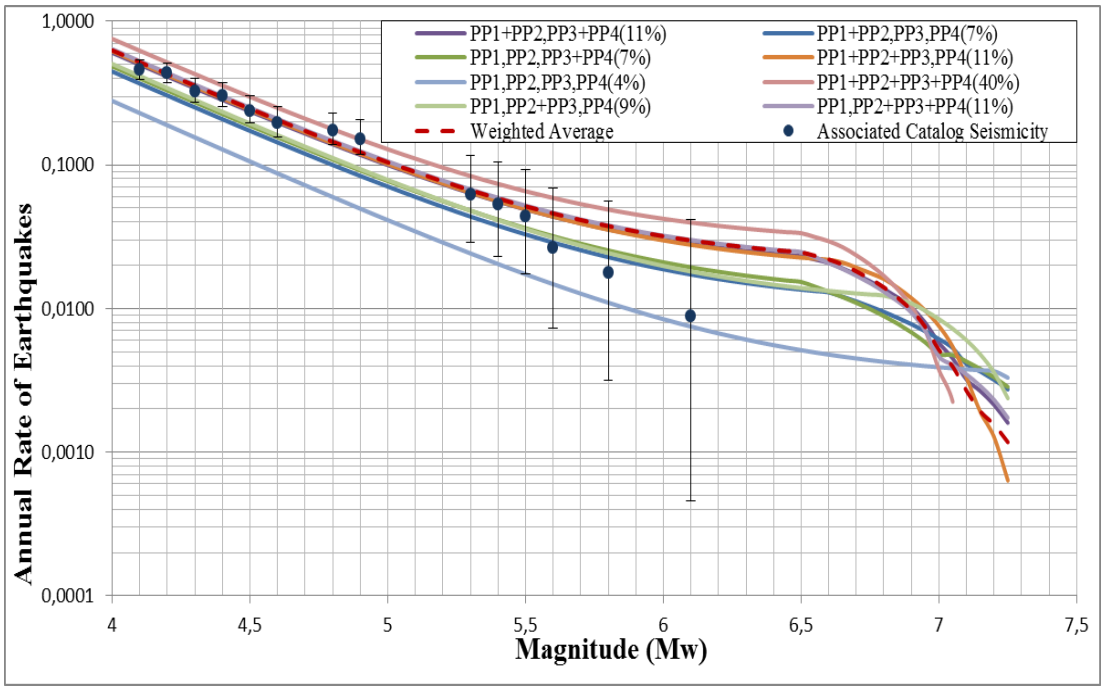


**Figure 2.27: Cumulative Rates of Catalog Events for Pütürge-Palu Rupture System and Proposed Magnitude Recurrence Model**

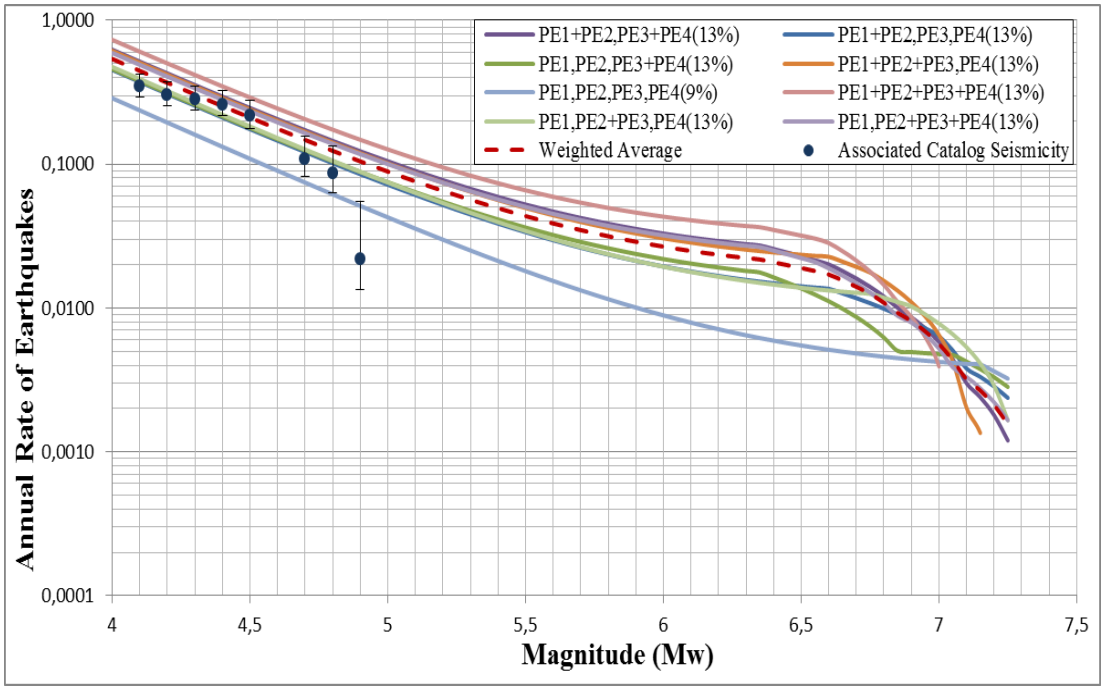


**Figure 2.28: Cumulative Rates of Catalog Events for Pazarcık-Erkenek Rupture System and Proposed Magnitude Recurrence Model**

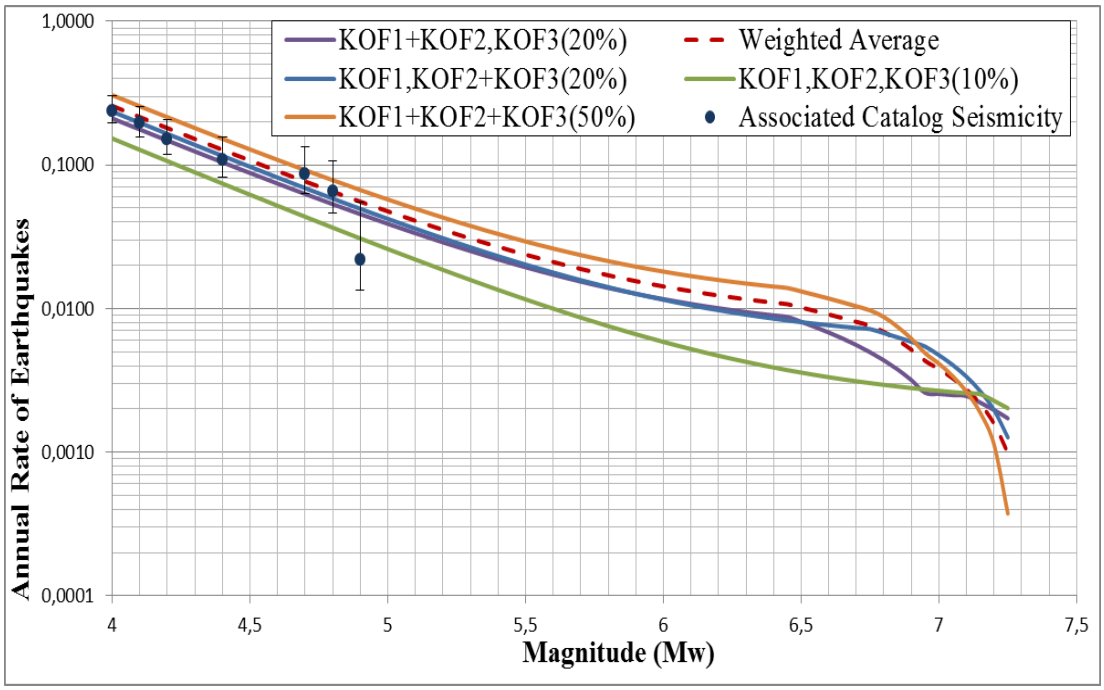


**Figure 2.29: Cumulative Rates of Catalog Events for Karataş-Osmaniye Rupture System (KOF) and Proposed Magnitude Recurrence Model**

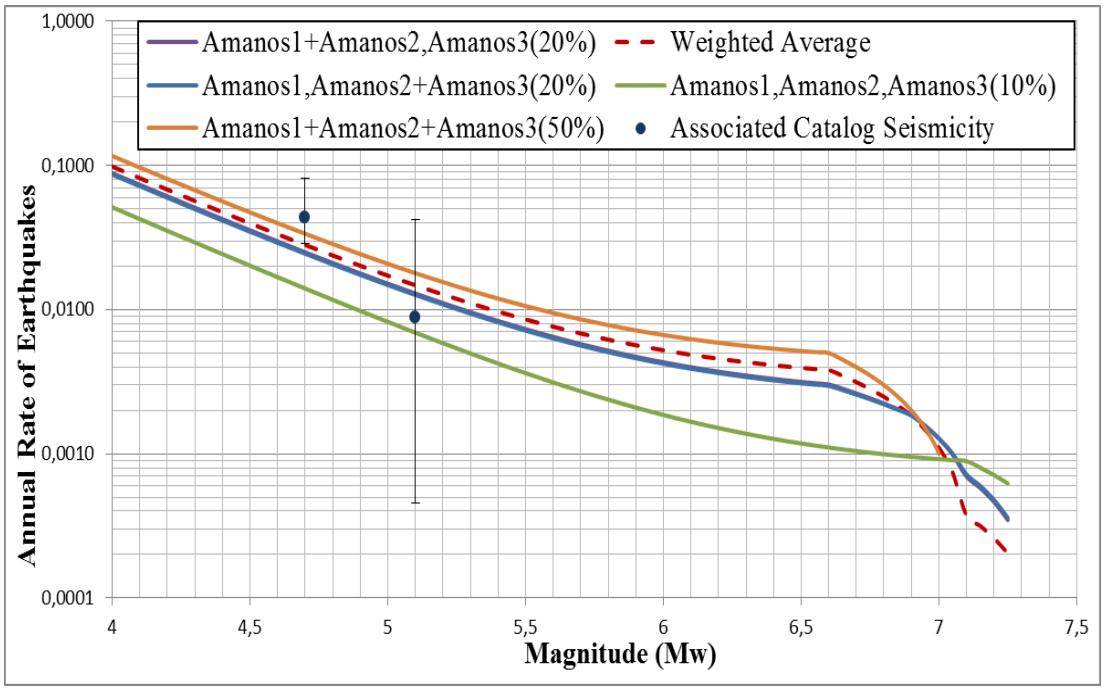


**Figure 2.30: Cumulative Rates of Catalog Events for Amanos Rupture System and Proposed Magnitude Recurrence Model**

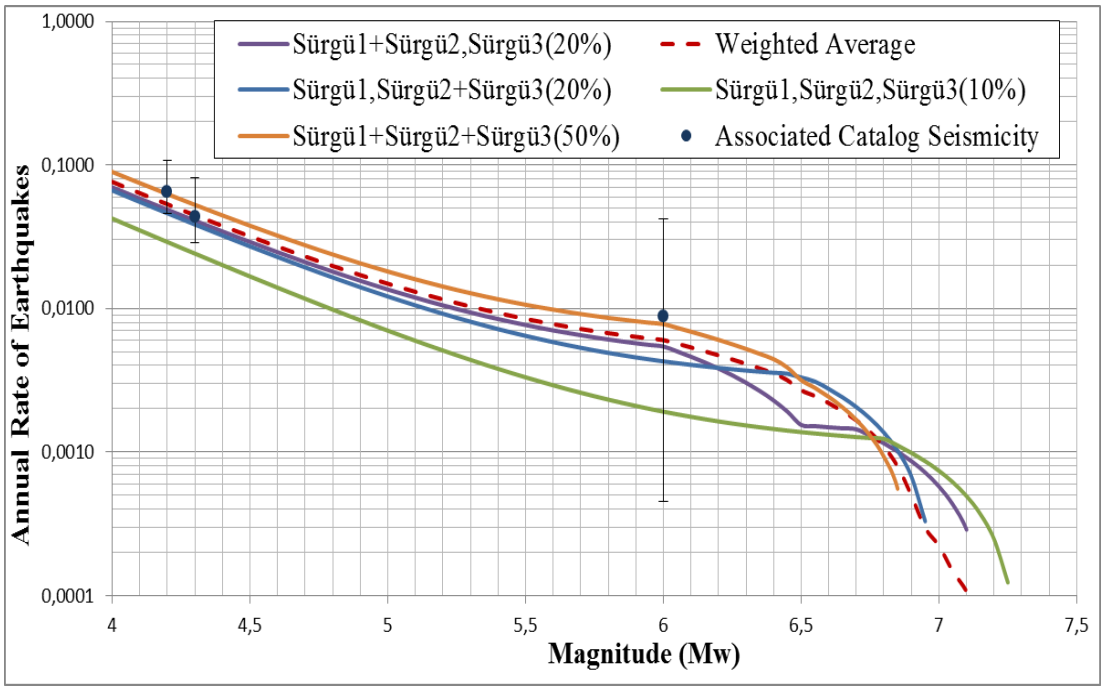


**Figure 2.31: Cumulative Rates of Catalog Events for Sürgü Rupture System and Proposed Magnitude Recurrence Model**

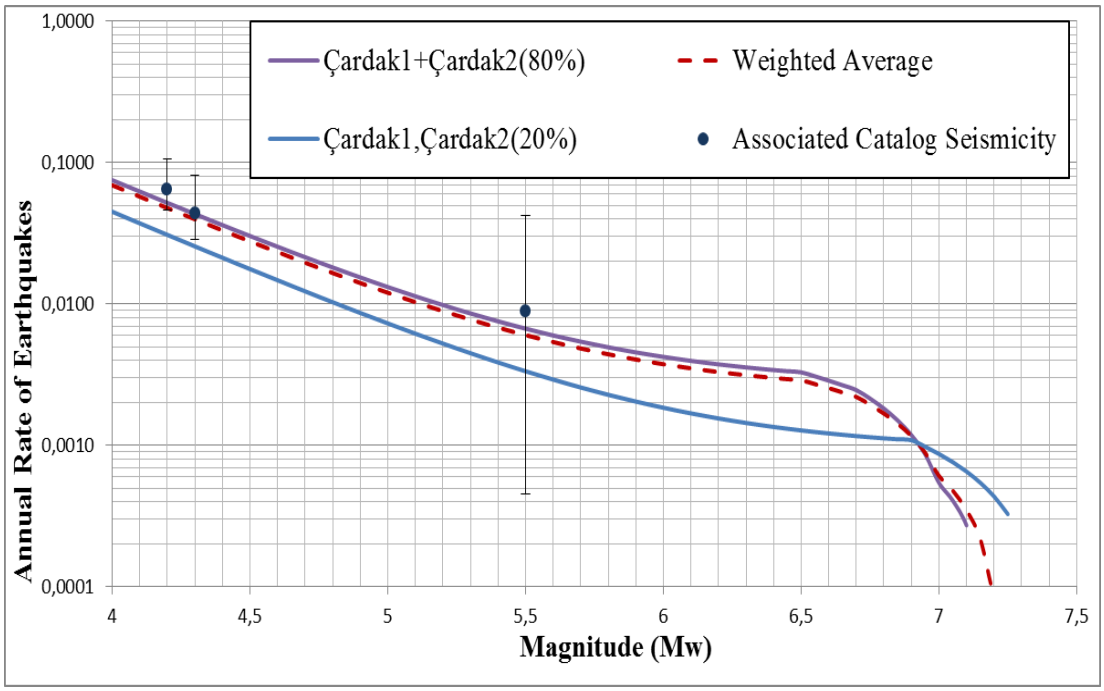


**Figure 2.32: Cumulative Rates of Catalog Events for Çardak Rupture System and Proposed Magnitude Recurrence Model**

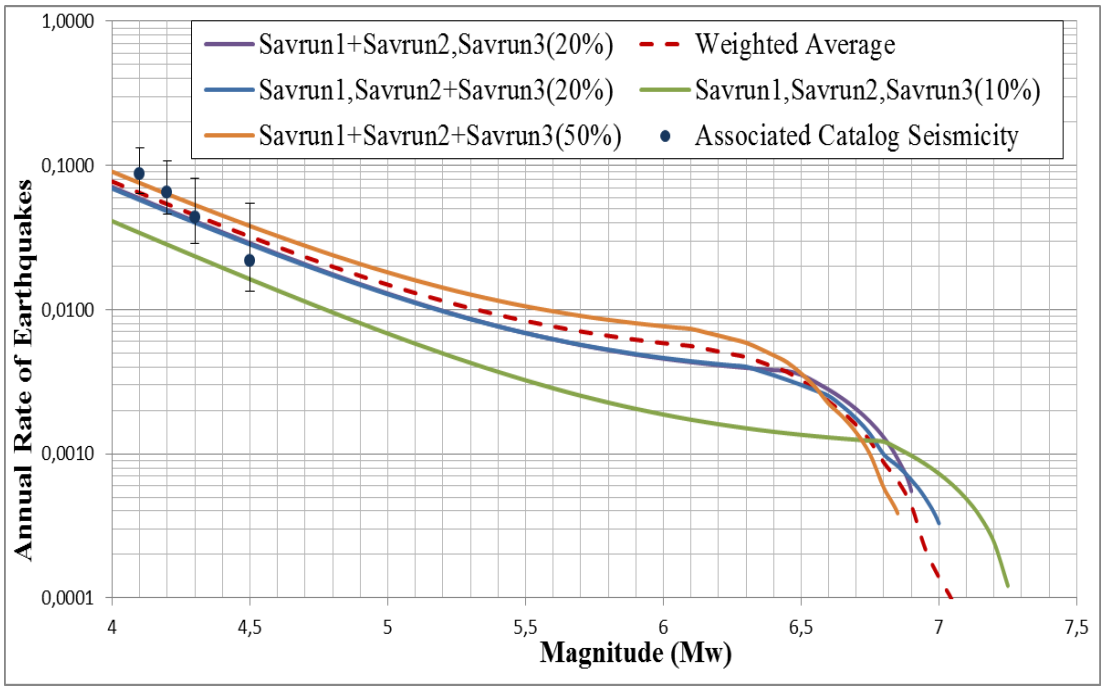


**Figure 2.33: Cumulative Rates of Catalog Events for Savrun Rupture System and Proposed Magnitude Recurrence Model**

# CHAPTER 3

# GROUND MOTION CHARACTERIZATION

Attenuation Relations or Ground Motion Prediction Equations (GMPEs) are used for the prediction of strong ground motion parameters and associated uncertainty based on the parameters such as magnitude, source-to-site distance, local soil conditions, fault mechanism, etc. GMPEs are widely used in both probabilistic and deterministic seismic hazard analysis as well as in many earthquake engineering applications like seismic analysis and design of structures, social and financial loss estimation, development of regional seismic hazard maps for use in building codes etc. In the last two decades, many global and local GMPEs have been developed as a result of enlarging, regional and global ground motion databases. The decision of which model to employ is a critical step in a PSHA study because the resulting design ground motions are strongly dependent on the chosen GMPEs. Local models are derived based on regional databases and they are more likely to reflect the regional tectonic characteristics compared to the global models. On the other hand, local GMPEs have smaller (and less stable) databases and generally do not extrapolate well to larger magnitude events. Also because of their limited databases, local GMPEs may not provide realistic constraints on some important features such as short distance scaling, style of faulting, and hanging wall effects (Gülerce et al., 2015). According to Bommer et al. (2010), local models may not give very precise results while adding larger uncertainty due to the problems related with the extrapolation of magnitude scaling determined from smaller events. On the other hand, global GMPEs have larger well compiled strong ground motion database which decrease the epistemic uncertainty in the models. However, global GMPEs do not reflect regional characteristics as well as local models and their applicability should be evaluated before implementing them in the PSHA study.

## 3.1 Regionalization of Global GMPEs

The Pacific Earthquake Engineering Research Center (PEER) launched an extensive research program in 2003 to develop state-of-the-art GMPEs for shallow crustal

earthquakes in active tectonic regions. In 2008, the research project ended up with a comprehensive database of strong ground motions recorded worldwide and a set of peer-reviewed GMPEs (NGA-West1 models) were published for horizontal ground motion component (Power et al., 2008). Slowly, NGA-West1 models have been used in PSHA studies in various regions, raising the issue of their applicability outside California. Recent studies by Stafford et al. (2008), Scasserra et al. (2009), Shoja-Taheri et al. (2010), and Bradley (2013) tested the applicability of the NGA-West1 GMPEs for Euro-Mediterranean Region, Italy, Iran, and New Zealand. Scasserra et al. (2009) have taken a further attempt and modified the distance scaling of the NGA-West1 GMPEs by re-regressing the model coefficients related to the distance attenuation and the constant term for PGA, 0.2, 0.5, 1 and 2 second spectral periods. Bradley (2013) found that the Chiou and Youngs (2008) model performed better than the other NGA-West1 models in capturing the difference between small magnitude scaling of the NGA-West1 and New Zealand datasets, especially after the small magnitude model proposed by Chiou et al. (2010) was included. However, several other features of the Chiou and Youngs (2008) GMPE had to be adjusted for New Zealand and coefficients of the modified model were provided by Bradley (2013).

### 3.1.1 TR-Adjusted NGA-West1 Models

Gülerce et al. (2015) performed a comprehensive study to evaluate the compatibility of the NGA-West1 GMPEs in terms of magnitude, distance and site effects scaling with respect to the Turkish strong ground motions. The authors systematically modified the incompatibilities between the NGA-West1 GMPEs and Turkish strong motion dataset and recommended a new set of Turkey-specific versions of the NGA-West1 GMPEs, the TR-Adjusted NGA-West1 GMPEs. Since the details of the TR-adjusted NGA-West1 models are discussed in Gülerce et al. (2015), only a brief summary is provided below:

- The Turkish strong motion dataset used by Gülerce et al. (2015) includes 1142 recordings from 288 events with the earthquake metadata, source-to-site distance metrics for the recordings, $V_{S30}$ values for the recording stations, and horizontal component spectral values in terms of GMRotI50 (Boore et al., 2006) for 23 spectral periods between 0.01 and 10 seconds.

- By using random-effects regression with a constant term, model residuals between the actual strong motion data and global model predictions are calculated for a period range of 0.01-10 seconds.
- From residual plots, the differences in the magnitude, distance, and site amplification scaling between the Turkish dataset and the NGA-West1 models are evaluated.
- Inter-event residuals indicated that the ground motions in the dataset are overestimated by all 5 NGA-West1 models. In order to preserve the well-constrained large magnitude scaling of the global dataset, only small-to-moderate magnitude scaling of the NGA-West1 GMPEs is modified.
- The distance scaling of the NGA-West1 models is not adjusted because no trend is observed in the intra-event residuals vs. rupture distance plots up to 100 kilometers. AS08 (Abrahamson and Silva, 2008) and CY08 (Chiou and Youngs, 2008) models with separate gamma terms are modified for the distances between 100 and 200 km.
- An adjustment function is fitted for $V_{S30}$ scaling in AS08 and CY08 models in order to modify overestimation at the stiff soil/engineering rock sites.

Turkey adjusted NGA models are compatible with the regional strong ground motion characteristics and preserve the well constrained feature of the global NGA models; therefore, they are suitable for ground motion characterization studies in Turkey (Gülerce et al., 2015). Gülerce et al. (2015) pointed out that the mean bias in the median predictions of TR-ID08 model (TR-adjusted version of the Idriss, 2008 model) remains for the long periods even after the adjustment; therefore, the TR-adjusted version of the ID08 model is excluded and all other TR-adjusted NGA-West1 models are included in the GMPE logic tree in this study.

### 3.2 NGA-West2 Ground Motion Prediction Models

Some important issues in the GMPE performance and supporting research projects were not addressed in the course of NGA-West1 project; therefore, NGA-West 2 project was launched in 2011 to update NGA-West1 project. The new project mainly targeted to: 1) expand the NGA-West1 database for small, moderate, and large-magnitude events; 2) revise the NGA-West1 GMPEs for the horizontal component of ground motion and develop new GMPEs for the vertical ground motion data; 3)

develop damping models to scale response spectra predicted by GMPEs to damping values different from the reference value; 4) evaluate directivity models and their effects on horizontal ground motion and directionality of horizontal ground motion. The GMPE developers of NGA-West2 research project are Abrahamson, Silva, and Kamai (ASK14 model); Boore, Stewart, Seyhan, and Atkinson (BSSA14 model); Campbell and Bozorgnia (CB14 model); Chiou and Youngs (CY14 model) and Idriss (I14 model). Within this project, the database has expanded to 21,332 (10,706 recordings associated with events with $3.0 \leq M_w \leq 4.5$) recordings with mainly three component-recordings. This new database has events with magnitude ranging from $M_w$=3 to $M_w$=7.9 and recordings with distance ranging from 0.05 km to 533 km. The applicable ranges for the ASK14, BSSA14, CB14 and CY14 models in terms of distance, magnitude, shear wave velocity and spectral periods are listed in Table 3.1.

**Table 3.1 Model Applicability Range of the Four NGA-West 2 GMPEs for Magnitude, Distance, Vs30, and Spectral Period**

| **NGA-West2 Model** | ASK14 | BSSA14 | CB14 | CY14 |
|---|---|---|---|---|
| Magnitude (Mw) | 3.8-8.5 | 3.0-8.5 (SS,RV) | 3.3-8.5 (SS) | 3.5-8.5 (SS) |
| (Mecahnism) | (All) | 3.3-7 (NM) | 3.3-8.0 (RV) 3.3-7.0 (NM) | 3.5-8.0 (RV,NM) |
| Distance (km) | 0-300 | 0-400 | 0-300 | 0-300 |
| $Vs_{30}$(m/s) | 180-1500 | 150-1500 | 150-1500 | 180-1500 |
| Period Range | PGA-10sec PGV | PGA-10sec PGV | PGA-10sec PGV | PGA-10sec |

It has been recognized that the NGA-West1 GMPEs lead to an over-prediction of ground motions from small to moderate events (Chiou et al. 2010, Atkinson and Boore 2011, Campbell 2011). Based on the new and large database, the magnitude scaling of NGA-West 2 models were changed to account for this over-prediction problem for small to moderate magnitude earthquakes. According to Gülerce et al. (2015), magnitude scaling of the NGA-West 2 and TR-adjusted NGA-West1 models is very similar for CB14 and CY14 models with more flexible functional forms, except for the small difference in 5<M<6.75 range. For smaller magnitudes (M<4),

predictions of NGA-West 2 models and TR-Adjusted NGA-West1 models are similar. The updated model by Idriss (2014, ID14) has approximately the same magnitude scaling with the previous version (ID08) and both models are significantly different than the TR-adjusted version. Therefore, NGA-West 2 model proposed by Idriss (2014) is excluded from the candidate GMPE list.

ASK14, BSSA14, CB14, and CY14 models acknowledged the regional differences in large distance scaling; however, regional terms were developed for regions like Taiwan, Japan, China and Italy with significant amount of data in the NGA-West 2 database. The number of Turkish recordings in the NGA-West 2 database is sparse (only 55 recordings); therefore, individual anelastic attenuation terms are not provided for the Turkey. BSSA14 model combined the recordings from Turkey with the recordings from China (defined as 'high Q' regions) and provided a China-Turkey modification on their $c_3$ term. In ASK14 model, Turkish recordings were grouped with ground motions from Iran under the "Middle East" subgroup; however, separate anelastic attenuation or site amplification coefficients are not provided for Middle East region after the evaluations. Similarly, CB14 and CY14 models did not find a difference between the large distance scaling of California and Turkish ground motions. Findings of Gülerce et al. (2015) support the findings of NGA-West 2 project: the distance scaling of the Turkish dataset is not significantly different than the distance scaling of NGA-West1 and West 2 models.

The suite of the NGA-West 2 models was found to provide median ground-motion predictions that agree to within factors of about 1.5 to 2. The biggest differences are realized for the cases in which the NGA-West 2 database is inadequate, such as for large earthquakes (Mw=8) at close distances, and for hanging-wall sites located over the rupture plane of shallow dipping earthquakes. Therefore, ASK14, BSSA14, CB14 and CY14 models are included in the GMPE logic tree to properly represent the epistemic uncertainty. A brief summary for each model is provided below.

### 3.2.1 Abrahamson et al., 2014 (ASK14) Model

ASK14 model is an update to the Abrahamson and Silva, 2008 (AS08) model based on the NGA-West 2 database (Ancheta et al. 2014). The input parameters of the model are the same as the parameters used by AS08 model; however, following modifications are included in the new model: the loading level for non-linear site effects is based on the spectral acceleration at the period of interest rather than the

PGA; the distance scaling for hanging wall (HW) effects includes a dependence on the source to-site azimuth; regional differences in large-distance attenuation and site amplification scaling between California, China, Japan and Taiwan are incorporated; the scaling for the hanging wall effect is developed based on constraints from numerical simulations; the standard deviation is magnitude-dependent with smaller magnitudes resulting larger standard deviations at short periods, but smaller standard deviations at long periods and different from the old model, small magnitude events (Mw=3) are included in the updated model. The functional form of ASK14 model is given in Equation 3.1 as;

$$\ln Sa(g)=f_1(M,R_{rup})+F_{RV}\,f_7(M)+F_N f_8(M)+F_{As} f_{11}(CR_{jb})+f_5(\hat{S}a_{1180},V_{S30}) + F_{HW} f_4(R_{jb},R_{rup},R_X,W,dip,Z_{TOR},M) +f_6(Z_{TOR})+f_{10}(Z_{1.0},V_{S30})+Reg(V_{S30},R_{rup}) \quad 3.1$$

where $f_1$ is the basic form of the magnitude and distance dependence for strike slip earthquakes, $f_7$ and $f_8$ are functions for style of faulting model, $f_{11}$ is aftershock scaling function, $f_5$ is the site response model using median spectral acceleration on hard rock, $f_4$ is hanging wall model, $f_6$ is depth to top of rupture model, $f_{10}$ is the soil depth model. Regionalization of $V_{S30}$ is also included in this model.

### 3.2.2 Boore et al., 2014 (BSSA14) Model

The new and improved BSSA14 model is provided as an update for Boore and Atkinson, 2008 (BA08) model to compute medians and standard deviations of average horizontal component of recorded ground motion amplitudes for shallow crustal earthquakes in active tectonic regions. Regional variability in source, path and site effects is considered, however the model does not address directivity effects. The functional form of the BSSA14 model is given in Equation 3.2 as:

$$\ln Y=F_E(M, \textit{mech})+F_P(R_{jb},M, \textit{region})+F_S(V_{S30},R_{jb},M,\textit{region},z1)+\varepsilon_n\sigma(M,R_{jb},V_{s30}) \quad 3.2$$

where Y represents the natural logarithm of a ground motion, $F_E$ is the source function, $F_P$ is the function related with path and $F_S$ is the site effect function, $\varepsilon_n$ is the fractional number of standard deviations of a single predicted value of lnY, $\sigma$ is the standard deviation; M, *mech* and $R_{jb}$ are the predictor variables.

### 3.2.3 Campbell and Bozorgnia, 2014 (CB14) Model

CB14 model is developed after Campbell and Bozorgnia, 2008 (CB08) model for estimating horizontal ground motion from shallow crustal continental earthquakes in active tectonic regions. This new model brings in the modifications for hanging wall effects over the rupture plane, improvements in small-magnitude and far-source estimates, and increase in inter-event variability for Mw > 5.5 due to the inclusion of earthquakes from additional active tectonic regions. Based on the large database of NGA-West 2, this model presents better constraints on magnitude scaling and attenuation of small magnitude events. The general form of the equation is given below as;

$$\begin{aligned} &\ln Y = \ln PGA && PSA<PGA \text{ and } T<0.25 \text{ s} \\ &\ln Y = f_{mag}+f_{dis}+f_{flt}+f_{hng}+f_{site}+f_{sed}+f_{hyp}+f_{dip}+f_{atn} && \text{otherwise} \end{aligned} \quad 3.3$$

where $f_{mag}$ is the magnitude term; $f_{dist}$ is the geometric attenuation term; $f_{flt}$ is the style of faulting term; $f_{hng}$ is the hanging wall term; $f_{site}$ is the shallow site response term; $f_{sed}$ is the basin response term; $f_{dip}$ is the fault dip term; $f_{hyp}$ is the hypocentral depth term; $f_{dip}$ is the fault dip term and $f_{atn}$ represents the anelastic attenuation term.

### 3.2.4 Chiou and Youngs, 2014 (CY14) Model

CY14 model is presented as an update model for Chiou and Youngs, 2008 (CY08) model to predict horizontal ground motion amplitudes caused by shallow crustal earthquakes occurring in active tectonic regions. The median ground-motion values predicted by CY14 model are similar with older model for magnitudes Mw>7, however the results are lower for magnitudes Mw< 5. The new CY14 model includes minor adjustments to CY08 form related to style of faulting effects, hanging wall function, scaling with the depth to top of rupture, scaling with sediment thickness, and the inclusion of additional terms for the effects of fault dip and rupture directivity. In addition, regional differences in far source (80 km < $R_{RUP}$ ≤ 500 km) distance attenuation and site effects between California and other active tectonic regions are included.

## 3.3 Comparison of the Hazard Curves for Selected GMPE Models

Selected TR-Adjusted NGA-West1 and NGA-West 2 models were implemented individually to quantify the effect of each model on the hazard outcome. The study was performed for two example sites with $R_{Rup}$=5km and $R_{Rup}$=15km and assuming

$V_{S30}$=450 m/s; 760m/s and 1100 m/s for the spectral periods of 0.01 s and 2.5s. For these analyses, all seismic sources defined in Chapter 2 with the full SSC logic tree were incorporated. The hazard curves for each individual GMPE is presented in Figures 3.1, 3.2 and 3.3 and following interpretations can be made based on these figures:

- In general, the PGA estimations of TR-Adjusted NGA-West1 models are slightly lower than the estimations of NGA-West 2 models. This result is expected since the magnitude scaling of the TR-Adjusted NGA-West1 models (in average) is smaller than the NGA-West 2 models (in average).
- Effect of the selected GMPE decreases as the distance from the source increases. The maximum difference between the estimated PGA values using different models is about 0.12g for $R_{rup}$=15 km case and 0.24g for $R_{rup}$=5 km case for the annual rate of exceedance level of 0.0021 (2% chance of exceeding in 50 years).
- For the annual rate of exceedance level of 0.001, the maximum difference between the models increases up to 0.14g for $R_{rup}$=15 km case and 0.28g for $R_{rup}$=5 km case. For smaller annual rate of exceedance levels (e.g. 0.01), the maximum difference between the models becomes insignificant, especially when the source to site distance increases.
- For $V_{S30}$=450m/s and T=2.5s spectral accelerations, TR_Adj_AS08 and ASK14 models' estimates are slightly lower than other models for $R_{Rup}$=5 km case.
- TR_Adj_AS08 model provides slightly lower PGA values and CB14 model estimates slightly higher GA values than other models for $V_{S30}$=1100 m/s and $R_{rup}$=15 km case. On the other hand, ASK14 model estimates are larger than other models for T=2.5 s.

Since there are no systematic differences between the hazard estimates of selected models in the high frequency and low frequency ranges, TR-adjusted NGA-West1 models (TR_Adj_AS08, TR_Adj_BA08, TR_Adj_CB08, TR_Adj_CY08) and four global NGA-West 2 models (ASK14, BSSA14, CB14, and CY14) were included into GMPE logic tree with equal weights (50 % weight is assigned to global and regionalized models (12.5 % each)).

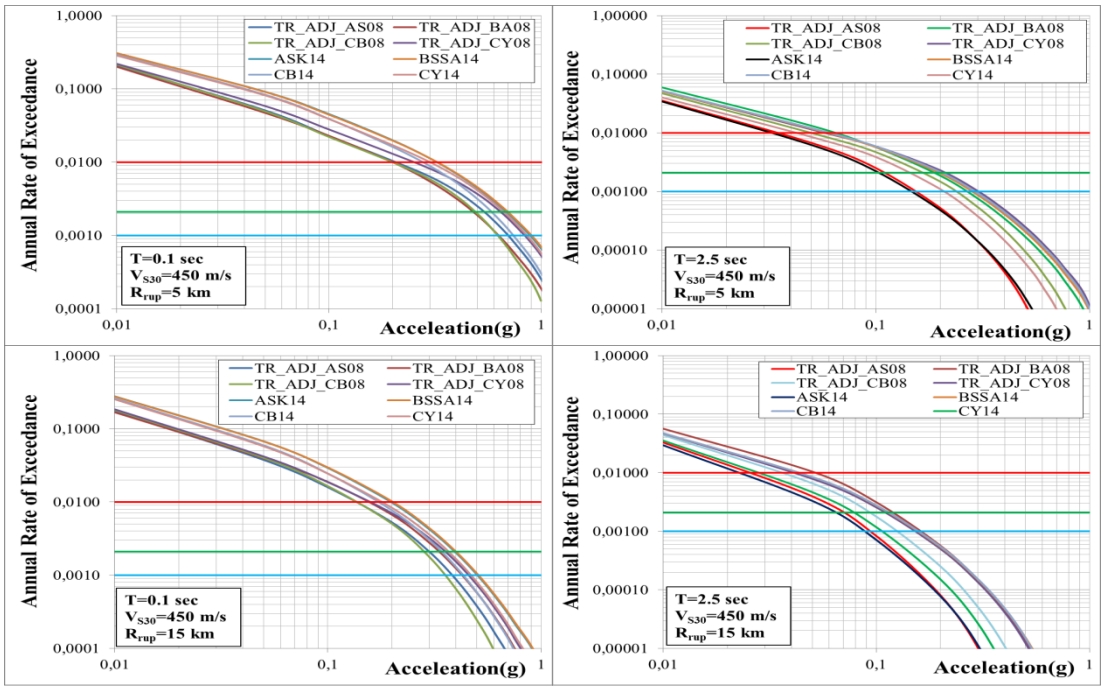


**Figure 3.1: Hazard Curves for T=0.01s and T=2.5s; using TR-Adjusted NGA-W1 models and NGA-West2 models (Vs30=450 m/s; Rrup=5 km and Rrup=15 km)**

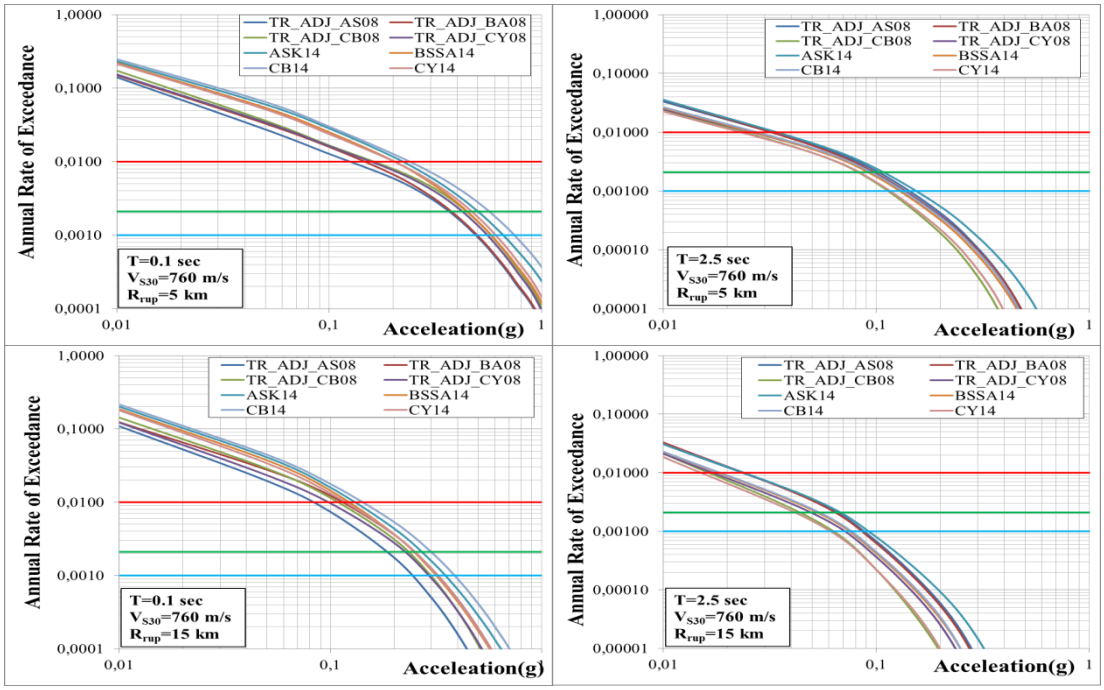


**Figure 3.2: Hazard Curves for T=0.01s and T=2.5s; using TR_Adj_NGA Models and NGA_West2 Models (Vs30=760 m/s; Rrup=5 km and Rrup=15 km)**

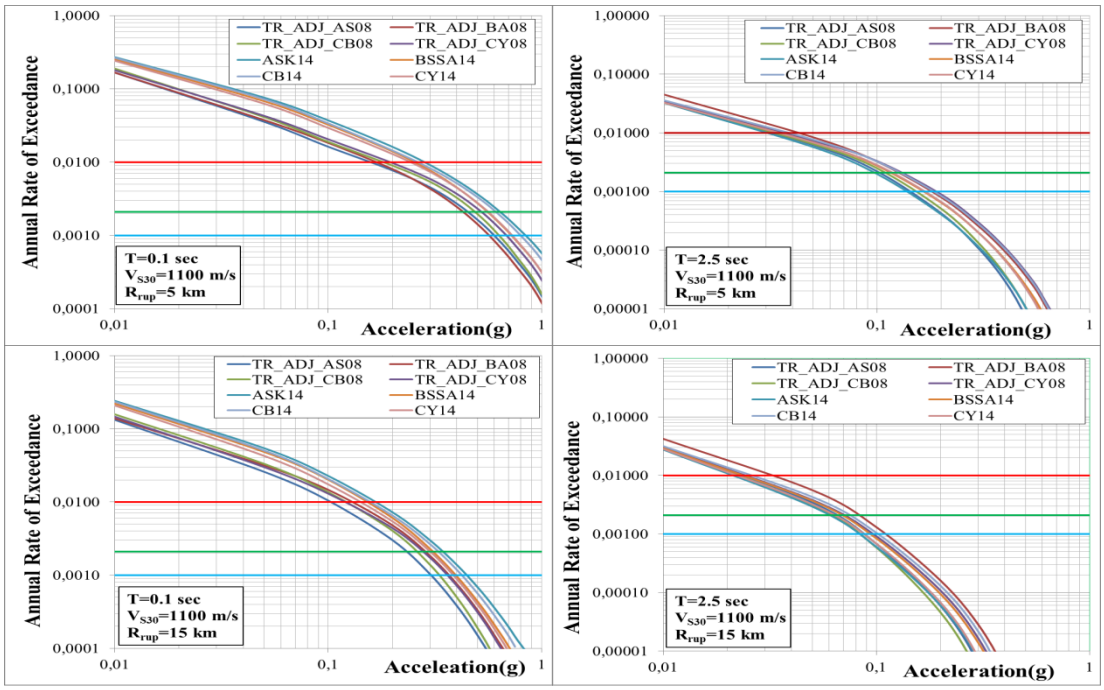


**Figure 3.3: Hazard Curves for T=0.01s and T=2.5s; using TR_Adj_NGA Models and NGA_West2 Models (Vs30=1100 m/s; Rrup=5 km and Rrup=15 km)**

# CHAPTER 4

# PROBABILISTIC SEISMIC HAZARD ANALYSIS RESULTS AND CONCLUSIONS

## 4.1 Probabilistic Seismic Hazard Assessment (PSHA) Methodology and Software

The target of many earthquake engineering analyses is to make sure that a structure can withstand a given ground-shaking level while maintaining the desired performance. However, there is a great deal of uncertainty about the size, location and resulting shaking intensity of future earthquakes. Probabilistic Seismic Hazard Analysis (PSHA) is a methodology that aims to quantify these uncertainties and estimate the annual frequency or probability per year of various levels of earthquake-caused ground motions that will be exceeded at the site for a given future time. The PSHA consists of definition of a suite of earthquake scenarios (seismic source characterization), estimation of the range of ground motions for each earthquake scenario (ground motion characterization), and computation of the rate of each combination of earthquake scenario and ground motion (Gulerce and Abrahamson, 2010). Cornell (1968) introduced a probabilistic seismic hazard methodology for the computation of seismic hazard at the site by giving the level of ground motion for corresponding probability of exceedance. The PSHA framework evolved significantly over the course of the years after 1968 and the current perspective was summarized by McGuire in 2004. In this study, the Cornell-McGuire approach is used to determine the seismic hazard where the hazard integral for a single point source is given by:

$$\nu\,(A>z)= N_{min}\cdot \int_M \int_R \int_\varepsilon f_M(M) f_R(M,R) f_\varepsilon(\varepsilon) P(A>z \mid M,R,\epsilon)\times dM\times dR\times d\varepsilon \qquad 4.1$$

In Equation 4.1, M represents the earthquake magnitude; R is the distance between the source and the site, $N_{min}$ is the annual rate of earthquakes with magnitude greater than or equal to the minimum magnitude, $f_M(M)$ and $f_R(M,R)$ are the probability density functions for the magnitude and distance, $\varepsilon$ is the number of standard deviations above or below the median, $f_\varepsilon(\varepsilon)$ is the probability density function for the

epsilon (given by a standard normal distribution), and P(A>z | M, R, ε) is either 0 or 1. In this equation, P(A > z|M, R, ε) selects those scenarios and ground motion combinations that lead to ground motions greater than the test level z. The computer code HAZ45 (developed by N. Abrahamson, PGE, 2010) is used for performing the numerical integrations of the PSHA integral. HAZ45 treats the epistemic uncertainties in the source characterization and the ground motion prediction models by using logic trees. All combinations of the logic tree branches are evaluated for each source in HAZ45.

## 4.2 Probabilistic and Deterministic SHA Results for Example Sites around EAFZ

Using the HAZ45 computer code, the seismic hazard for 6 selected locations (marked by yellow stars in Figure 4.1): Bingöl ($R_{Rup}$= 1 km), Elazığ ($R_{Rup}$= 27 km), Kahramanmaraş ($R_{Rup}$ = 15 km), Osmaniye ($R_{Rup}$ = 2 km), Pütürge ($R_{Rup}$= 5 km) and Hasanbeyli ($R_{Rup}$ = 8 km) is analyzed for PGA, T=0.2 second and T=1.0 second spectral accelerations for $V_{S30}$=760 m/s and shown in Figures 4.2, 4.3, and 4.4, respectively. These figures show the relation between the distance to the fault and the level of hazard; highest level of hazard is observed in Bingöl (PGA=0.68 g for 475-years return period) since this location is very close to EAFZ. Osmaniye is also close to the EAFZ however the slip rate of the rupture systems near Osmaniye is lower than the slip rate of the rupture systems near Bingöl; therefore, the hazard in Osmaniye (PGA=0.42 g for 475-years return period) is lower than the hazard in Bingöl. The lowest hazard is observed in Elazığ (PGA=0.42 g for 475-years return period) since this location is farther away from the faults when compared to other locations.

The hazard curves give the merged effects of all magnitudes and distances on the probability of exceeding the specified ground motion level. In order to find out which events are more important for the hazard at a given ground motion level, the hazard curve is broken down into its contributions from different earthquake scenarios (Gülerce and Abrahamson, 2010). This process is called deaggregation (Bazzurro and Cornell, 1999). The PGA deaggregation plots for 475-years and 2475-years return periods for $V_{S30}$=760 m/s are presented in Figures 4.5 to 4.16 for the same locations. These figures show that when the accepted hazard level increases, the percentage contribution of the dominating scenario to the total hazard decreases.

However, the dominating scenario for 475-year hazard level is not different than the dominating scenario for 475-year hazard level at any of the selected locations. The dominating scenario for Bingöl has a magnitude range of 6.5-7.0 and distance range of 0-5 km. For Elazığ, the dominating scenario has a magnitude range of 7.0-7.5 and a distance range of 20-30 km. (Figure 4.6 and 4.12). Kahramanmaraş has the dominating scenario with magnitude range of 6.5-7.0 and distance range of 10-15 km. Osmaniye has the dominating scenario with magnitude range of 7-7.5 and distance range of 0-5 km. Pütürge (Figure 4.9 and 4.15) and Hasanbeyli (Figure 4.10 and 4.16) have the dominating scenarios with magnitude range of 6.5-7.0 km and distance range of 5-10 km. These values are consistent with the distance to the nearest fault system and the characteristic magnitude of the nearby rupture systems.

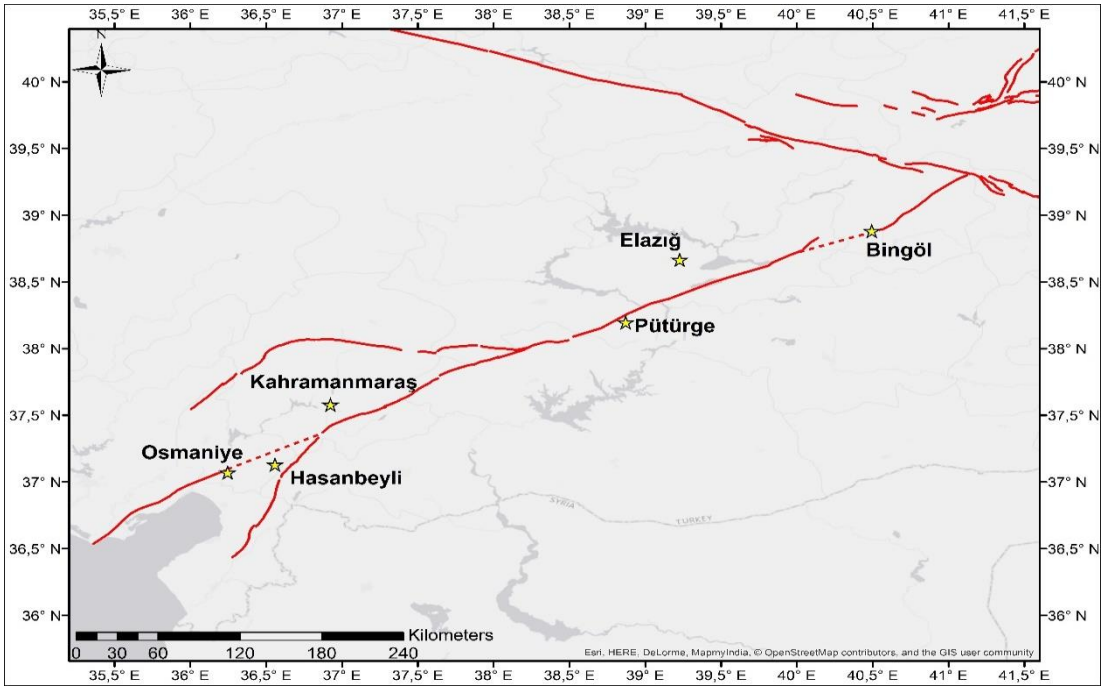


**Figure 4.1: The Six Locations where the Analysis are Performed**

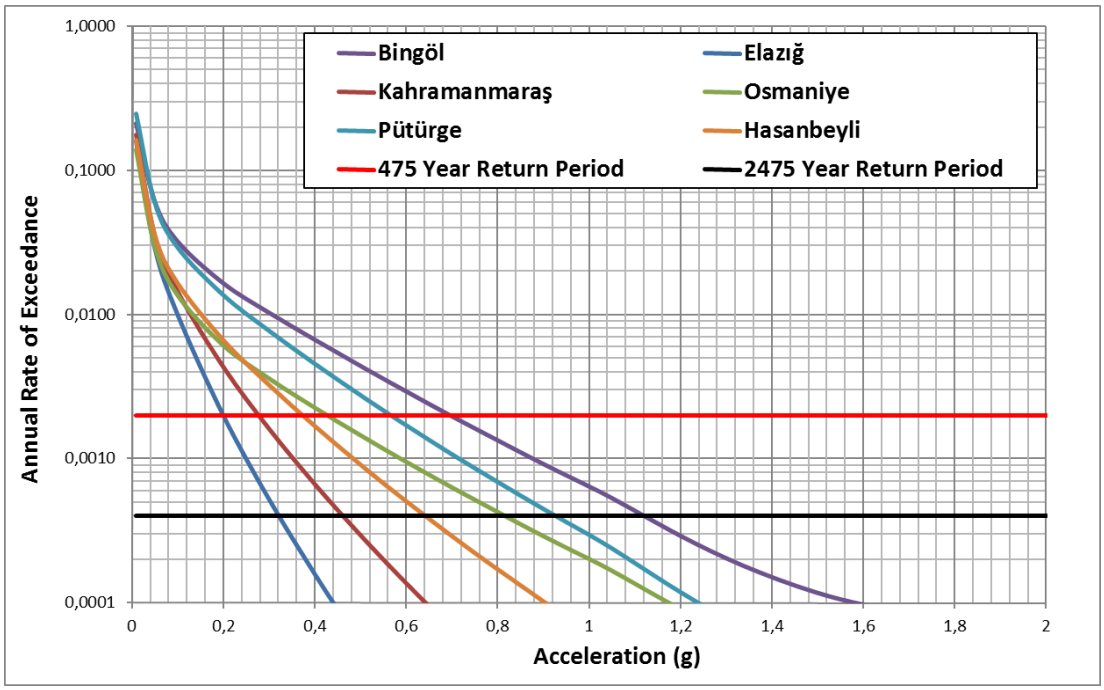


**Figure 4.2: PGA Hazard Curves for Bingöl, Elazığ, Kahramanmaraş, Osmaniye, Pütürge and Hasanbeyli for Vs30=760 m/s.**

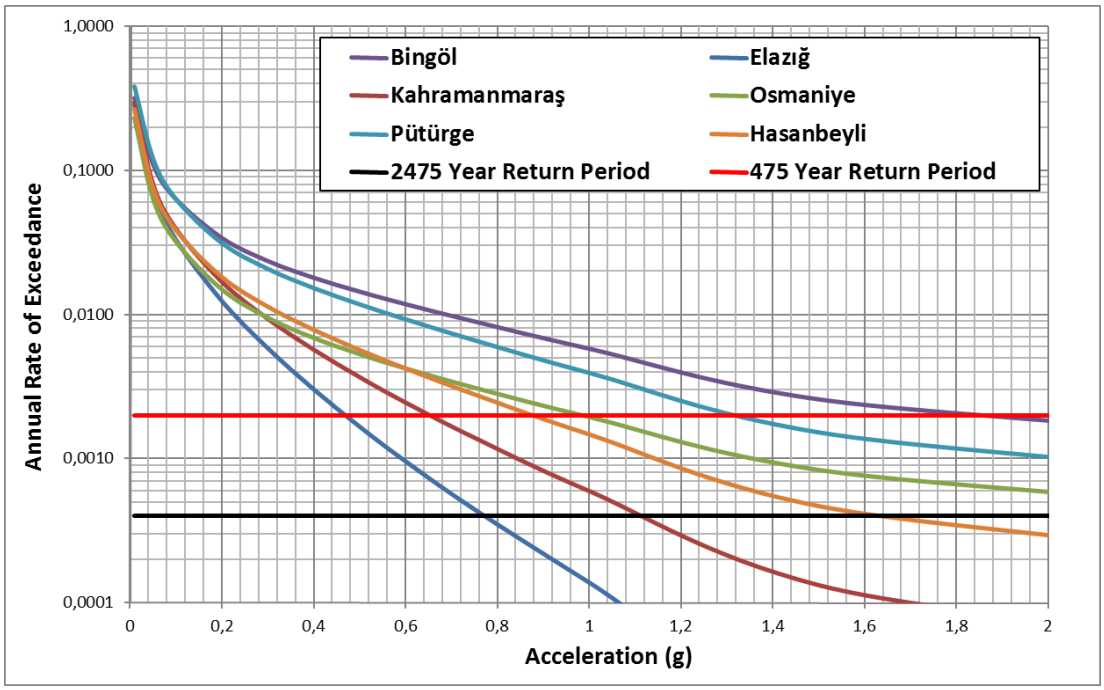


**Figure 4.3: Hazard Curves (T=0.2s) for Bingöl, Elazığ, Kahramanmaraş, Osmaniye, Pütürge and Hasanbeyli for Vs30=760 m/s.**

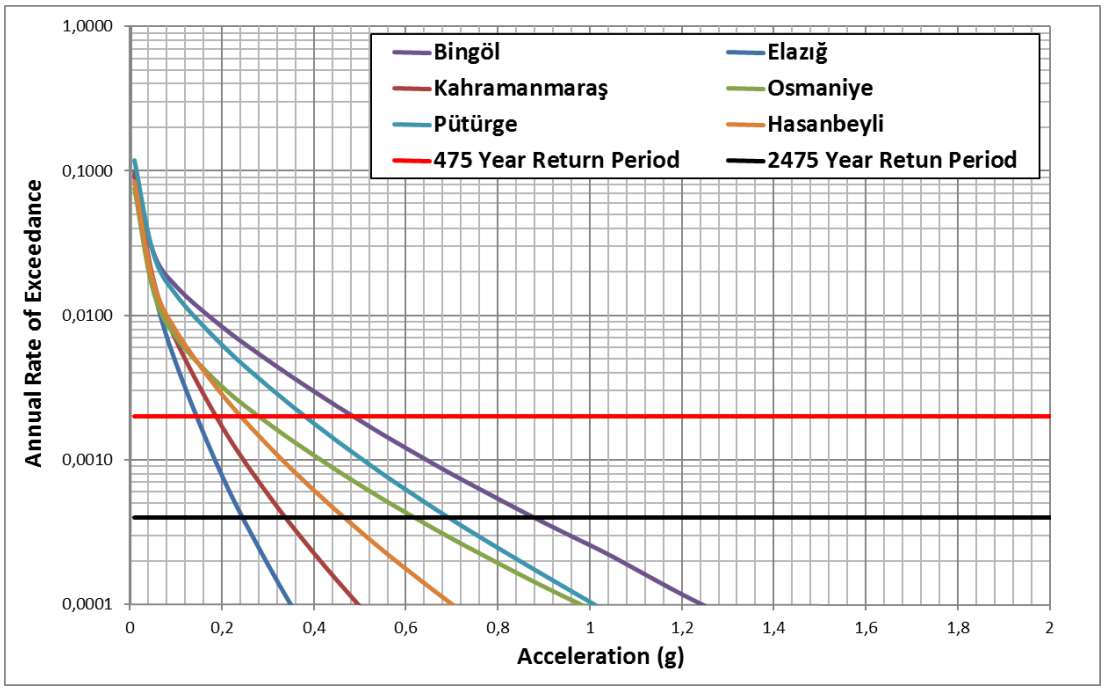


**Figure 4.4: Hazard Curves (T=0.1s) for Bingöl, Elazığ, Kahramanmaraş, Osmaniye, Pütürge and Hasanbeyli for Vs30=760 m/s.**

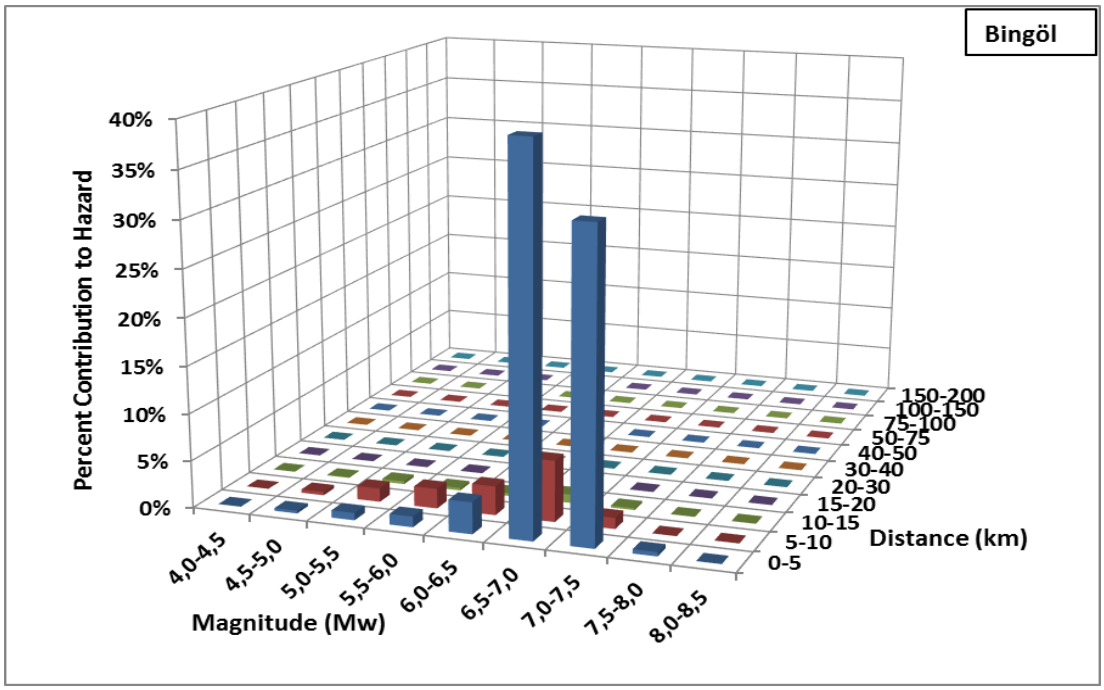


**Figure 4.5: Deaggregation for Bingöl for 475 Year Return Period (Vs30=760m/s, PGA)**

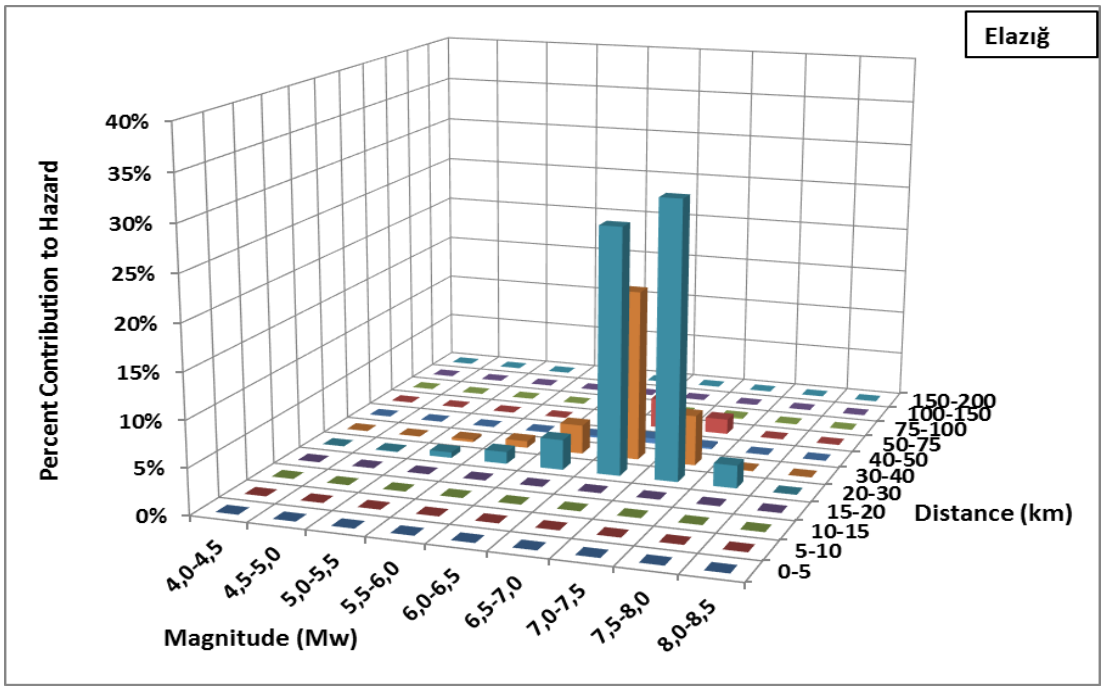


**Figure 4.6: Deaggregation for Elazığ for 475 Year Return Period (Vs30=760m/s, PGA)**

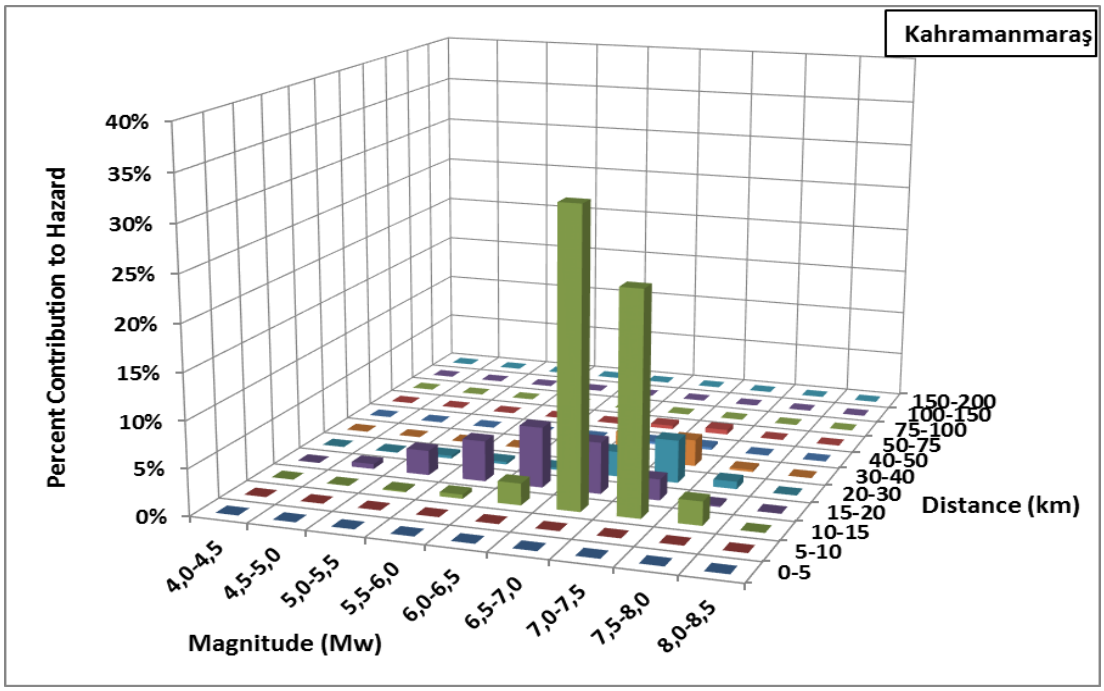


**Figure 4.7: Deaggregation for Kahramanmaraş for 475 Year Return Period (Vs30=760m/s, PGA)**

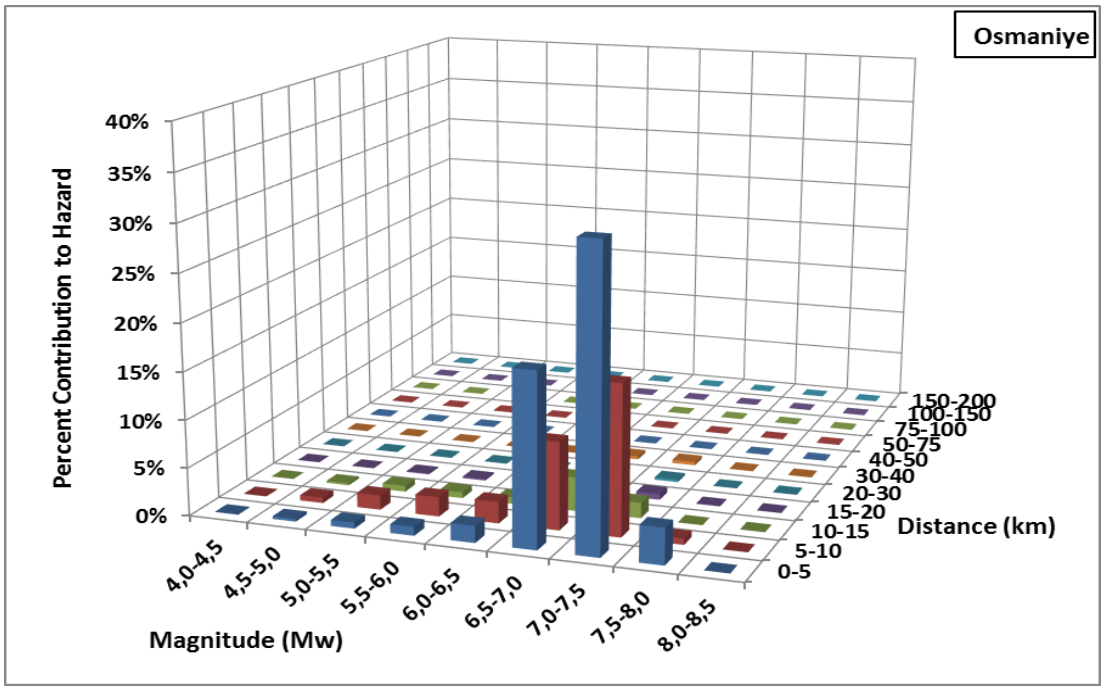


**Figure 4.8: Deaggregation for Osmaniye for 475 Year Return Period (Vs30=760m/s, PGA)**

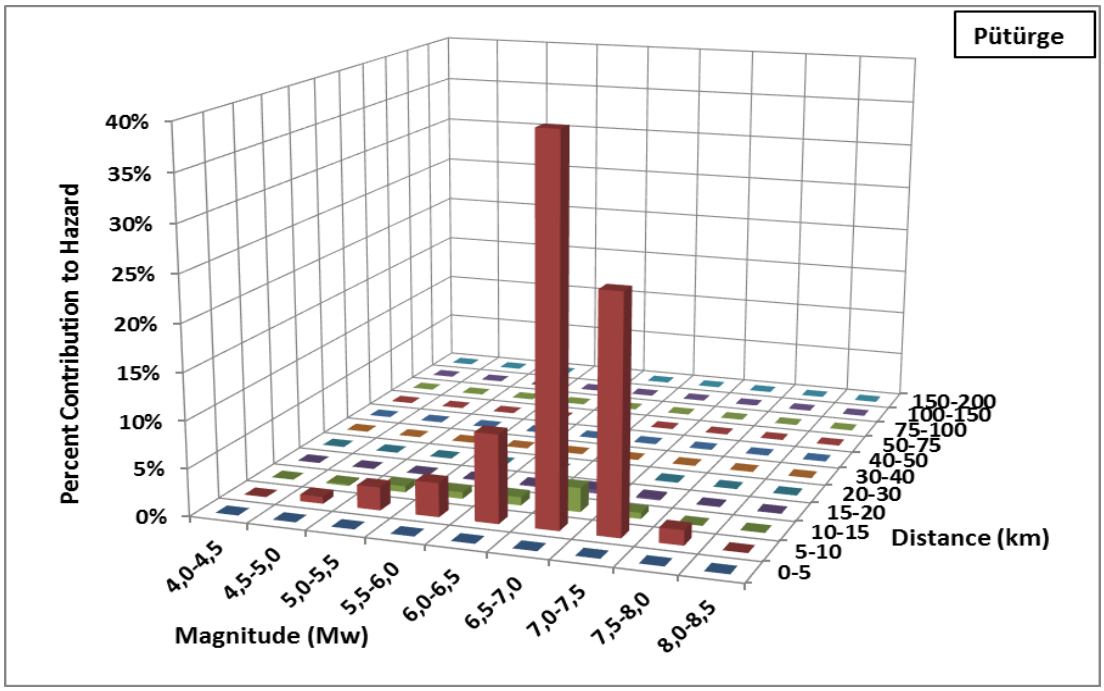


**Figure 4.9: Deaggregation for Pütürge for 475 Year Return Period (Vs30=760m/s, PGA)**

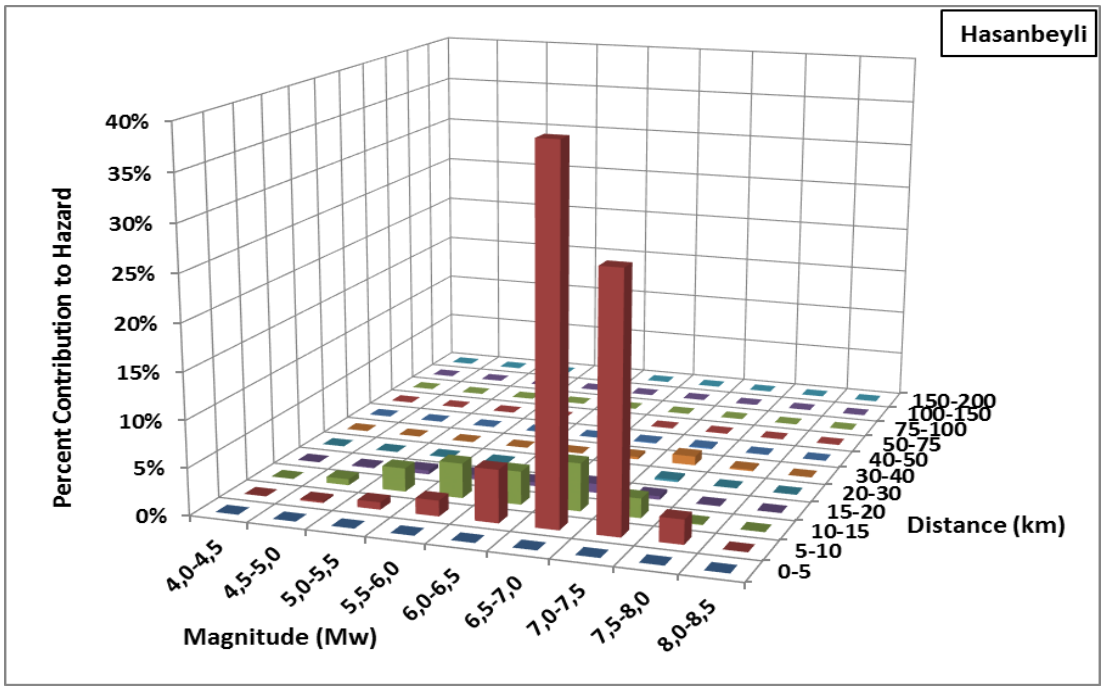


**Figure 4.10: Deaggregation for Hasanbeyli for 475 Year Return Period (Vs30=760m/s, PGA)**

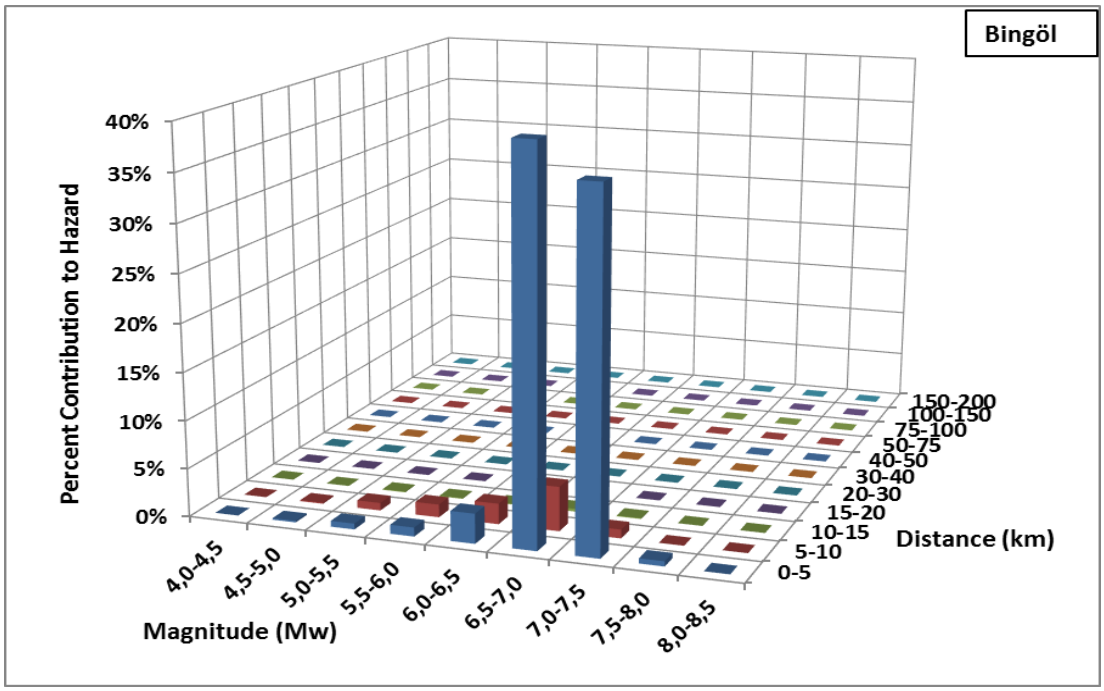


**Figure 4.11: Deaggregation for Bingöl for 2475 Year Return Period (Vs30=760m/s, PGA)**

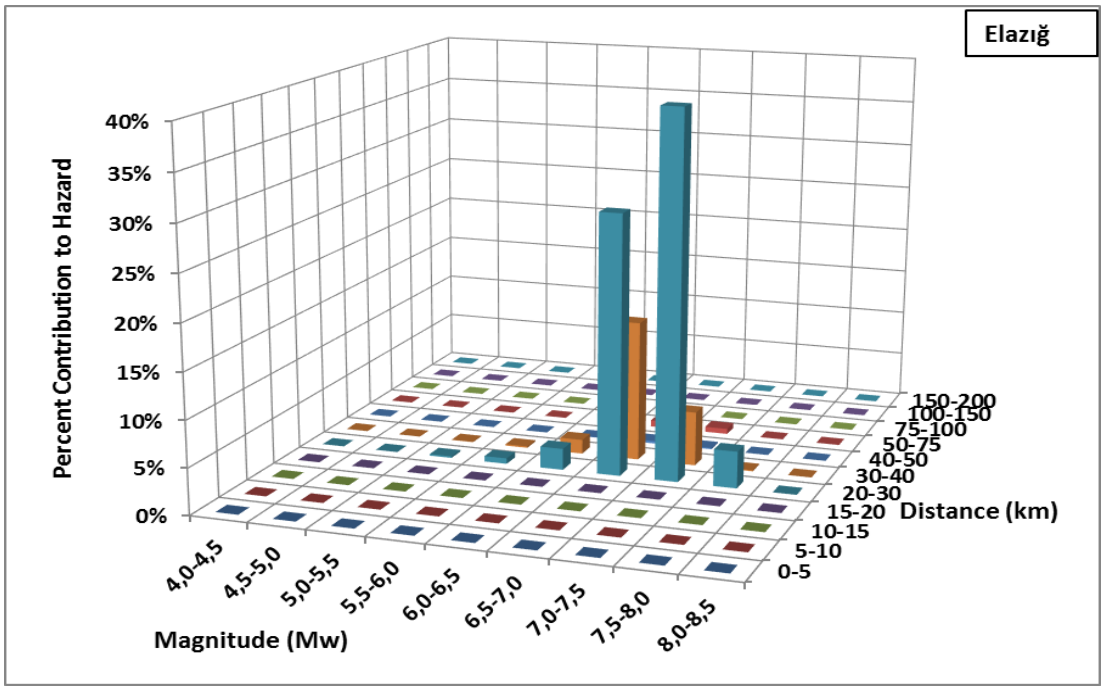


**Figure 4.12: Deaggregation for Elazığ for 2475 Year Return Period (Vs30=760m/s, PGA)**

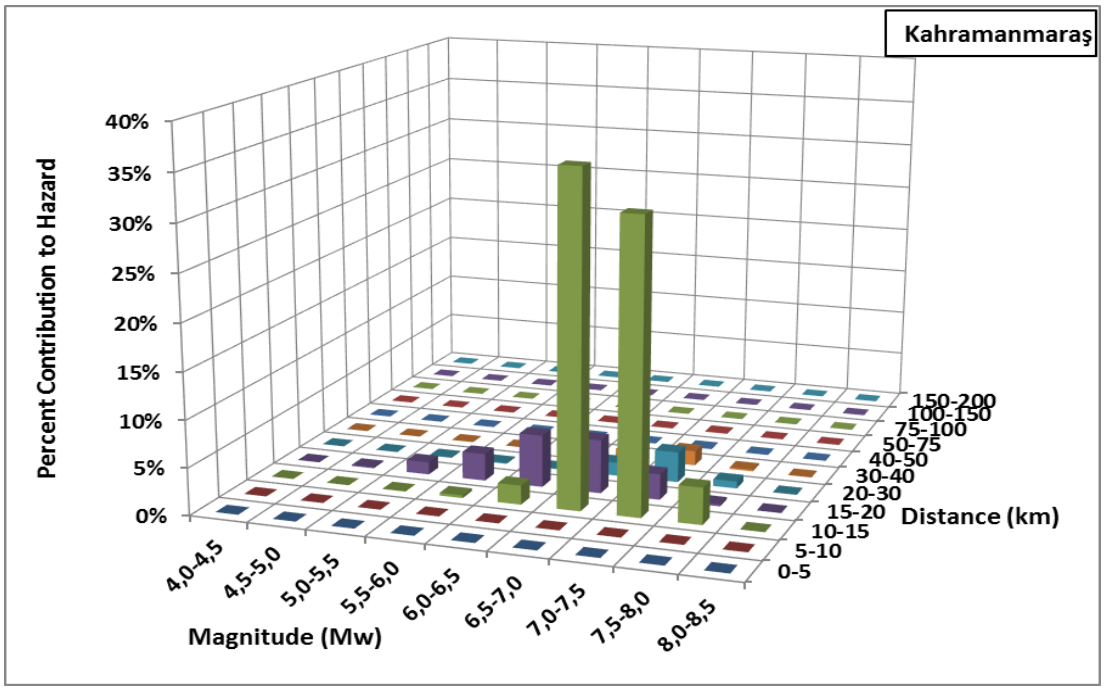


**Figure 4.13: Deaggregation for Kahramanmaraş for 2475 Year Return Period (Vs30=760m/s, PGA)**

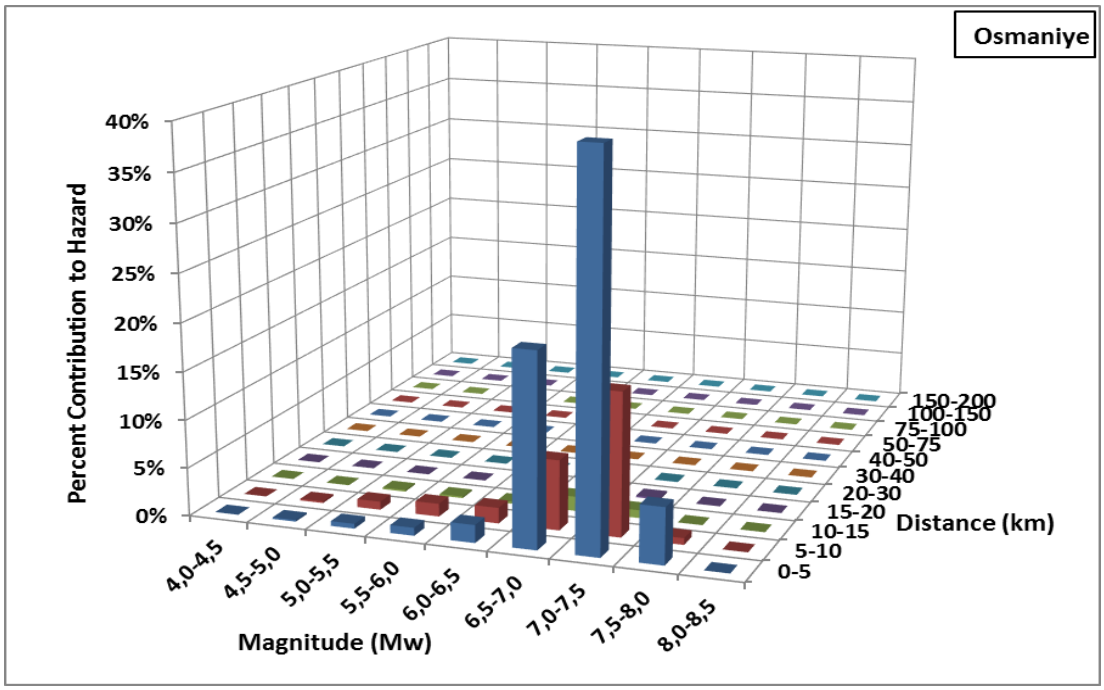


**Figure 4.14: Deaggregation for Osmaniye for 2475 Year Return Period (Vs30=760m/s, PGA)**

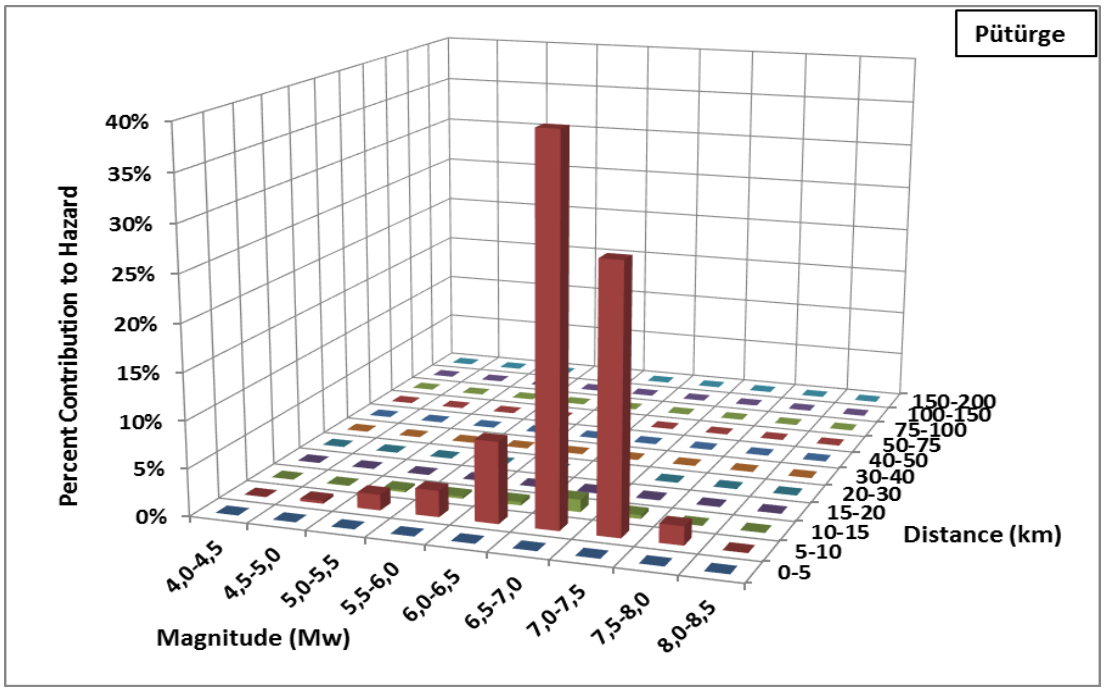


**Figure 4.15: Deaggregation for Pütürge for 2475 Year Return Period (Vs30=760m/s, PGA)**

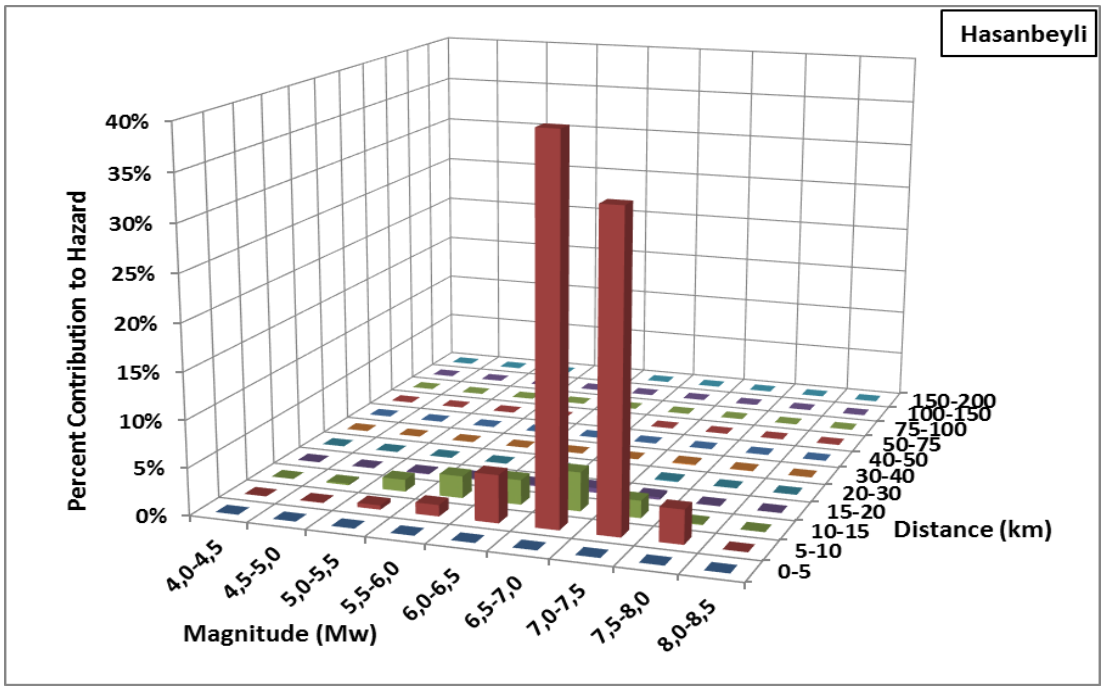


**Figure 4.16: Deaggregation for Hasanbeyli for 2475 Year Return Period (Vs30=760m/s, PGA)**

Deterministic Seismic Hazard Assessment (DSHA) is another basic methodology to carry out seismic hazard analysis in order to quantify future earthquake threat at a site. In DSHA approach, critical earthquake scenario that will produce the largest ground motion at the site is selected (maximum possible earthquake magnitude occurring at a seismic source with minimum distance to the site). The ground motion at the site is predicted for this earthquake scenario based on the magnitude, distance and site characteristics. DSHA is based on the most adverse earthquake scenarios regardless of how unlikely they may be. Since single deterministic values are selected for earthquake magnitude and site to source distance, this method is called as the deterministic seismic hazard analysis. In Figures 4.17 to 4.22, comparison of the hazard curves for $V_{S30}$=760 m/s and PGA are given for 6 selected sites (Bingöl, Elazığ, Kahramanmaraş, Osmaniye, Pütürge and Hasanbeyli). In general, it is observed from the figures that the difference between the hazard levels estimated by PSHA and DSHA is insignificant for the sites close to faults (Figure 4.17 (Bingöl, $R_{Rup}$ =1km). However as shown in Figure 4.18 (Elazığ, $R_{Rup}$ =27km), as the source to site distance increases PSHA estimates higher results than DSHA.

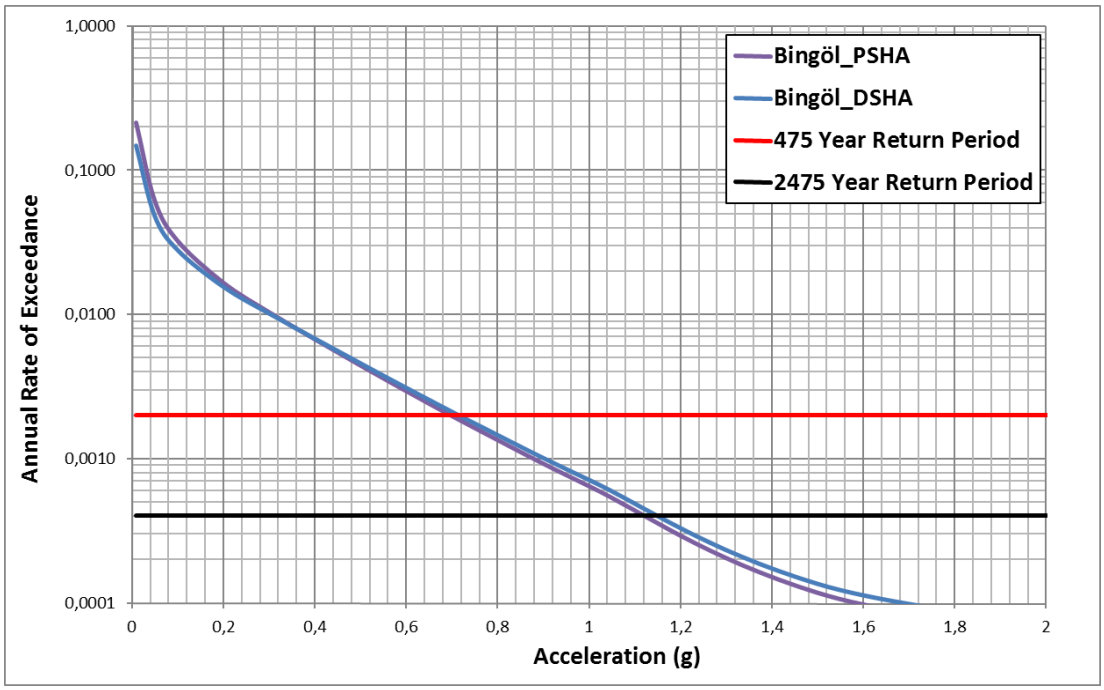


**Figure 4.17: Comparison of PSHA and DSHA Results for Bingöl (Vs30=760m/s, PGA)**

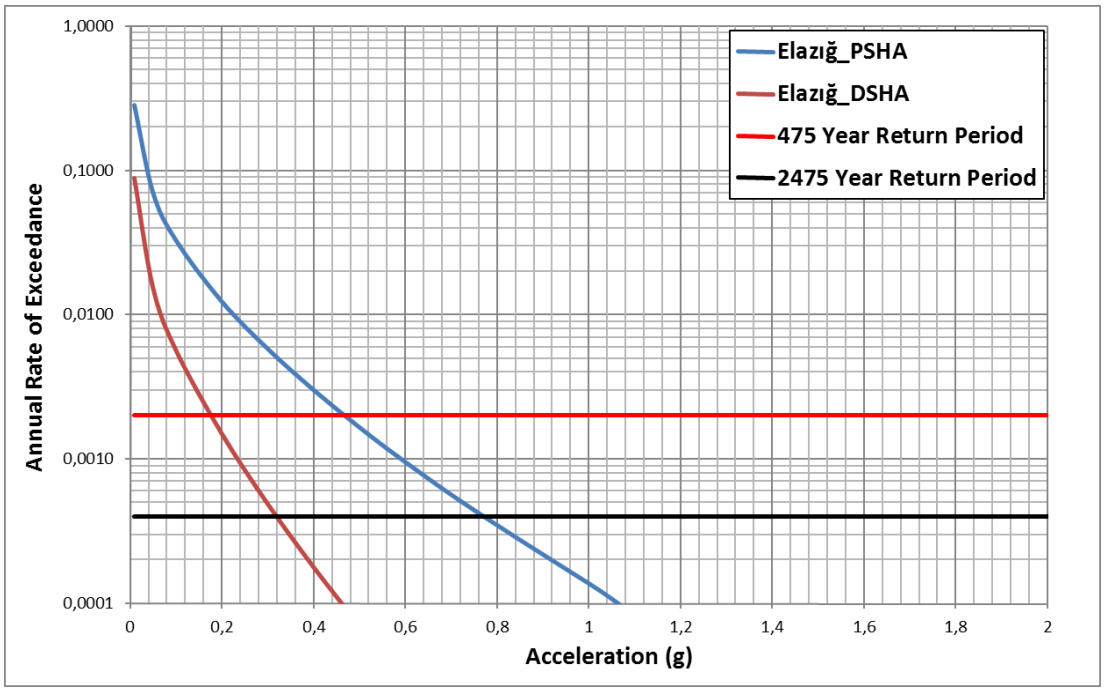


**Figure 4.18: Comparison of PSHA and DSHA Results for Elazığ (Vs30=760m/s, PGA)**

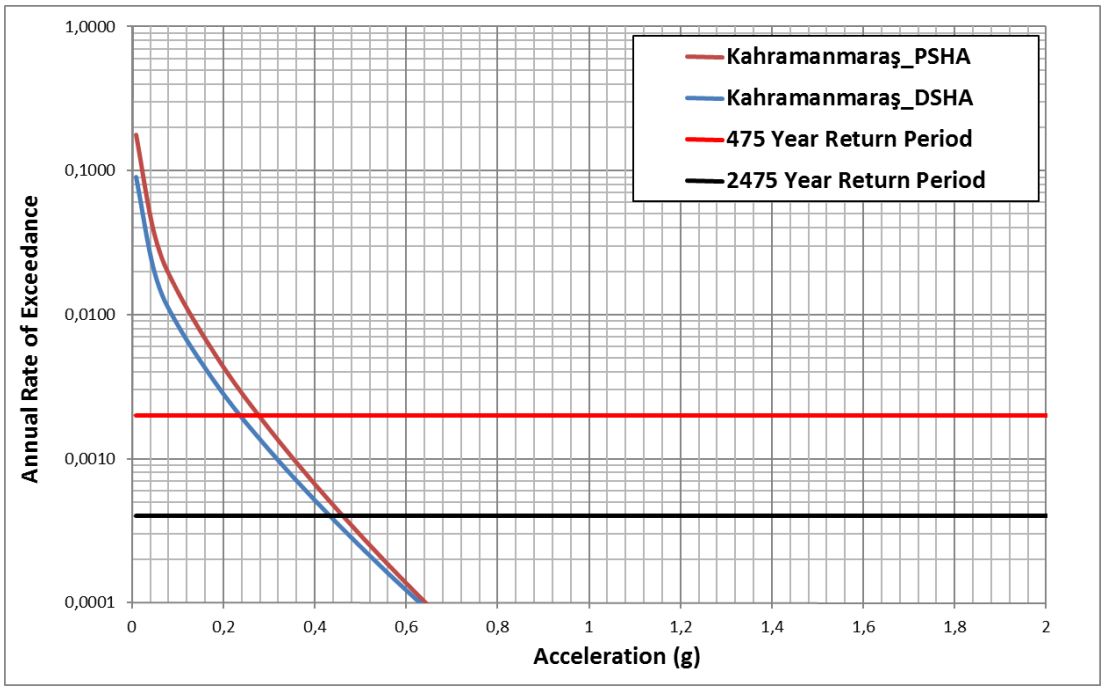


**Figure 4.19: Comparison of PSHA and DSHA Results for Kahramanmaraş ($V_{S30}$=760m/s, PGA)**

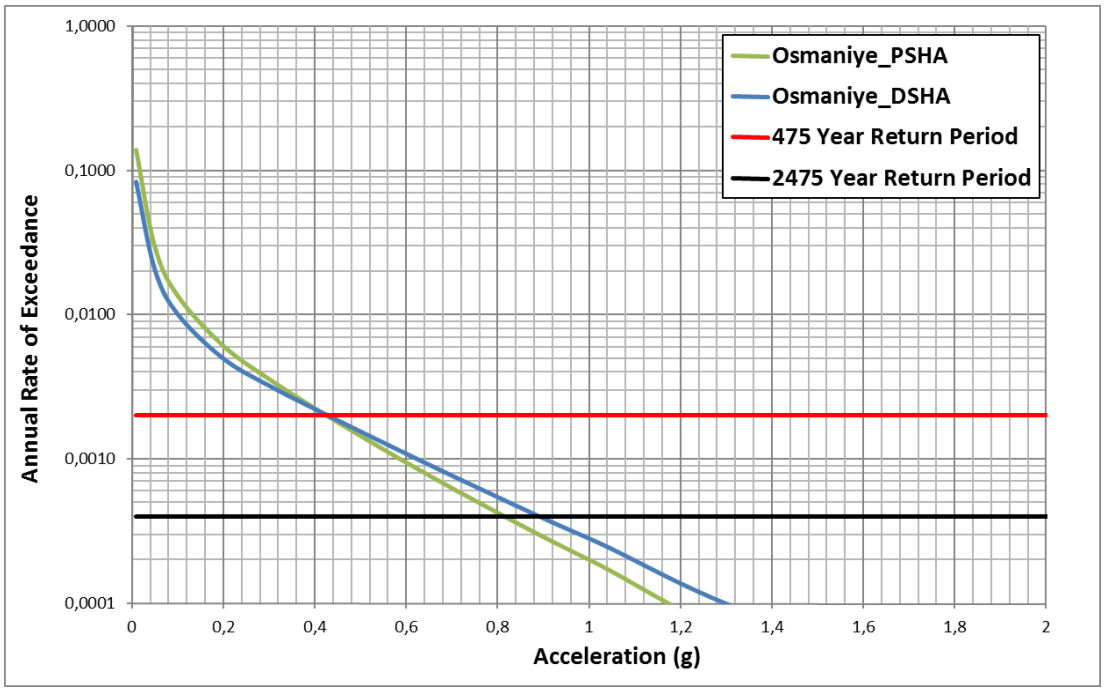


**Figure 4.20: Comparison of PSHA and DSHA Results for Osmaniye (Vs30=760m/s, PGA)**

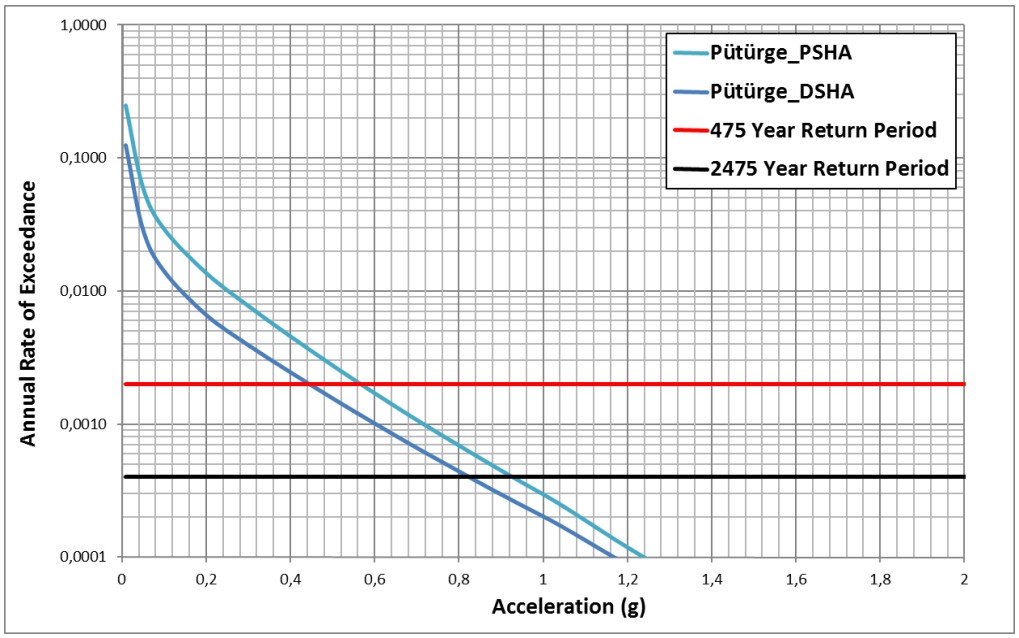


**Figure 4.21: Comparison of PSHA and DSHA Results for Pütürge (Vs30=760m/s, PGA)**

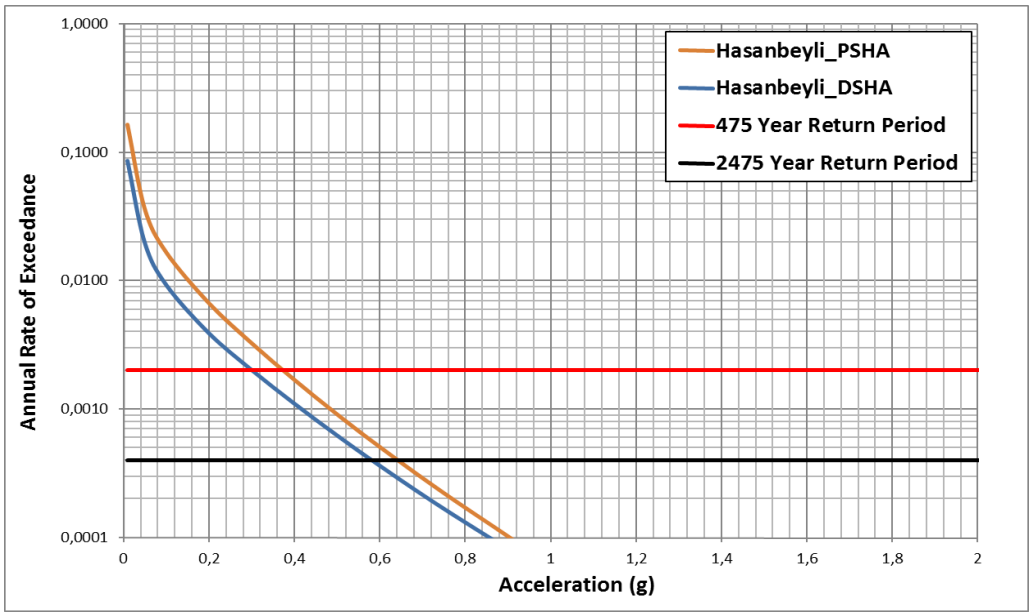


**Figure 4.22: Comparison of PSHA and DSHA Results for Hasanbeyli (Vs30=760m/s, PGA)**

## 4.3 Seismic Hazard Maps for the East Anatolian Fault Zone

Seismic hazard maps for PGA, T=0.02 and T=1.0 second spectral periods corresponding to return periods of 475 (10% chance of exceedance at 50 years) and 2475 (2% chance of exceedance at 50 years) around EAFZ are prepared based on two alternative representations of the seismicity in Gökdere Restraining Bend and

two alternative generic rock site conditions. In **Alternative 1**, an areal source zone is defined to model the seismicity in Gökdere region whereas in **Alternative 2**, a fault segment connecting the southern end of the Ilıca-Karlıova Rupture System with the Pütürge-Palu Rupture System is added to Ilıca-Karlıova Rupture System (please refer to Section 2.1.1 for details). Additionally, two different rock site conditions; **Rock 1** being the B/C boundary in NEHRP site classification system ($V_{S30}$=760 m/s) and **Rock 2** being the reference rock site conditions to be used in site-specific response analysis are defined ($V_{S30}$=1100 m/s). Based on these alternatives, 4 combinations for each spectral period are considered and individual hazard maps representing these combinations are provided in Figures 4.24 to 4.35. Please note that the southern end of the hazard maps provided in each figure are indifferent but the design ground motions around Gökdere Restraining Bend changes significantly in Part(a) and (b). In order to prepare the seismic hazard maps, 604 grid points (0.1° to 0.1°) are defined around EAFZ and PSHA analysis is performed at each grid node (please see Figure 4.23 for the grid points). For more accurate results, the density of the grid points is increased (0.1° to 0.05°) for areas that are within the close vicinity of the fault plane (±5.5 km). Last set of points in the grid is 33 km away from the fault plane.

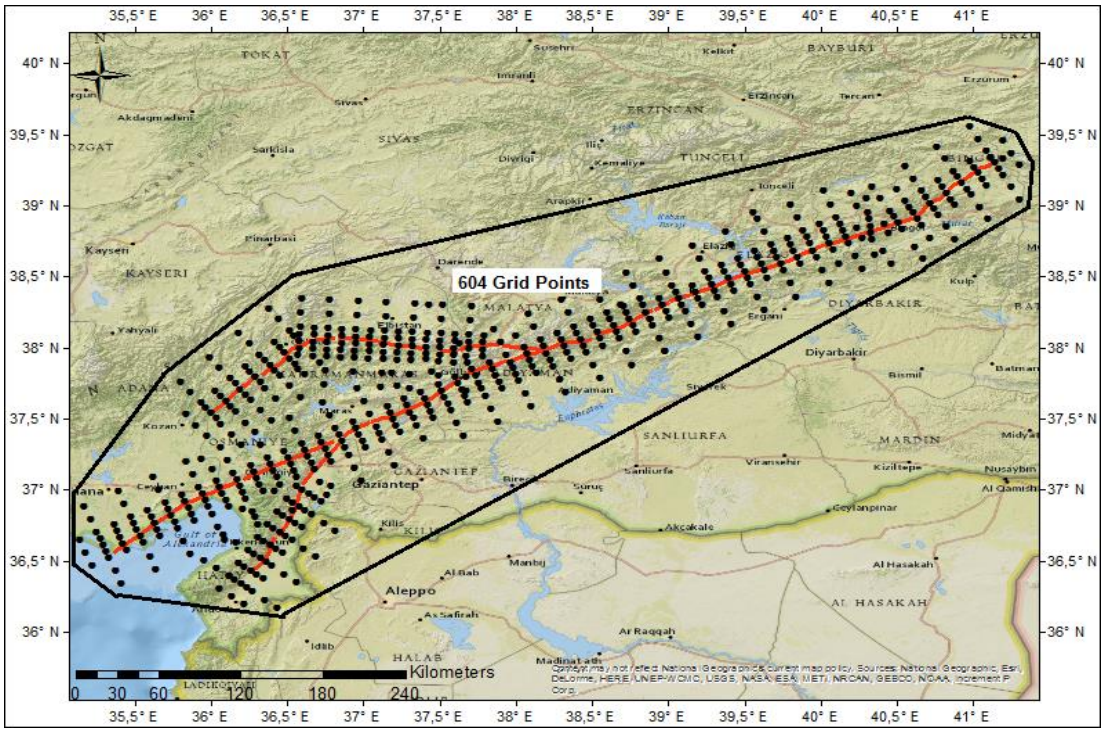


**Figure 4.23: Location of the Grid of Points at which the PSHA was performed with respect to the Seismic Sources**

Seismic hazard maps provided in Figures 4.24 to 4.35 show that the contours of hazard follow the fault lines as expected and larger values are observed along the close vicinity of the fault lines. At the end of each rupture system or at the segmentation points where the surface interpretations of the fault planes are discontinuous, a certain reduction in the design ground motions is observed. This observation is particularly significant in Gökdere Restraining Bend. As the source-to site distance increases, the design ground motion values attenuates quite abruptly. Following interpretations can be made based on the hazard maps provided in Figures 4.24 to 4.35 and hazard maps from previous studies:

1. Highest ground motions are estimated in the vicinity of Pütürge-Palu Rupture System where the annual slip rate is 10 mm/yr.
2. The highest value of 475-year return period PGA is 0.82g for Rock 1 conditions and 0.72g for Rock 2 conditions. As the acceptable hazard level increases, the design ground motions also increase considerably. The maximum 2475-years return period PGA value is equal to 1.40g and 1.21g for Rock 1 and Rock 2 site conditions, respectively.
3. Estimated values are comparable with the recent design ground motion estimates around the NAFZ. The maximum 2475-year return period PGA was found to be between 1.50-1.65g by Kalkan et al. (2009), Erdik et al. (2004), and Gülerce and Ocak (2013) for $V_{S30}$=760 m/s. Please note that the values estimated around NAFZ are higher than the ones estimated around EAFZ since the annual slip rate of the NAFZ is higher than that of EAFZ.
4. The hazard map proposed by Erdik et al. (1999) (Figure 1.2) is quite similar to results obtained in this study (Figure 4.24). In both studies, there is a narrow band around the fault where the 475-year return period PGA values are higher than 0.6g. The high-PGA zone provided by Erdik et al. (1999) is larger and more homogenous than the high-PGA zone shown in Figure 4.24 since the seismicity was uniformly distributed in the areal source zone around EAFZ by Erdik et al. (1999). Same interpretation can be made for the hazard map proposed by Kayabalı (2002).
5. Since the activity of the Northern Strand of EAFZ was only recently acknowledged, the design PGA values for 475-year return period around the Sürgü-Çardak-Savrun Rupture Systems estimated in this study is higher than

the design ground motions proposed in previous works (see Figures 1.2 and 1.3 for comparison).

6. In this study, Karataş-Osmaniye and Amanos Rupture Systems share the annual slip rate where the majority of the slip rate is assigned to Karataş-Osmaniye system. Therefore, the estimates of Erdik et al., (1999) and Kayabalı (2002) are slightly higher than the 475-year return period PGA values shown in Figure 4.24 in Hatay-Kırıkhan region.
7. The seismic hazard maps proposed in SHARE project and this study is very similar between Karlıova and Türkoğlu, except that the high-PGA zone in SHARE map (Figure 1.4) is larger and more homogenous than the high-PGA zone shown in Figure 4.24. Also, the design ground motions proposed for the region between Karlıova and Türkoğlu is higher than the design ground motions in the Hatay-Kırıkhan region, indicating that reduction in the annual slip rate of Amanos Rupture System was also considered in SHARE project.
8. The hazard map for PGA proposed by EMME is similar to the 475-year return period PGA maps proposed by SHARE and this study along the main strand of EAFZ. Additionally, the shape of the EMME PGA map (Figure 1.5) is similar to Figure 4.24 around the Karataş-Osmaniye Rupture System but the EMME estimates are slightly higher than this study for southern continuation of EAFZ from Türkoğlu.
9. The highest value of spectral acceleration at T= 0.2 sec for the return period of 475 years is about 1.92g for Rock 1 conditions and 1.54g for Rock 2 conditions. These high spectral accelerations are estimated for the sites right on top of the fault lines, but hazard values reduce quickly after the near-field zones. Again, these values are comparable with the recent estimates around the NAFZ by Kalkan et al. (2009) and Gülerce and Ocak (2013).

### 4.4 Comparison with the Turkish Earthquake Code (2007) Requirements

Even if it is not explicitly mentioned in the Turkish Earthquake Code (TEC-2007), the official Earthquake Hazard Zone Map of Turkey were adopted from the PGA values at 10% probability of exceedance in 50 years proposed by Gülkan et al. (1993) for each seismic zone (Kalkan et al., 2009). To be able to compare the TEC-2007 requirements with the design ground motions in this study, the zonation map of TEC-2007 is digitized using the actual hazard values given in Middle East Technical

University Disaster Management Center Archives (http://dmc.metu.edu.tr/en/round-table-meetings-and-dmc-archive, last accessed in December 2015). According to the zonation map of TEC-2007, the EAFZ is mostly situated in a first-degree earthquake hazard zone (Zone I) where the design PGA is equal to 0.4g (Figure 4.36). However, the southernmost segments of Karataş-Osmaniye Rupture System and Çardak Rupture System is located in Zone II where the design PGA=0.3g and Savrun Rupture System is located in Zone III where the design PGA=0.2g. The contours of 475-year return period PGA proposed in this study are overlaid on top of Zone I and II of the TEC-2007 zonation map for Alternative 1 and 2 in Figure 4.36(a) and (b), respectively.

It is notable that the actual 475-year return period PGA values proposed by Gülkan et al. (1993) are not exactly equal to the design PGA values recommended for Zones I-II-III. The 475-year return period PGA values proposed by Gülkan et al. (1993) can be as high as 0.61 g and as low as 0.32 g along the main strand of EAFZ even if the site is located in Zone I. Therefore, a second set of maps are prepared to allow the comparison between the 475-year return period PGA values proposed by Gülkan et al. (1993) and in this study (Figure 4.37). Since the average shear wave velocity at the top 30 meters employed by Gülkan et al. (1993) in hazard calculations are unknown, direct comparison between the hazard maps provided here and TEC-2007 requirements is a challenging task. In Figures 4.36 and 4.37, the 475-years return period PGA values calculated for $V_{S30}$=760 m/s are preferred to imitate site conditions considered by Gülkan et al. (1993).

Figures 4.36 indicates that the "high hazard zone" (where the 475-years return period PGA is higher than 0.4g) is thinner than Zone I and more concentrated around EAFZ. The design PGA values are higher than 0.4g within the ±15 km of the fault plane for the main strand (until Türkoğlu) but as the slip rate decreases, thickness of the "high hazard zone" also reduces to ±10 km in Karataş-Osmaniye region. Design PGA values larger than 0.4g are rarely observed along the northern strand of EAFZ and along the Amanos Rupture System. On that sense, biggest change in the design ground motions proposed by this study is in Hatay Region. However, one of the important shortcomings of the hazard maps proposed in this study is the neglected contribution of nearby tectonic structures. When the southern continuation of EAFZ (or the Dead Sea Fault Zone) is considered, the design ground motions in Hatay region will increase. The contours of hazard estimates of Gülkan et al. (1993) are

different than the zonation map of TEC-2007 and this study. The 475-years return period PGA values proposed by Gülkan et al. (1993) are relatively smaller than the TEC-2007 requirements around Türkoğlu Triple Junction even where the fault plane is continuous. An interesting feature of Figure 4.37 is the high PGA values observed in between the parallel Karataş-Osmaniye and Amanos Rupture Systems. Possible explanations for this inconsistency with the tectonic structures are the use of areal source zones and inaccuracy in the site coordinates given in Gülkan et al. (1993). Since the Sürgü, Çardak and Savrun Rupture Systems are not considered in the zonation map of TEC-2007 and Gülkan et al. (1993), the design PGA values in these regions are lower than the 475-year return period PGA estimates of this study.

### 4.5 Recommendations for Future Work

The objective of this study is to update the design ground motions and seismic hazard maps of the region using the planar source models that combine the recently published information on source geometry and fault kinematics. This study also proposes a substantial change from the other available studies in terms of the ground motion characterization framework. Recently developed NGA-West 2 GMPEs (Bozorgnia et al., 2014) and the Turkey-Adjusted NGA-West 1 (Gülerce et al., 2015) models that were regionalized based on Turkish strong motion database are employed for ground motion estimates and variability. The seismic hazard maps are provided for two different site conditions; $V_{S30}$=760 m/s representing the B/C boundary of NEHRP site classification scheme and $V_{S30}$=1100 m/s to provide the reference rock site conditions that might be used in site-specific response analysis. Proposed design ground motions are compared to the TEC (2007) requirements and the significant differences are thoroughly discussed.

It is notable that this study does not include any floating seismic sources to model the earthquakes that may occur outside the buffer zones. Contribution of other nearby seismic sources such as Bitlis Suture Zone and NAFZ is neglected. Therefore, the PSHA maps proposed in this study underestimate the hazard at the northeastern tip of EAFZ, on the east of Gölbaşı and in the area that lies in between Karataş-Osmaniye and Amanos Rupture Systems. The annual slip rate distribution between parallel Karataş-Osmaniye and Amanos Rupture Systems is still under debate and this distribution has a significant effect on our results. Proper evaluation of associated slip rates on these parallel segments by GPS measurements and state of the art block

models will reduce the uncertainty in these parameters and will lead to more accurate estimation of design ground motion levels. The recurrence intervals for the characteristic event for any segment of EAFZ are not available; therefore, time dependent hazard methodologies are not employed in this study. Determination of paleoseismic recurrence periods will provide a substantial contribution in the PSHA practice of Turkey and eventually will lead to a decrease in the hazard estimates when the time dependent methods are utilized.

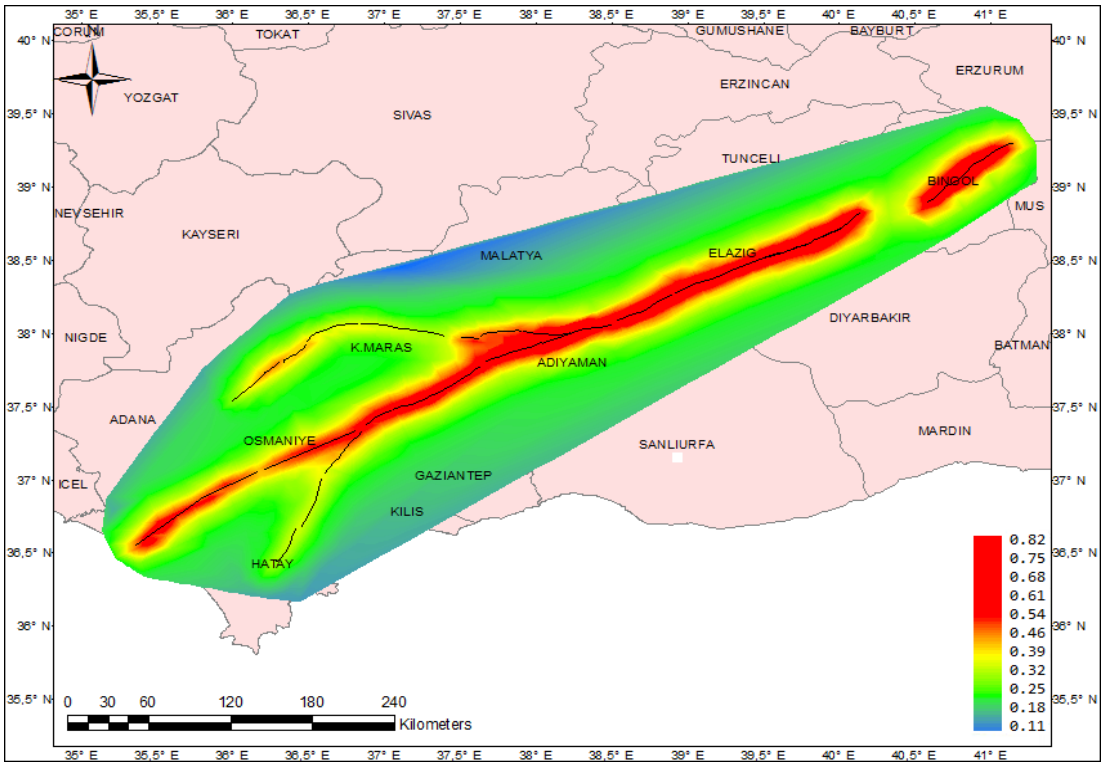


**(a)**

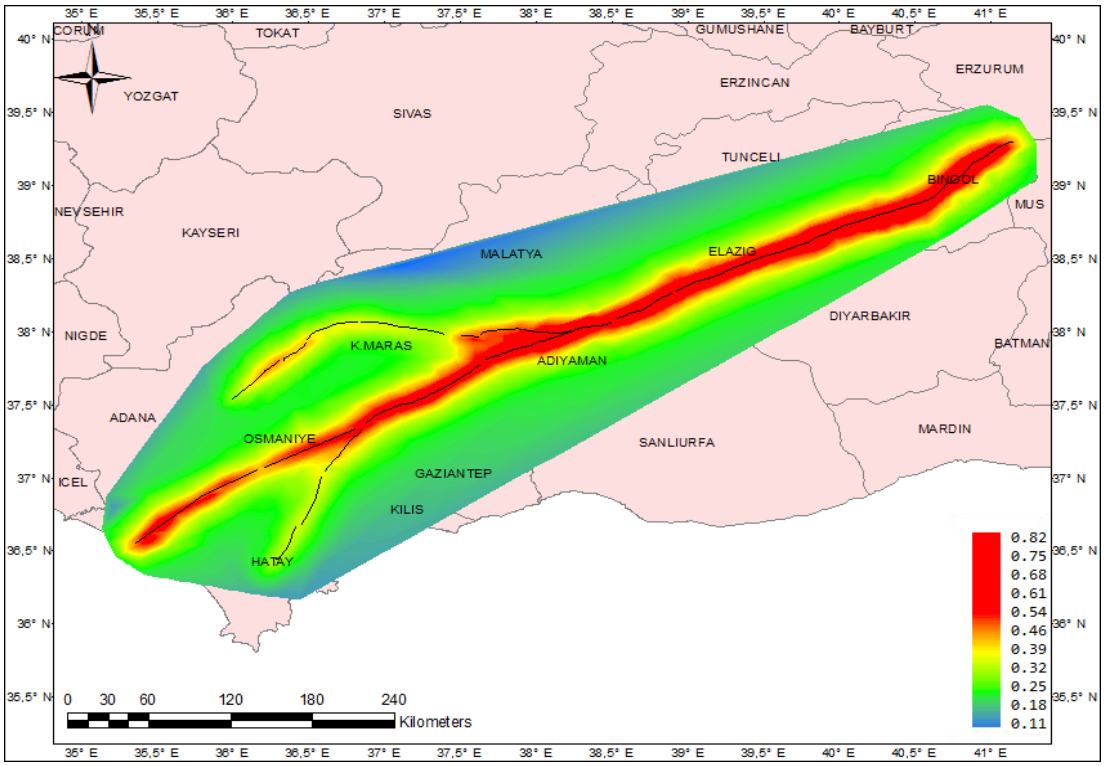


**(b)**

**Figure 4.24: PSHA Map of 475-Year Return Period PGA for Rock 1 Conditions Considering (a) Alternative 1 (b) Alternative 2 for Gökdere Restraining Bend**

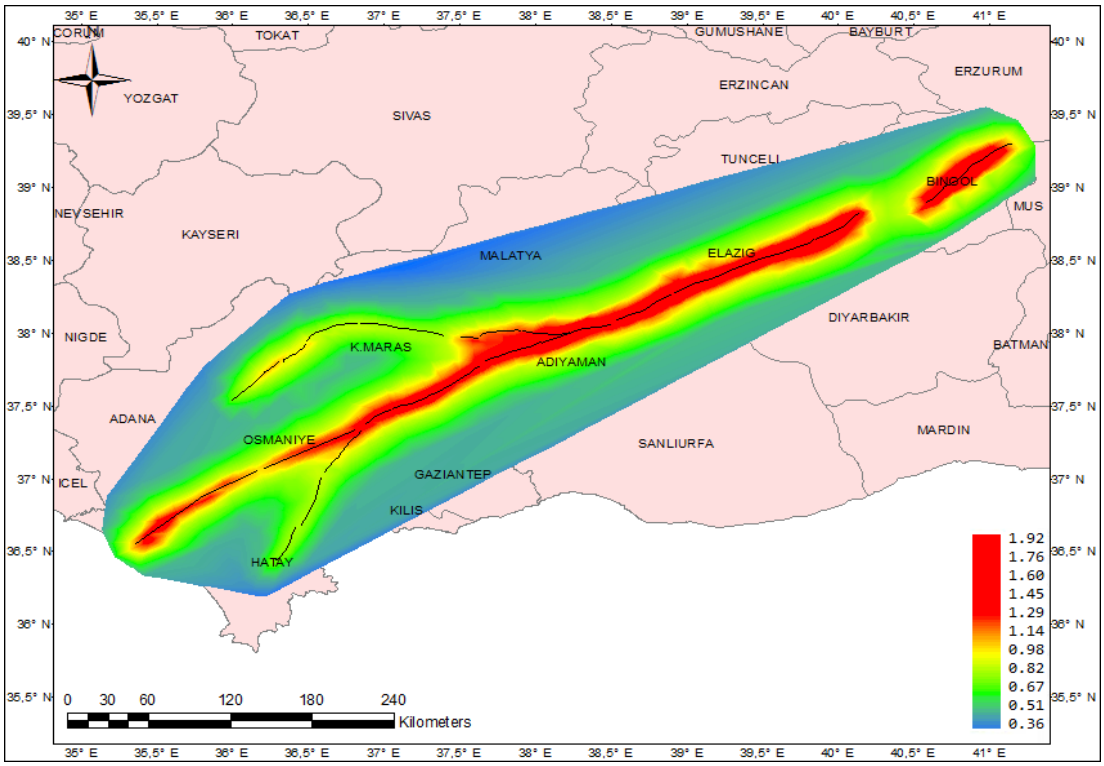


**(a)**

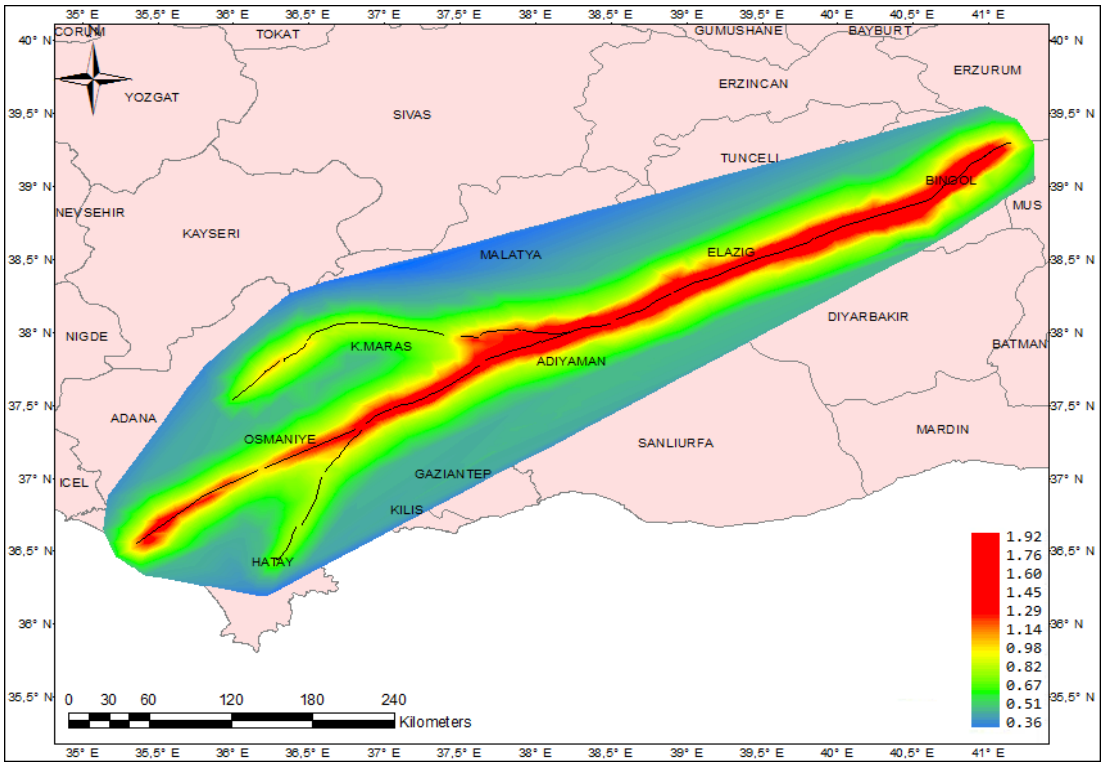


**(b)**

**Figure 4.25: PSHA Map of 475-Year Return Period (T=0.2s) for Rock 1 Conditions Considering (a) Alternative 1 (b) Alternative 2 for Gökdere Restraining Bend**

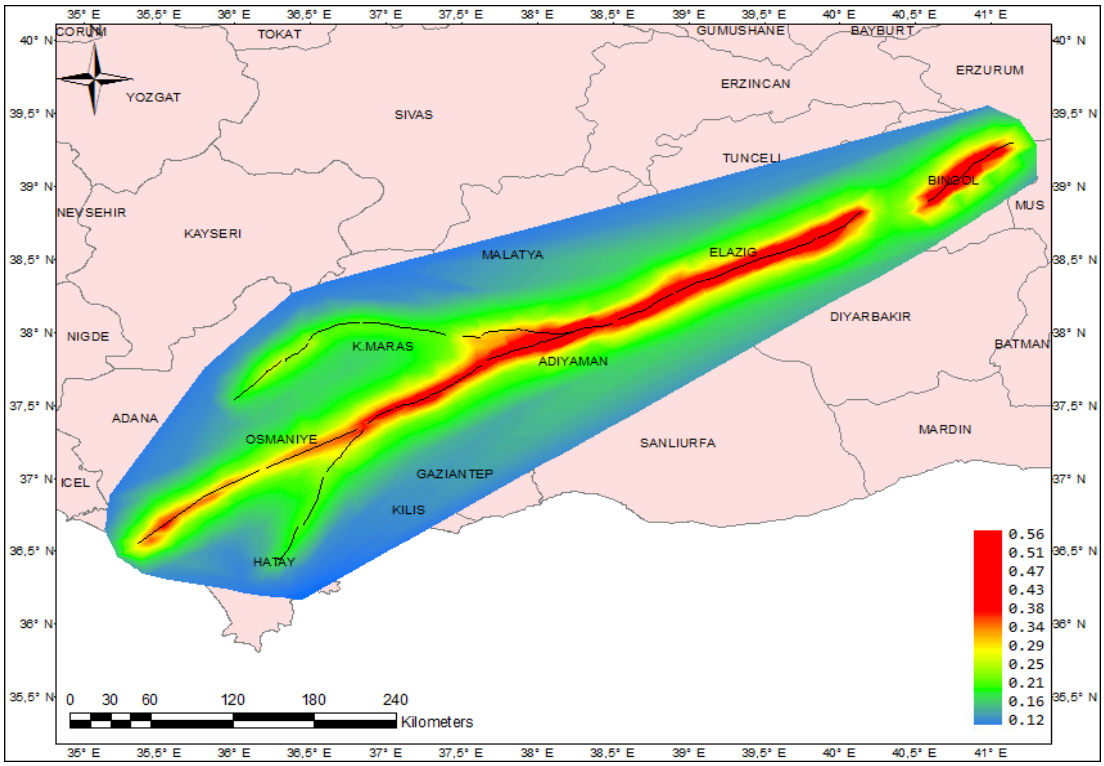


**(a)**

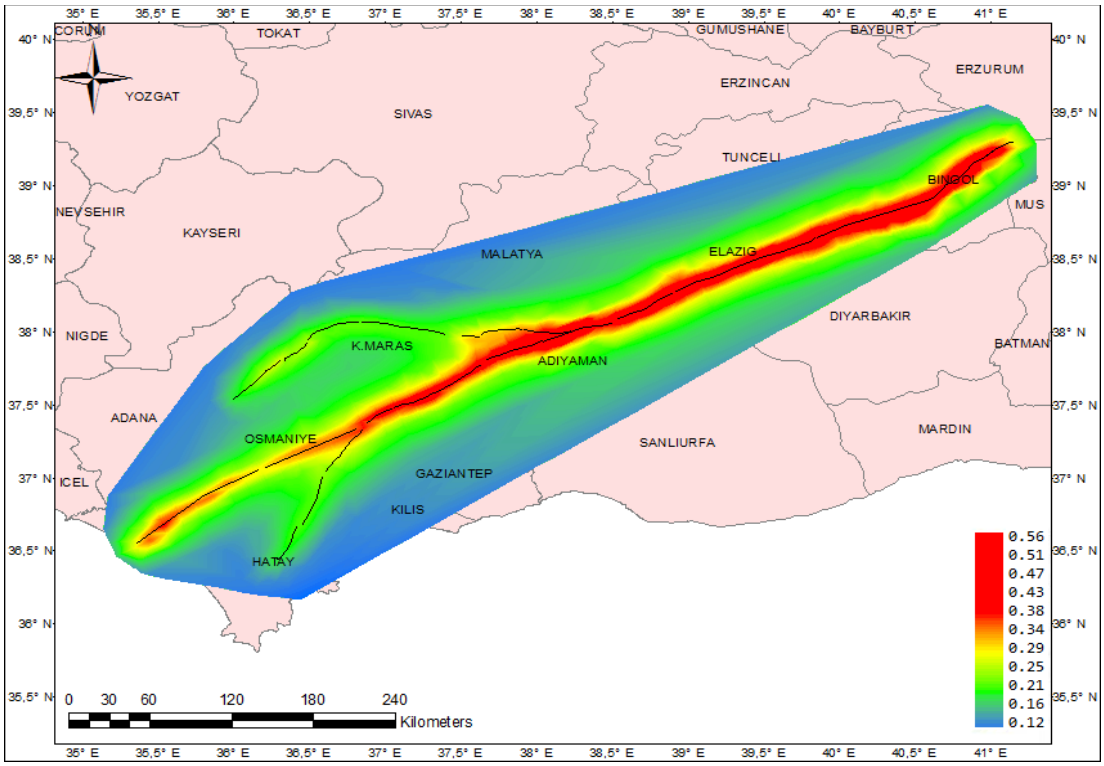


**(b)**

**Figure 4.26: PSHA Map of 475-Year Return Period (T=1.0s) for Rock 1 Conditions Considering (a) Alternative 1 (b) Alternative 2 for Gökdere Restraining Bend**

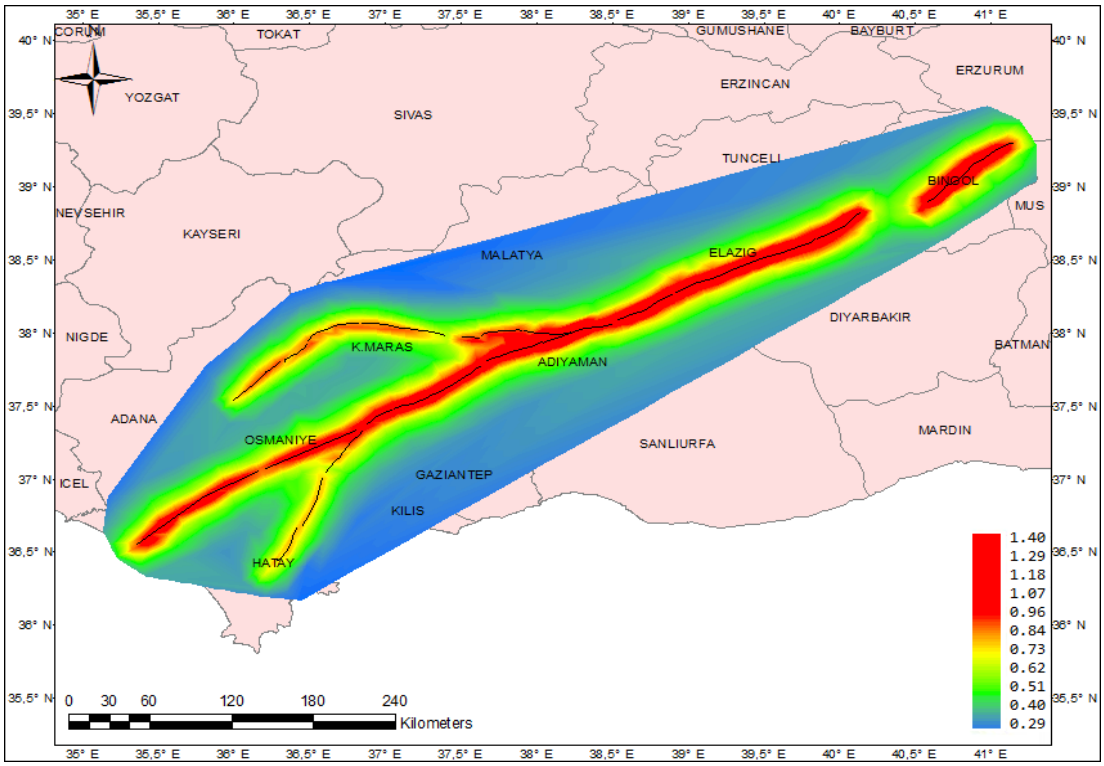


**(a)**

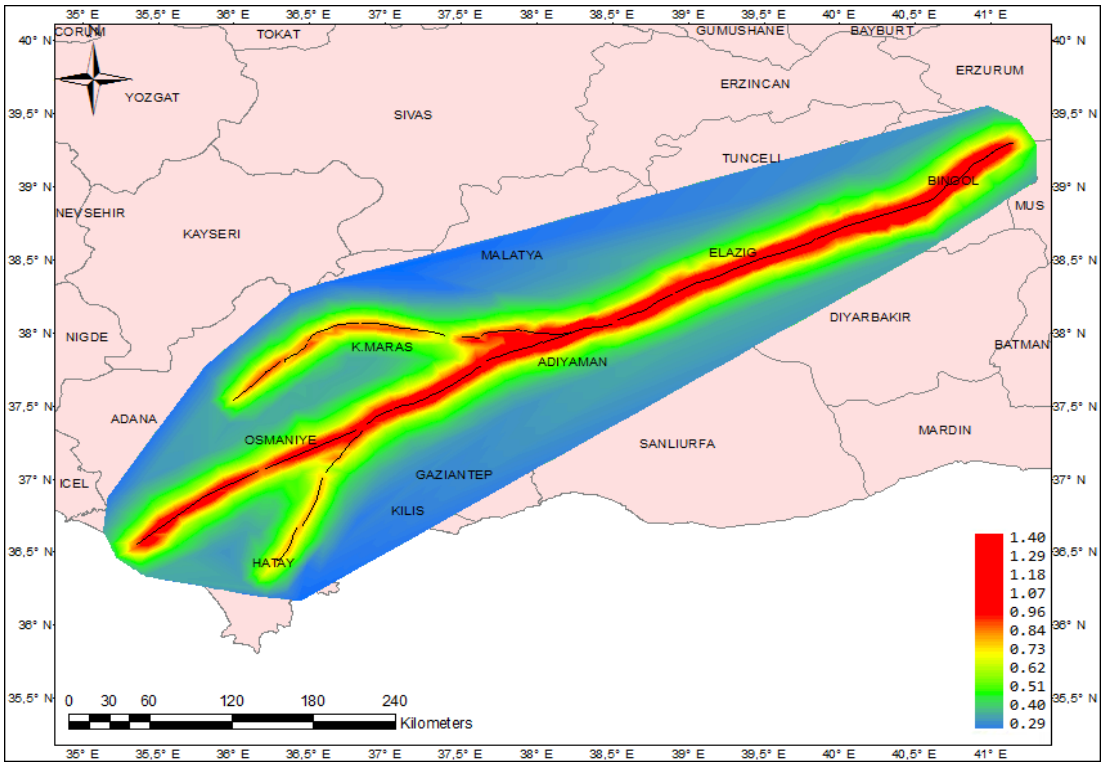


**(b)**

**Figure 4.27: PSHA Map of 2475-Year Return Period (PGA) for Rock 1 Conditions Considering (a) Alternative 1 (b) Alternative 2 for Gökdere Restraining Bend**

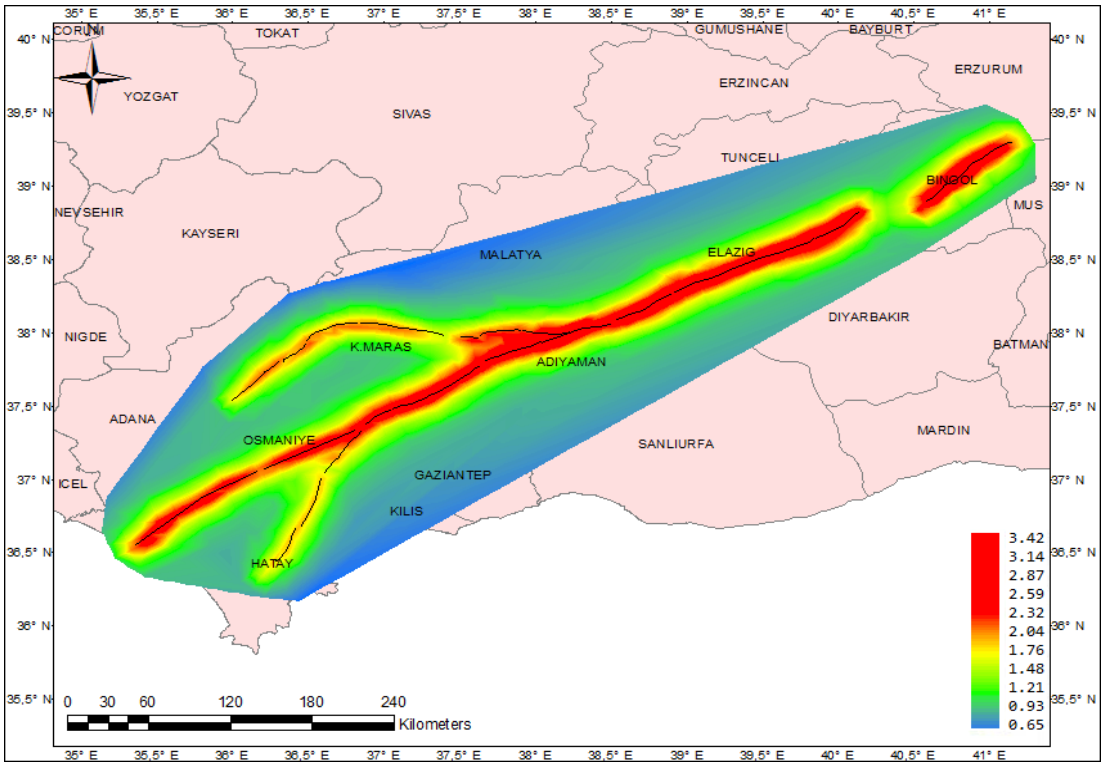


**(a)**

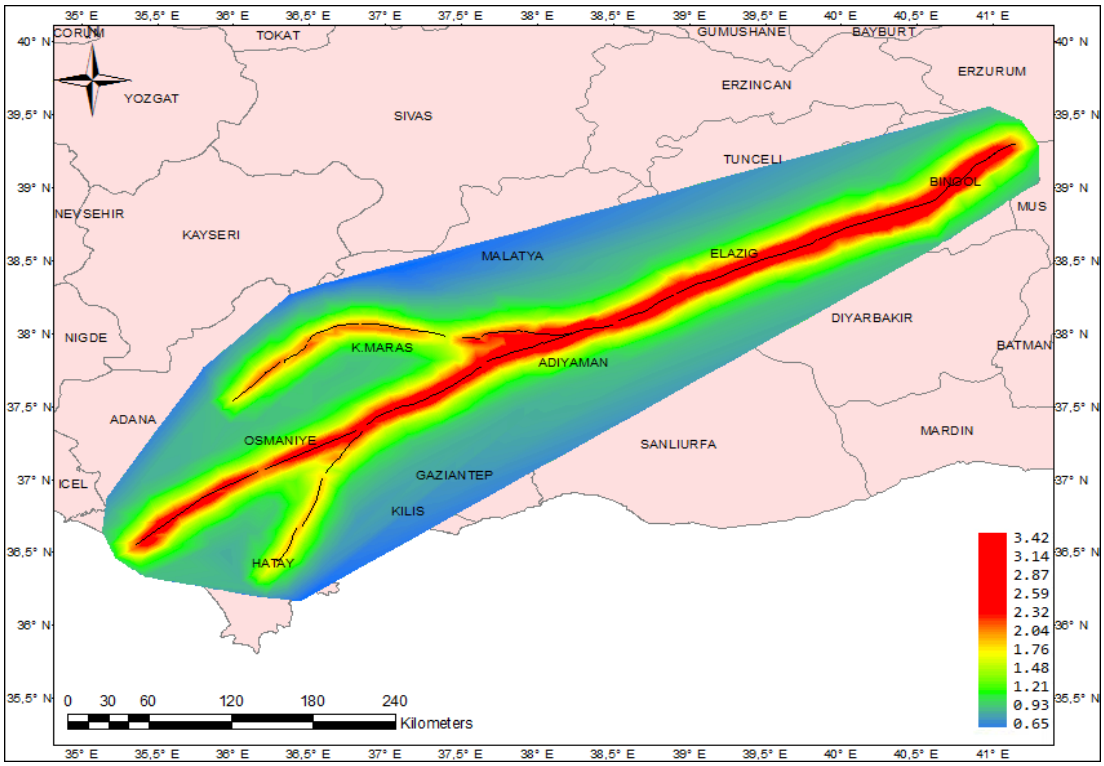


**(b)**

**Figure 4.28: PSHA Map of 2475-Year Return Period (T=0.2s) for Rock 1 conditions Considering (a) Alternative 1 (b) Alternative 2 for Gökdere Restraining Bend**

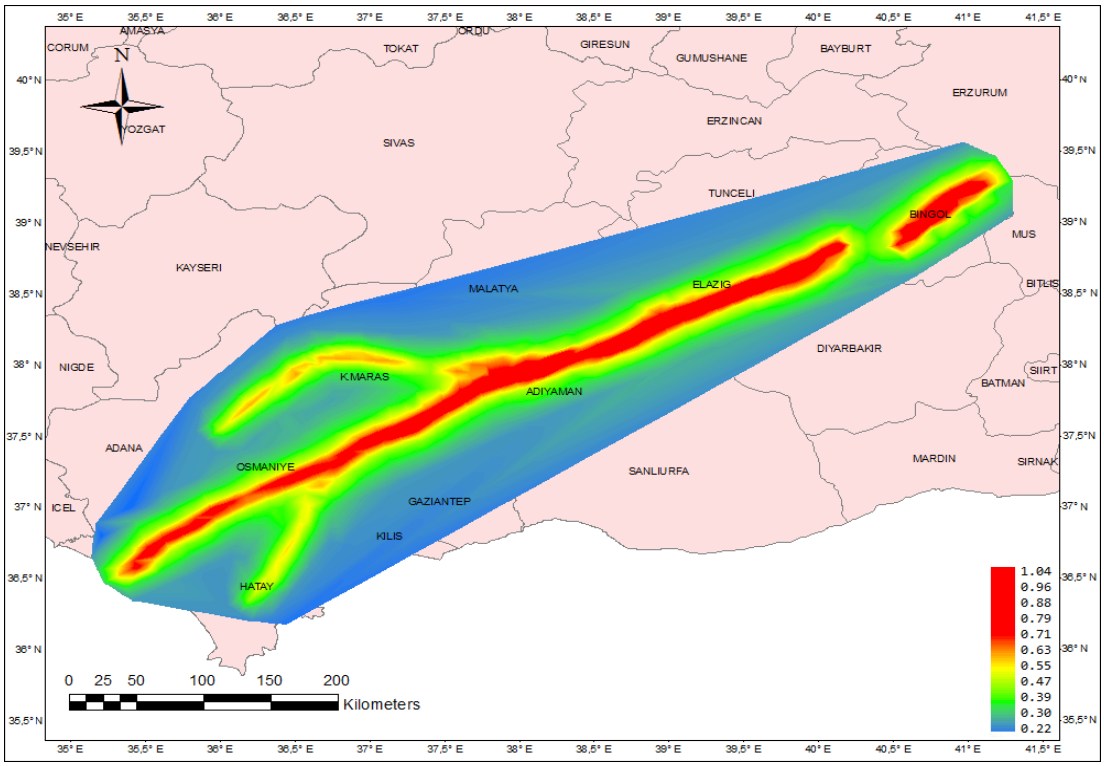


**(a)**

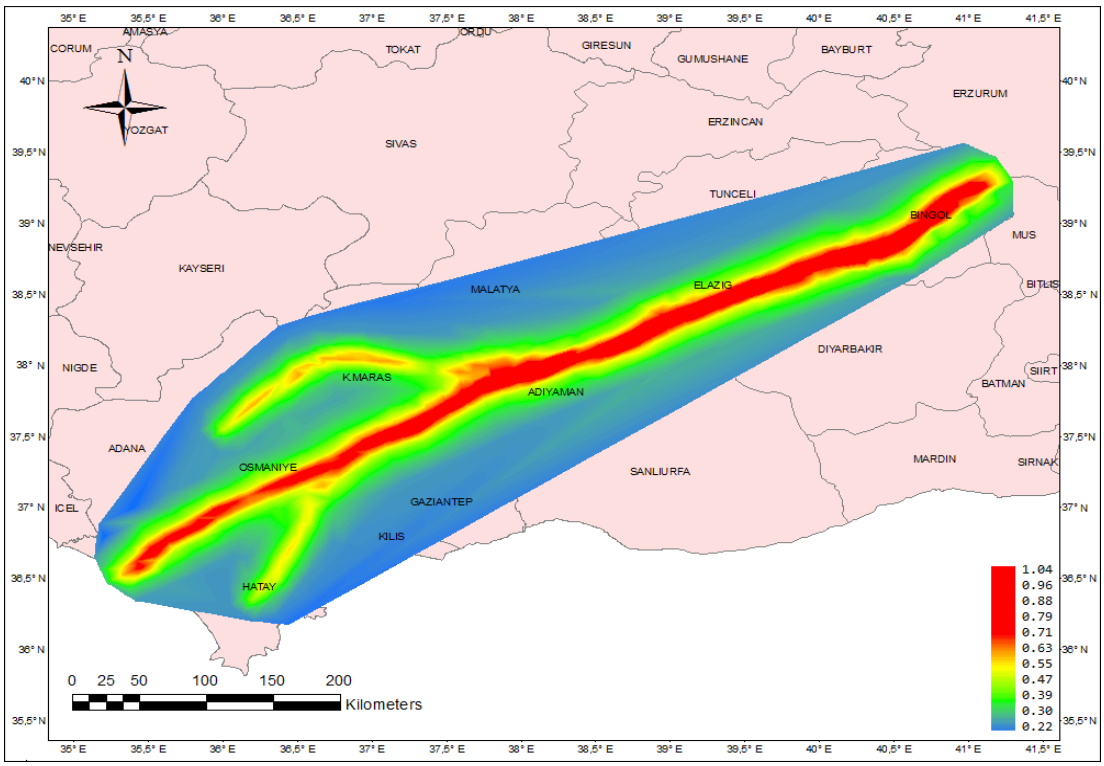


**(b)**

**Figure 4.29: PSHA Map of 2475-Year Return Period (T=1.0s) for Rock 1 Conditions Considering (a) Alternative 1 (b) Alternative 2 for Gökdere Restraining Bend**

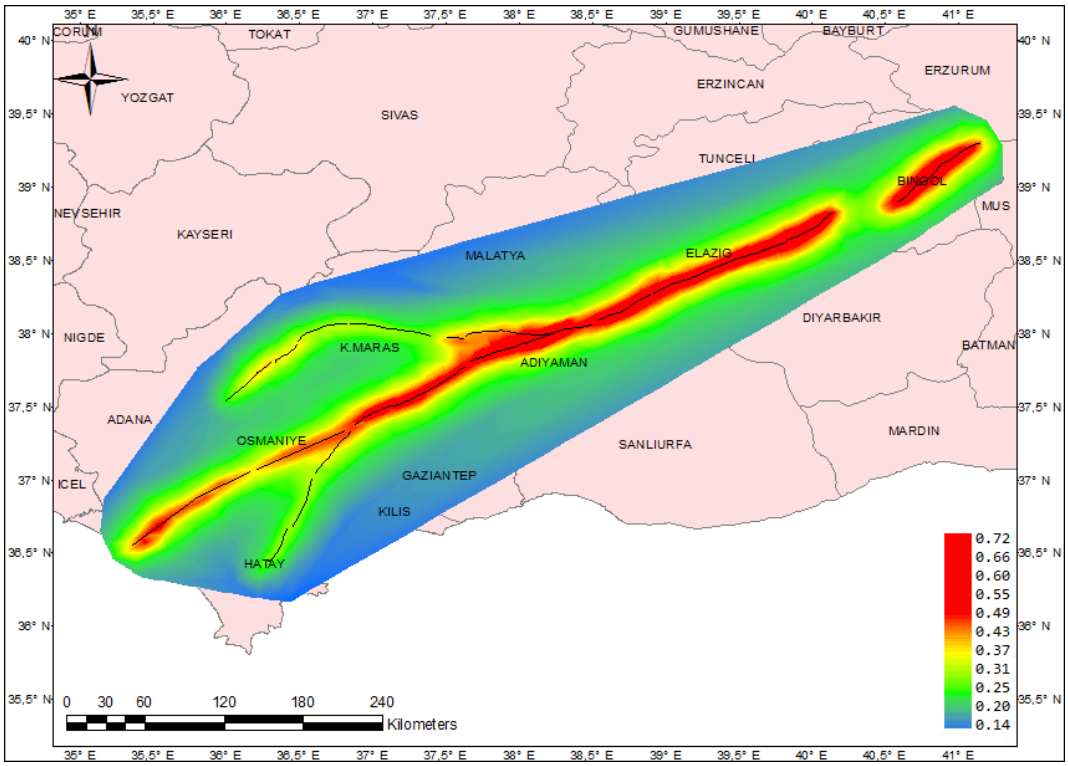


**(a)**

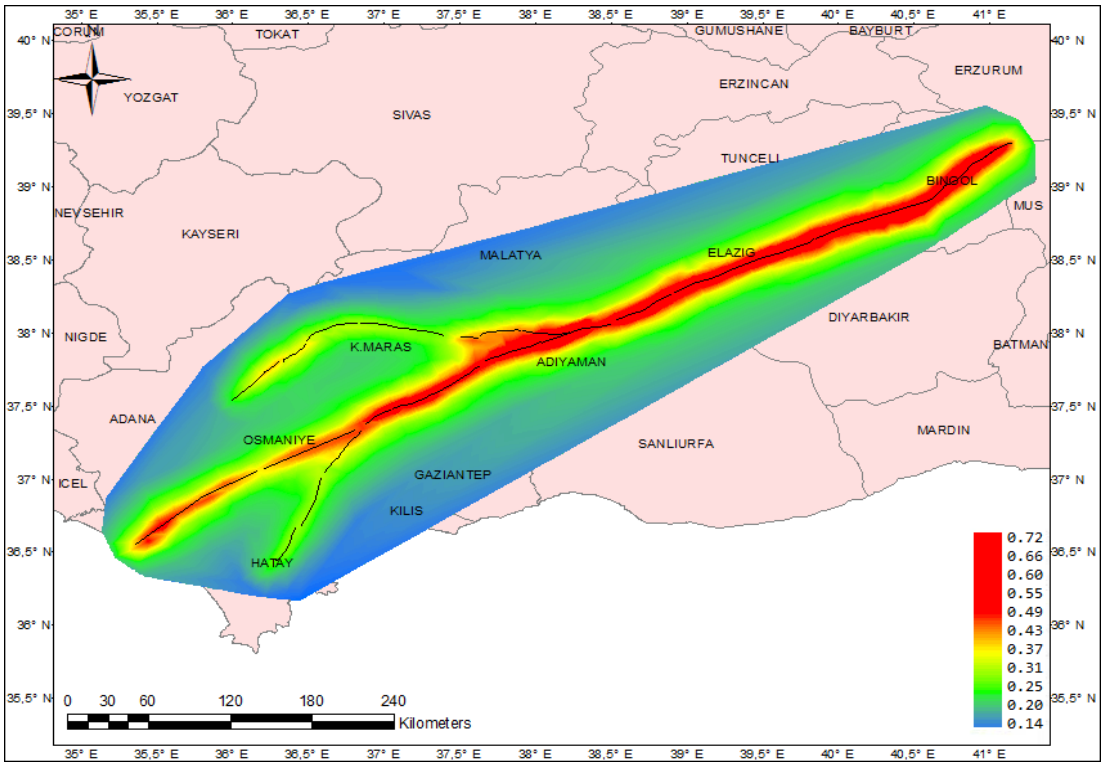


**(b)**

**Figure 4.30: PSHA Map of 475-Year Return Period (PGA) for Rock 2 Conditions Considering (a) Alternative 1 (b) Alternative 2 for Gökdere Restraining Bend**

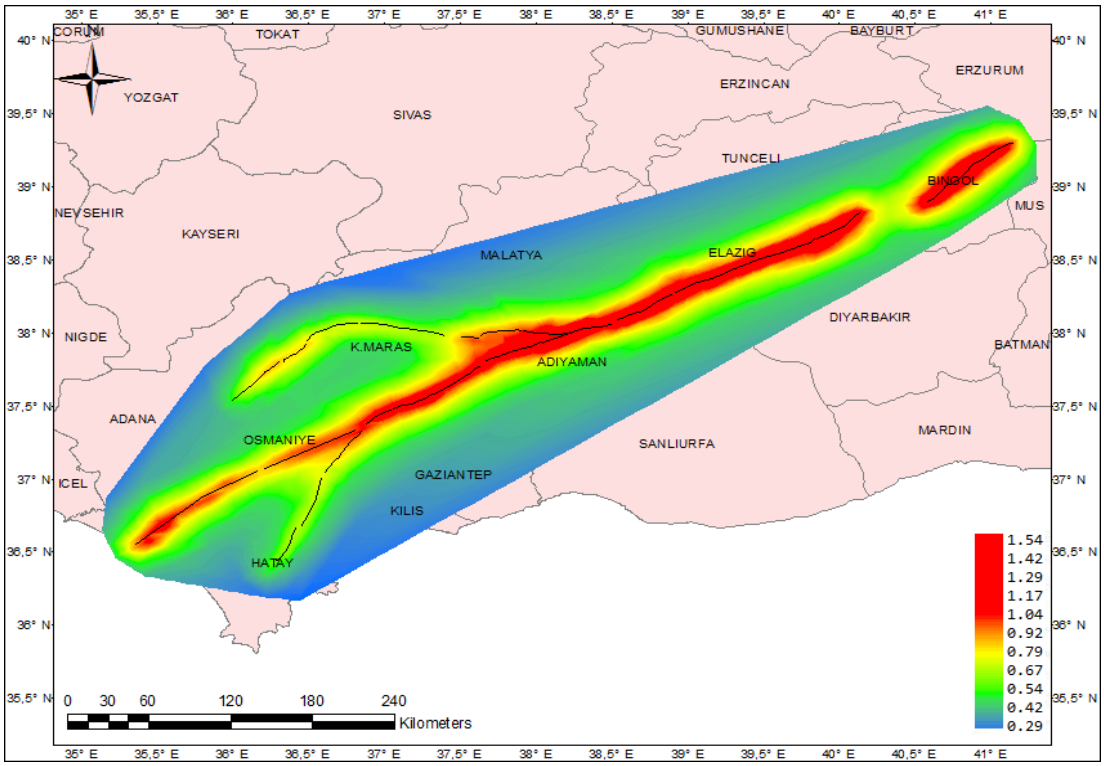


**(a)**

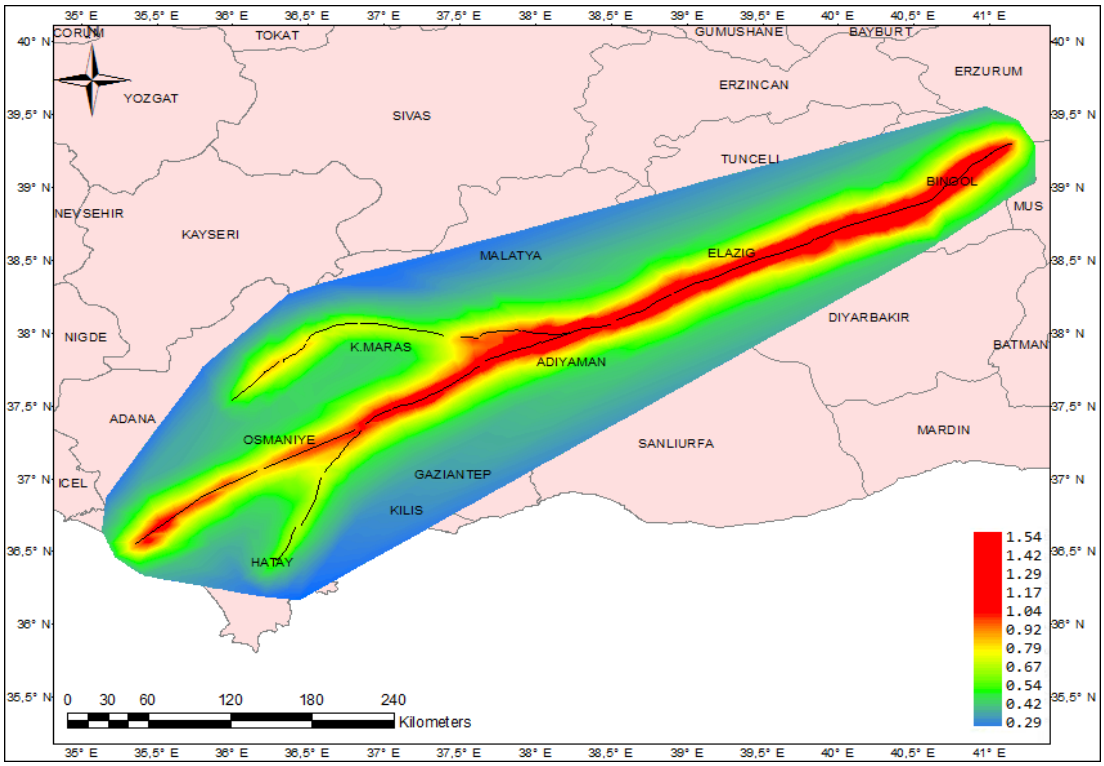


**(b)**

**Figure 4.31: PSHA Map of 475-Year Return Period (T=0.2s) for Rock 2 Conditions Considering (a) Alternative 1 (b) Alternative 2 for Gökdere Restraining Bend**

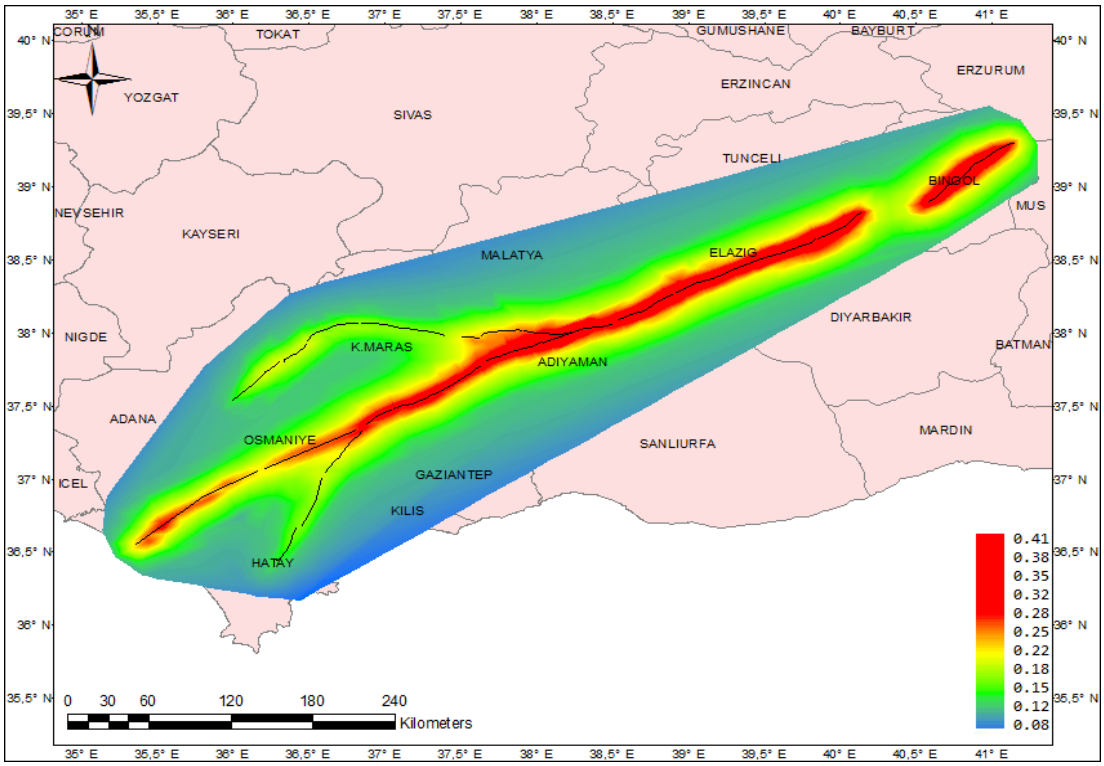


**(a)**

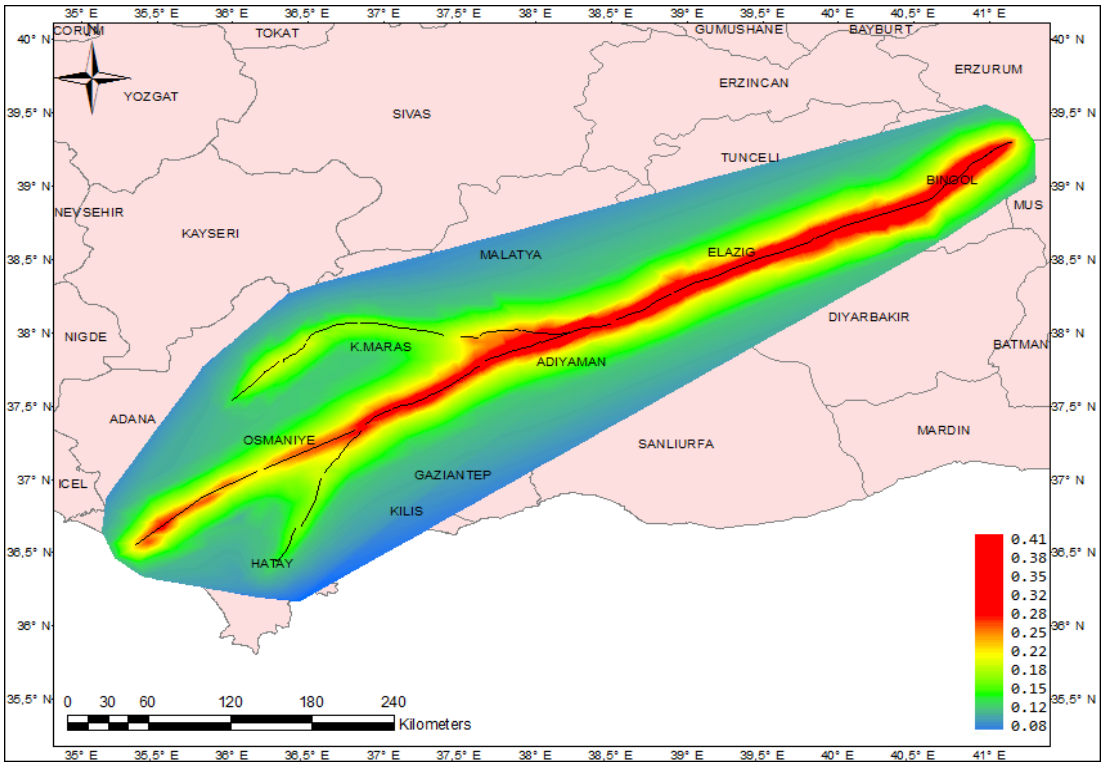


**(b)**

**Figure 4.32: PSHA Map of 475-Year Return Period (T=1.0s) for Rock 2 Conditions Considering (a) Alternative 1 (b) Alternative 2 for Gökdere Restraining Bend**

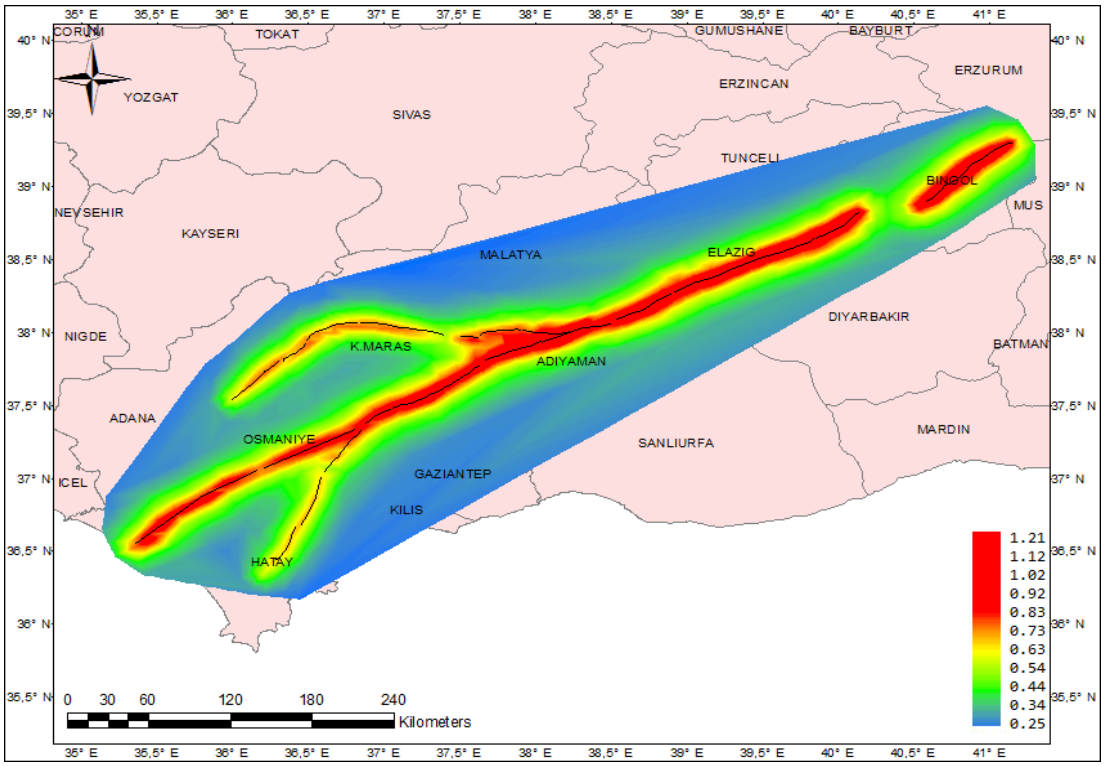


**(a)**

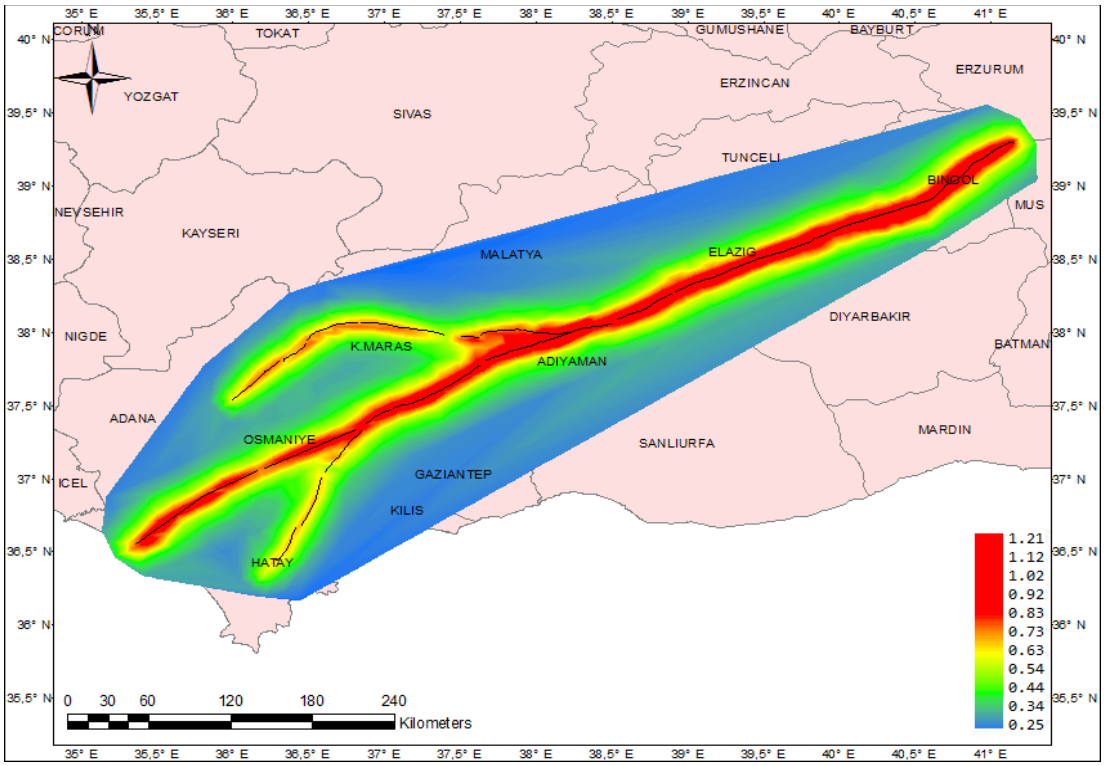


**(b)**

**Figure 4.33: PSHA Map of 2475-Year Return Period (PGA) for Rock 2 Conditions Considering (a) Alternative 1 (b) Alternative 2 for Gökdere Restraining Bend**

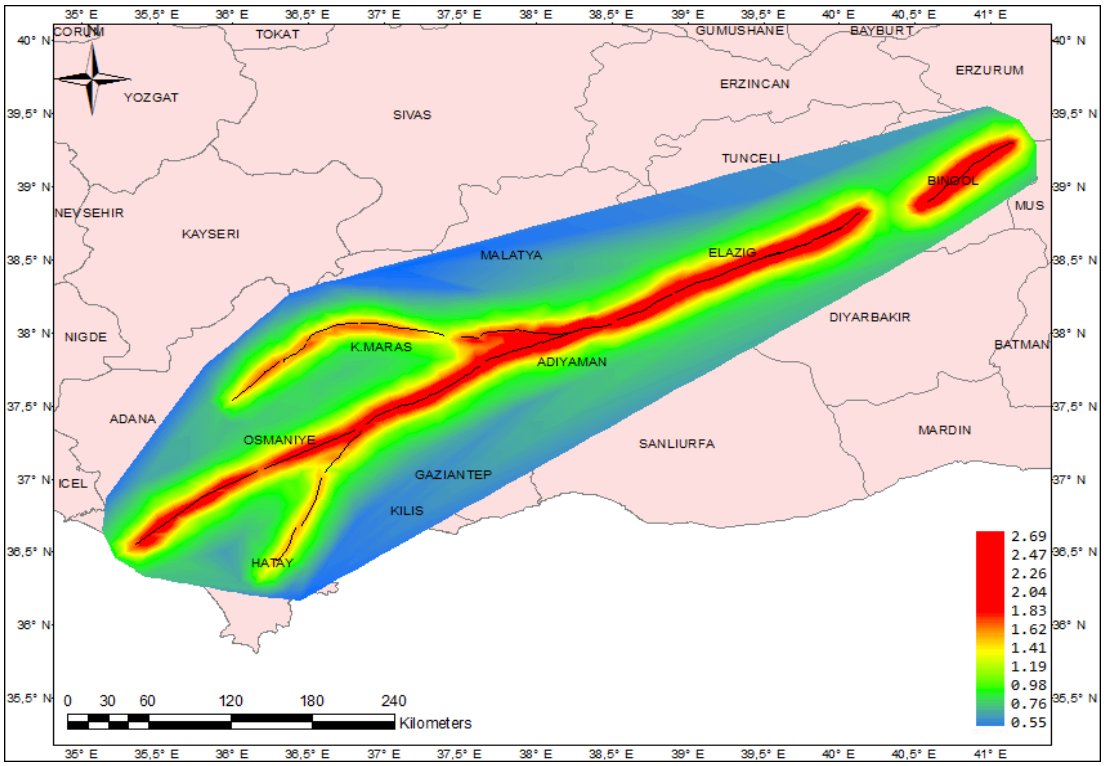


**(a)**

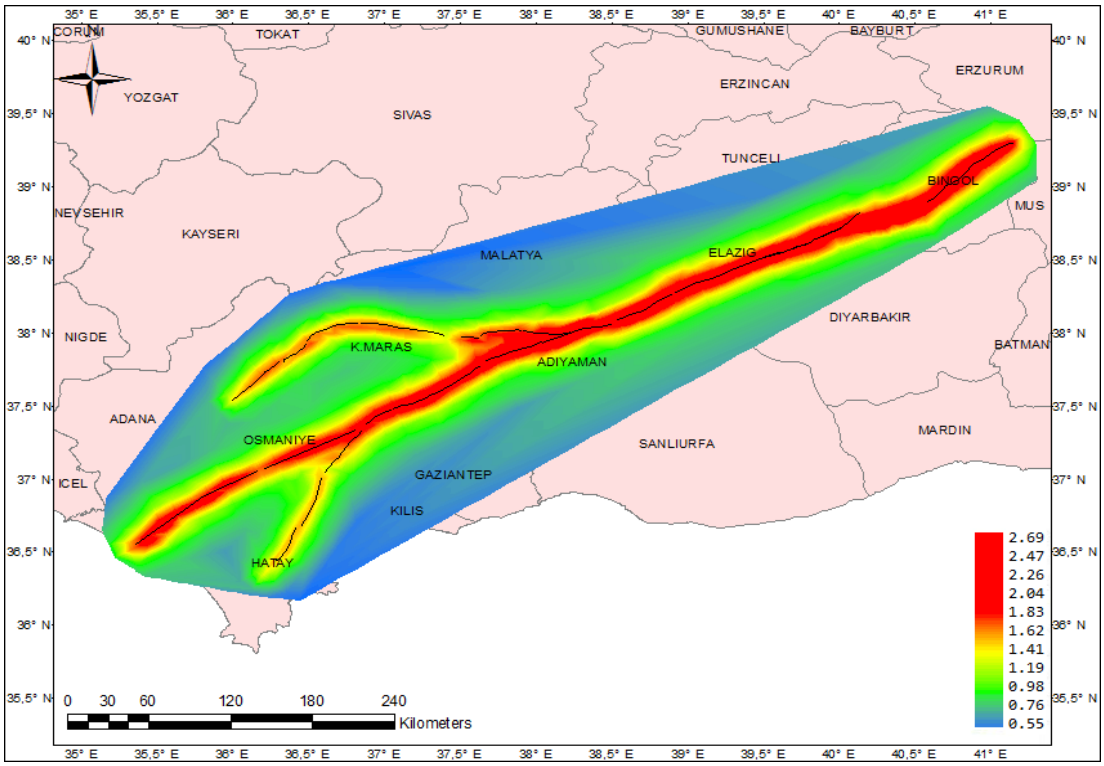


**(b)**

**Figure 4.34: PSHA Map of 2475-Year Return Period (T=0.2s) for Rock 2 Conditions Considering (a) Alternative 1 (b) Alternative 2 for Gökdere Restraining Bend**

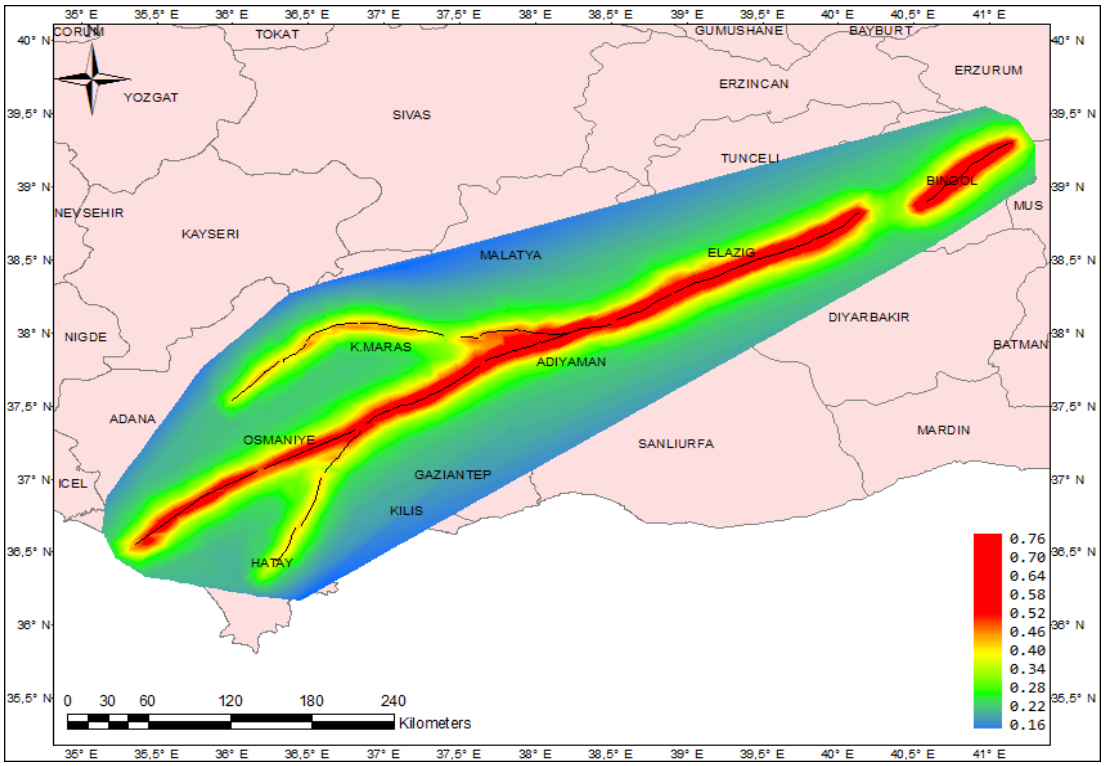


**(a)**

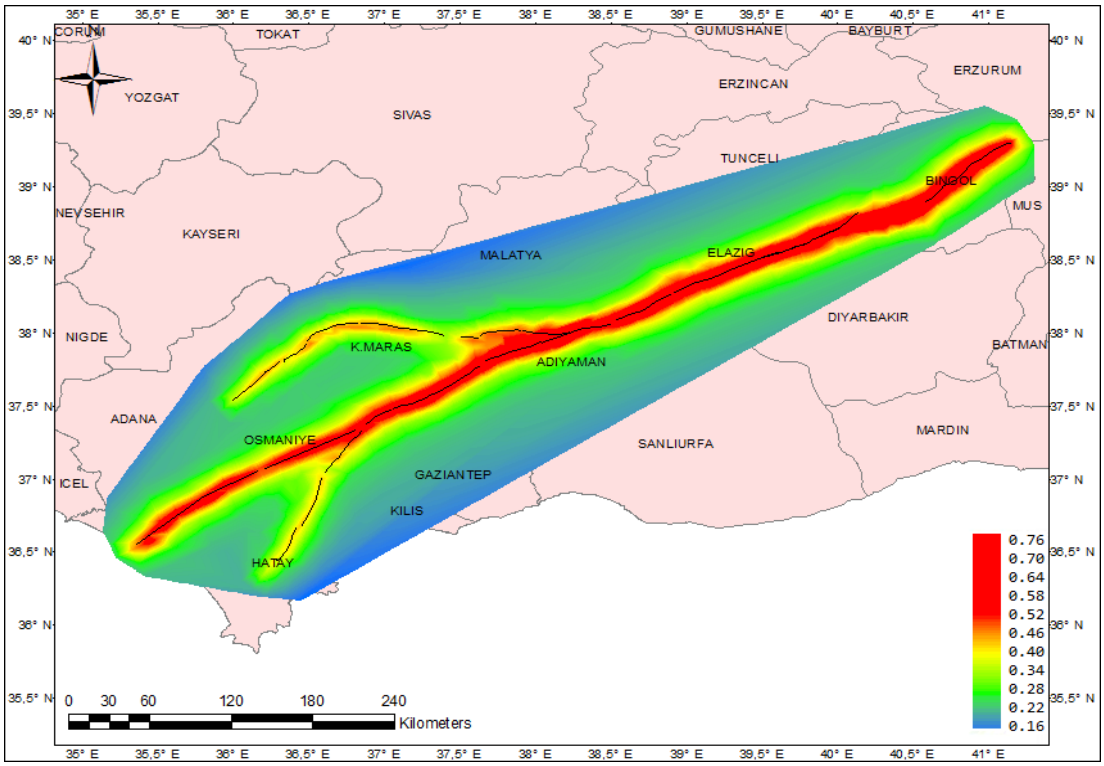


**(b)**

**Figure 4.35: PSHA Map of 2475-Year Return Period (T=1.0s) for Rock 2 Conditions Considering (a) Alternative 2 (b) Alternative 1 for Gökdere Restraining Bend**

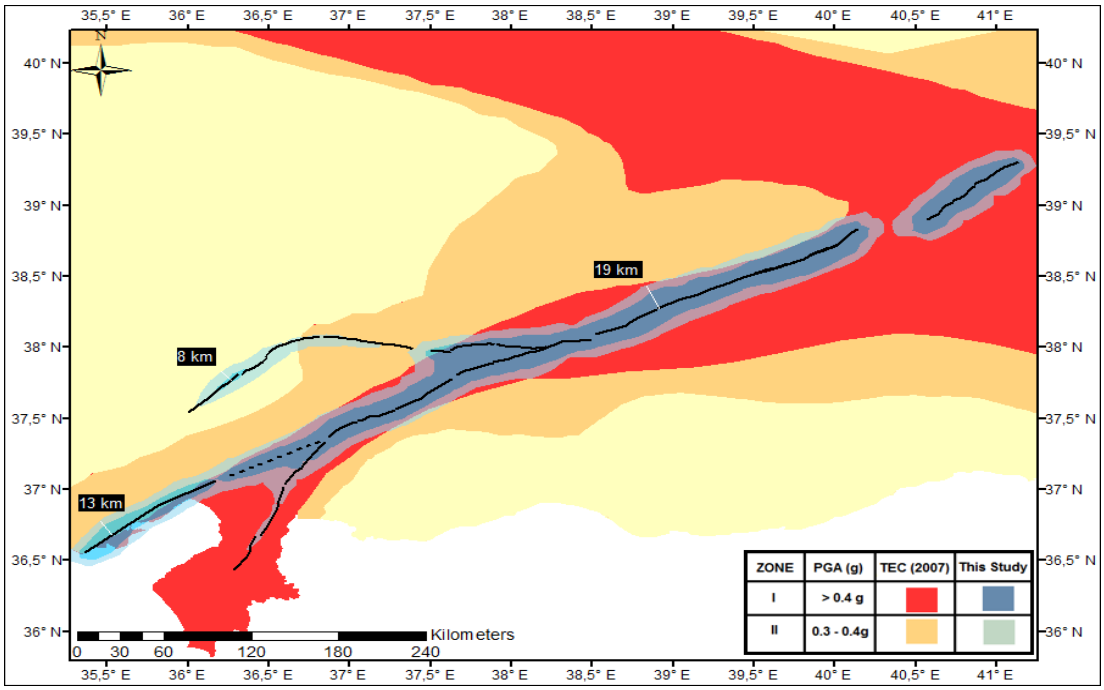


**(a)**

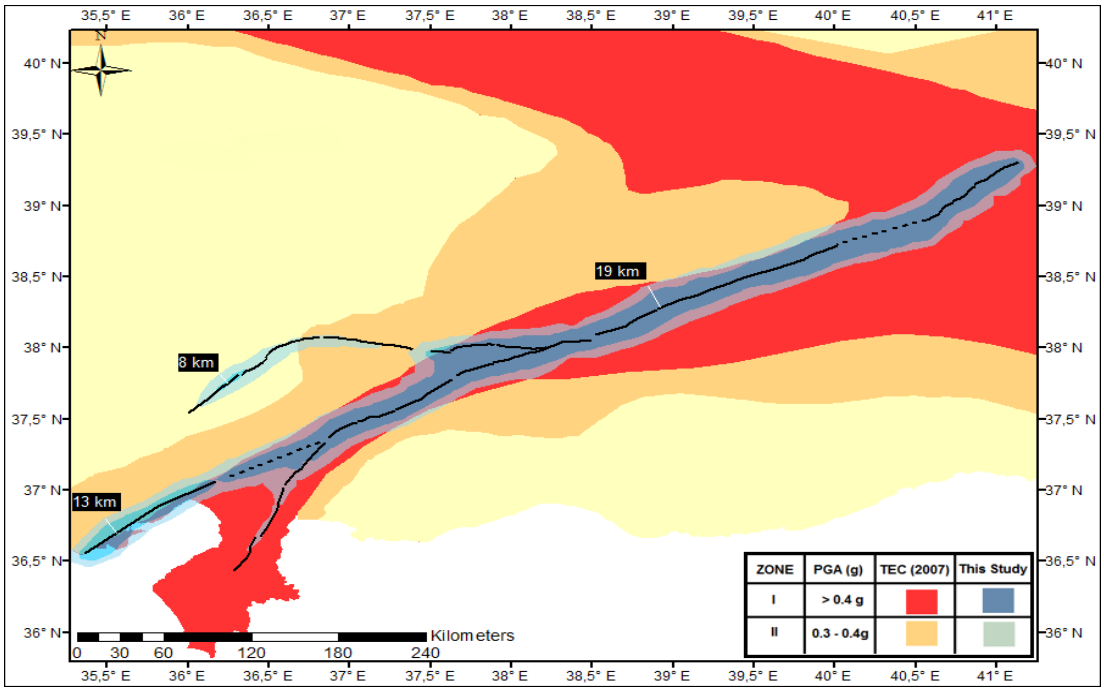


**(b)**

**Figure 4.36: Zone I and II of the TEC- 2007 Zonation Map Overlaid by the Contours of 475-Year Return Period PGA for Rock 1 Conditions Considering (a) Alternative 1 (b) Alternative 2 for Gökdere Restraining Bend**

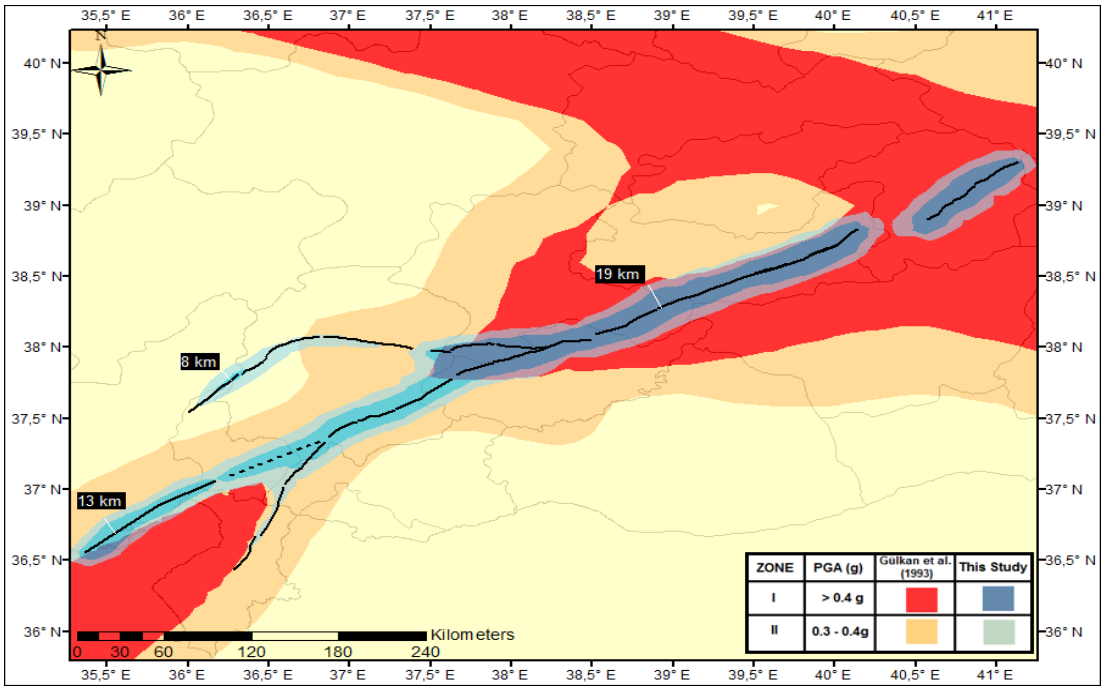


**(a)**

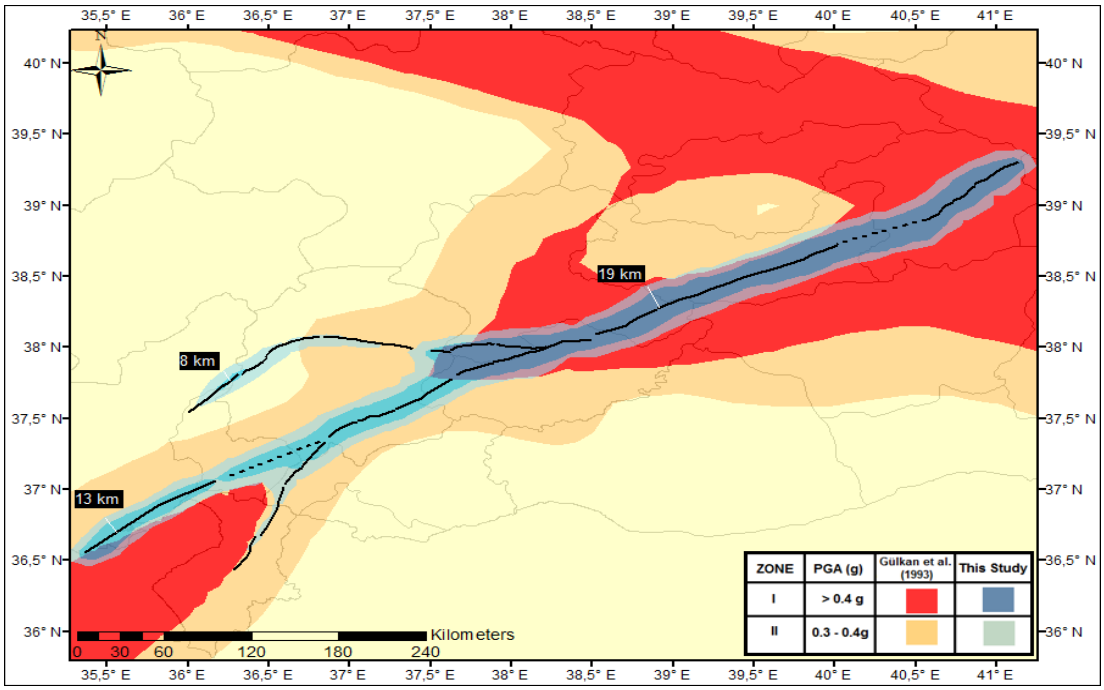


**(b)**

**Figure 4.37: Contours of 475-Year Return Period PGA Values Proposed by Gülkan et al. (1993) Overlaid by the Contours of 475-Year Return Period PGA for Rock 1 Conditions Considering (a) Alternative 1 (b) Alternative 2 for Gökdere Restraining Bend**

## REFERENCES


Aki K (1965) Maximum Likelihood Estimate of b in the Formula log N = a - bM and Its Confidence Limits. Tokyo Univ. Bull. Earthq. Res. Inst 43:237–239.

Akkar, S., and Bommer, J.J.2010. Empirical Equations for the Prediction of PGA, PGV and Spectral Accelerations in Europe, the Mediterranean Region and the Middle East. Seismological Research Letters, 81(2), 195–206.

Akkar, S. and Cagnan, Z., 2010. A Local Ground-motion Predictive Model for Turkey and its Comparison with Other Regional and Global Ground-motion Models. Bulletin of the Seismological Society of America 100, 2978-2995.

Akkar, S., Cagnan, Z., Yenier, E., Erdogan, E., Sandikkaya, M.A., Gulkan, P., 2010. The Recently Compiled Turkish Strong-motion Database: Preliminary Investigation for Seismological Parameters, Journal of Seismology, 14, 457-479.

Aksu, A. E., T. J. Calon, D. J. W. Piper, S. Turgut, and E. Izdar, Architecture of Late Orogenic Quaternary Basins in Northeastern Mediterranean Sea, Tectonophysics,210, 191 – 213, 1992a.

Aksu, A. E., A. Ulug, D. J. W. Piper, Y. T. Konuk, and S. Turgut, Quaternary Sedimentary History of Adana, Cilicia and Iskenderun Basins: Northeast Mediterranean Sea, Mar. Geol., 104, 55 – 71, 1992b.

Al-Tarazi, E., Rajab, J.A., Gomez, F., Cochran, W., Jaafar, R., Ferry, M., 2011. GPS Measurements of Near-field Deformation along the southern Dead Sea Fault System. Geochemistry, Geophysics, Geosystems 12, Q12021.

Alchalbi, A., Daoud, M., Gomez, F., McClusky, S., Reilinger, R., Romeyeh, M.A., Alsouod, A., Yassmin, R., Ballani, B., Darawcheh, R., 2010. Crustal Deformation in Northwestern Arabia from GPS Measurements in Syria: Slow Slip Rate along the Northern Dead Sea Fault. Geophysical Journal International 180, 125–135.

Alptekin Ö (1978) Magnitude–Frequency Relationships and Deformation Release for the Earthqukes in and around Turkey. Thesis for Promoting to Associate Professor Level, Karadeniz Technical University,107.

Ambraseys, N. N., Temporary Seismic Quiescence: SE Turkey, Geophys. Journal, 96, 311–331, 1989.

Ambraseys, N. N. and M. Barazangi, The 1759 Earthquake in the Bekaa Valley: Implications for Earthquake Hazard Assessment in the Eastern Mediterranean region, J. Geophys. Res., 94, 4007–4013, 1989.

Ambraseys, N. N. and C. P. Melville, Historical Evidence of Faulting in Eastern Anatolia and Northern Syria, Ann. Geophys., 38, 337–344, 1995.

Ambraseys, N. N. and Jackson, J. A. 1998. Faulting Associated with Historical and Recent Earthquakes in the Eastern Mediterranean Region. Geophysical Journal International, 133, 390–406.

Ancheta, T. D., Darragh, R. B., Stewart, J. P., Seyhan, E., Silva, W. J., Chiou, B. S. J., Wooddell, K. E., Graves, R. W., Kottke, A. R., Boore, D. M., Kishida, T., Donohue, J. L., 2014, PEER NGA-West2 Database. Earthquake Spectra, EERI, Pre-Print.

Arger J., Michell J. And Westeway R. 1996. Neogenea and Quaternary Volcanism in Eastern Turkey: Potassium-Argon Dating and Its Tecronic Implications. Technoscience. Newcastle Upon Tyne. UK. Open-File Science Reports. 1996/1.

Arpat, A. E. 1971. 22 Mayıs, 1971 Bingöl Depremi-Ön Rapor. Institute of Mineral Research and Exploration Report 4697.

Arpat, E. ve Şaroğlu, F., 1972. Doğu Anadolu Fayı ile İlgili Bazı Gözlemler ve Düşünceler. Maden Tetkik Ve Arama Enstitüsü. Ankara Ss:44-50.

Arpat, E. and Şaroğlu, F., 1975 Some Recent Tectonic Events in Turkey Bull. Geol. Soc. Turkey18 91–101.

Aslan, E., Tezucan, L. & Bhth, M., 1975. An Earthquake Catalogue for Turkey for The Interval 1913-1970. Common Report No. 7-75 Of Kandilli Observatory, Turkey and Seismic Institute, Uppsala, Sweden.

Atakan, K., Ojeda, A., Meghraoui, M., Barka, A.A., Erdik, M. And Bodare, A., (2002). Seismic Hazard in Istanbul Following The 17 August 1999 Izmit and 12 November 1999 Düzce Earthquakes, Bulletin of The Seismological Society of America, 92, 466-482.

Atkinson, G. M., And Boore, D. M., 2011. Modifications to Existing Ground-Motion Prediction Equations in Light of New Data, Bull. Seismol. Soc. Am. 101, 1121–1135.

Barka, A. A. And Kadinsky-Cade, K., 1988. Strike-Slip Fault Geometry in Turkey and Its Influence on Earthquake Activity. Tectonics, Vol.7, No.3, Pp. 663-684, June 1988.

Bayrak E., Yılmaz Ş., Softa M., Türker T., Bayrak Y. Earthquake Hhazard Analysis for East Anatolian Fault Zone, Turkey (2014). Nat Hazards doi: 10.1007/s11069-014-1541-5.

Bazzurro, P., and Cornell, C. A. (1999). Disaggregation of Seismic Hazard. Bulletin of the Seismological Society of America, 89(2), 501-520.

Bender and Perkins, 1987 B. Bender, D.M. Perkins SEISRISK 3: A Computer Program for Seismic Hazard Estimation US Geol. Surv. Bull. (1987), P. 48.

Bertrand S., Meghraoui M., Mcclusky S., Altunel E., Ergintav S. and Reilinger R. Present-Day Crustal Motions at The Triple Junction Between the Dead Sea Fault, The East Anatolian Fault and The Cyprus Arc (SE Turkey) Geophysical Research Abstracts, Vol. 8, 10004, 2006 Sref-ID: 1607-7962/Gra/EGU06-A-10004 © European Geosciences Union 2006.

Biricik, A.S.,1994, Gölbaşı Depresyonu. Türk Coğrafya Dergisi,29, 53-81

Bommer, J. J., Stafford P., And Akkar S., 2010. Current Empirical Ground Motion Prediction Equations for Europe and Their Application to Eurocode 8, Bull. Earthq. Eng. 8, 5–26.

Bommer, J.J., J. Douglas, F. Scherbaum, F. Cotton, H. Bungum and D. Fäh., 2010. On The Selection of Ground-Motion Prediction Equations for Seismic Hazard Analysis. Seismological Research Letters, 81(5), 794-801.

Bonilla, M. G., Mark, R. K., And Lienkaemper, J. J. (1984). Statistical Relations Among Earthquake Magnitude, Surface Rupture Length, And Surface Fault Displacement, Bull. Seism. Soc. Am., 74, 2379-241.

Boore, D. M., W. B. Joyner, And T. E. Fumal (1997). Equations for Estimating Horizontal Response Spectra and Peak Acceleration from Western North American Earthquakes: A Summary of Recent Work, Seism. Res. Letters 68, 128-153.

Bozorgnia, Y. and 31 other authors, 2014. NGA-West 2 research project, Earthquake Spectra, 30, 973-987

Bradley, B. A., 2013. A New Zealand-Specific Pseudospectral Acceleration Ground-Motion Prediction Equation for Active Shallow Crustal Earthquakes Based on Foreign Models, Bull. Seismol. Soc. Am. 103, 1801–1822.

Bulut, F., Y. Ben-Zion, and M. Bohnhoff (2012), Evidence for a Bimaterial Interface along the Mudurnu Segment of the North Anatolian Fault Zone from polarization analysis of P waves, Earth Planet. Sci. Lett., 327, 17 –22.

Campbell, K. W. (1997). Empirical Near-Source Attenuation Relationships for Horizontal and Vertical Components of Peak Ground Acceleration, Peak Ground Velocity, And Pseudo-Absolute Acceleration Response Spectra, Seismol. Res. Lett. 68, 154–179.

Campbell, K. W., 2011. Ground Motion Simulation Using the Hybrid Empirical Method: Issues and Insights, In Earthquake Data in Engineering Seismology, S. Akkar, P. Gülkan, And T. Van Eck (Editors.), Geotechnical, Geological, And Earthquake Engineering 14, Chapter 7, Springer, Berlin, 81–95.

Cauzzi, C., and E. Faccioli (2008), Broadband (0.05 s to 20 s) Prediction of Displacement Response Spectra Based on Worldwide Digital Records, J. Seismol., Vol.12, No. 4, pp. 453-475.

Çetin, H., Güneyli, H. and Mayer, L. 2003. Paleoseismology of the Palu-Lake Hazar Segment of the East Anatolian.

Chiou, B. S.-J., and Youngs, R. R. 2008. An NGA Model for The Average Horizontal Component of Peak Ground Motion and Response Spectra. Earthquake Spectra, 24(1), 173–215.

Chiou, B. S.-J., Youngs, R. R., Abrahamson, N. A., and Addo, K., 2010. Ground Motion Attenuation Model for Small to Moderate Shallow Crustal Earthquakes in California and Its Implications on Regionalization of Ground Motion Prediction Equations, Earthquake Spectra 26, 907–926.

Chorowicz, J., Luxey, P., Lyberis, N., Carvalho, J., Parrot, J.F., Yürür, T. and Gündoğdu, N., 1994. The Maraş Triple Junction (Southern Turkey) Based on Digital Elevation Model and Satellite Imaginery Interpretation. Journal of Geophysical Research, 99, 20225-20242.

Cornell, C.A.: Engineering Seismic Risk Analysis. Bulletin of the Seismological Society of America 58 (5), 1583-1606, 1968.

Cornell, C. A., 1971. Bayesian Statistical Decision Theory and Reliability Based Design. In Freudenthal, A. M. (Ed.), Proceedings of the International Conference on Structural Safety and Reliability, April 9-11, 1969. Smithsonian Institute: Washington D.C., Pp. 47-66.

Crowley, H. and Bommer, J.J. 2006. Modelling Seismic Hazard in Earthquake Loss Models with Spatially Distributed Exposure. Bulletin of Earthquake Engineering 4(3): 249–273.

Demirtaş, R., Yılmaz, R., 1996. Seismotectonics of Turkey: Preliminary Approach to Earthquake Forecasting Based on Long-Term Variations in Seismic Activity and Present Seismicity. Republic of Turkey Ministry of Public Works and Settlement, Ankara. 95 Pp.

Dewey J.F., Hempton M.R., Kidd W.S.F., Saroglu F., Sengör A.M.C. 1986 Shortening of Continental Lithosphere: The Neotectonics of Eastern Anatolia - A Young Collision Zone Incollision Tectonics Eds 19 3–36.

Duman. T.Y. and Emre Ö (2013). The East Anatolian Fault: Geometry, Segmentation and Jog Characteristics Geological Society, London, Special Publications.

Emre, Ö., Duman, T. Y., Özalp, S. and Elmacı, H. (2010). 8 Mart 2010 Başyurt-Karakoçan (Elazığ) Depremi Değerlendirme Raporu. Institute of Mineral Research and Exploration Report 11298.

Emre, Ö., Duman, T.Y., Duman, Ş., Özalp, S. 2012. Türkiye Diri Fay Haritası (Yenilenmiş), Maden Tetkik ve Arama Yayınları, Ankara.

Emre, Ö., Duman.T.Y., Özalp, S., Elmacı, H., Olgun, Ş., Şaroğlu, F., 2013. Türkiye Diri Fay Haritası. Maden Tetkik ve Arama Genel Müdürlüğü, Özel Yayın Serisi-30. Ankara-Türkiye.

Erdik, M., V. Doyuran, N. Akkas and P. Gulkan (1985). A Probabilistic Assessment of the Seismic Hazard in Turkey. Tecthonophysics, 117, 295-344.

Erdik, M., Alpay, B. Y., Onur, T., Sesetyan, K., And Birgoren, G., 1999, Assessment of Earthquake Hazard in Turkey and Neighboring Regions, Annali Di Geofisica, 42, 1125- 1138.

Erdik, M., Demircioglu, M., Sesetyan, K., Durukal, E. And Siyahi, B., (2004). Earthquake Hazard in Marmara Region, Turkey, Soil Dynamics and Earthquake Engineering, 24, 605-631.

Ergin, K., U. Guclu, And Z. Uz, A Catalogue of Earthquakes for Turkey and Surrounding Area (11AD to 1964AD), Tech. Univ. Mining Eng. Fac.Publ., 24, 189, 1967.

Fletcher, J. M., O. J. Teran, T. K. Rockwell, M. E. Oskin, K. W. Hudnut, K. J. Mueller, 378 R. M. Spelz, S. O. Akciz, E. Masana, G. Faneros, Et Al.,

Assembly of A Large Earthquake 379 from a Complex Fault System: Surface Rupture Kinematics of the 4 April 2010 El Mayor–380 Cucapah (Mexico) Mw 7.2 Earthquake, Geosphere, 10(4), 797–827, 2014.

Gomez, F., Karam, G., Khawlie, M., Mcclusky, S., Vernant, P., Reilinger, R., Jaafar, R., Tabet, C., Khair, K., Barazangi, M., 2007. Global Positioning System Measurements of Strain Accumulation and Slip Transfer Through the Restraining Bend along the Decrowlead Sea Fault System in Lebanon. Geophysical Journal International 168, 1021–1028.

Grünthal G, Wahlstro ¨M R, Stromeyer D (2013) The SHARE European Earthquake Catalogue (SHEEC) For The Time Period 1900–2006 and Its Comparison to The European-Mediterranean Earthquake Catalogue (EMEC). J Seismol 17:1339–1344. Doi:10.1007/S10950-013-9379-Y.

Gülen, L., Barka, A., Toksoz, M.N., 1987. Kıtaların çarpışması ve ilgili komplex deformasyon: Maraş üçlü eklemi ve çevre yapıları. Yerbilimleri, 14, 319-336.

Gülerce, Z. and Abrahamson, N. A. (2010) Vector-valued Probabilistic Seismic Hazard Assessment for the Effects of Vertical Ground Motions on the Seismic Response of Highway Bridges, Earthquake Spectra, Volume 26, No. 4, 999 – 101.

Gülerce, Z., Ocak S., 2013. Probabilistic Seismic Hazard Assessment of Eastern Marmara Region. Bulletin of Earthquake Engineering, Doi: 10.1007/S10518-013-9443-6.

Gülerce, Z., Kargıoğlu, B., and Abrahamson, N. A. (2015). Turkey-Adjusted NGA-West1 Horizontal Ground Motion Prediction Models. Earthquake Spectra, Doi:10.1193/022714EQS034M.

Gülerce, Z. and Vakilinezhad, M., (2015). Effect of Seismic Source Model Parameters on the Probabilistic Seismic Hazard Assessment Results: A Case Study for North Anatolian Fault Zone. Bulletin of Seismological Society of America, 105(5).

Gülkan, P., M.S. Yucemen, A. Kocyigit, V. Doyuran and N. Basoz (1993). Seismic Zoning Map of Turkey Based On Most Recent Input. Middle East Technical University Earthquake Eng. Res. Ctr., 93-01.

Güneyli, H., 2008. Paleoseismicity of the Golbasi-Turkoglu Segment of the East Anatolian Fault System) TUBITAK Project Report 104Y157.

Gutenberg, B., and C. F. Richter (1944). Frequency of Earthquakes in California, Bull. Seismol. Soc. Am. 34, 185–188.

Haeussler, P., D. P. Schwartz, T. E. Dawson, H. D. Stenner, J. J. Lienkaemper, B. Sherrod, F. Cinti, P. Montone, P. Craw, A. Crone, and S. Personius (2004). Surface Rupture and Slip Distribution of the Denali and Totschunda Faults in the 3 November 2002 Mw 7.9 Earthquake, Alaska, Bull. Seismol. Soc. Am. 94, S25–S52.

Hanks, T. C., and H. Kanamori, A Moment Magnitude Scale, J. Geo- Phys. R Es., 84, 2348-2350, 1979.

Hanks T.C., Bakun W.H. M-log a Models and Other Curiosities. Bull. Seism. Soc. Am. 2014;104(5):2604-2610.

Hempton, M. R., Dewey, J. F. and Şaroğlu, F. 1981. The East Anatolian Transform Fault: Along Strike Variations in Geometry and Behavior. Transactions, American Geophysical Union, EOS 62, 393.

Hempton, M. R. 1985. Structure and Deformation History of the Bitlis Sture Near Lake Hazar, Southeastern Turkey. Geological Society of America Bulletin, 96, 233–243.

Hempton, M. R., Constraints On Arabian Plate Motion and Extensional History of the Red Sea, Tectonics, 6, 687 – 705, 1987.

Herece, E. and Akay, E. 1992. Karlıova-Çelikhan Arasında Doğu Anadolu Fayı. Proceeding of The 9th Petroleum Congress of Turkey. 17–21 February 1992, Ankara, Turkey, 361–372.

Herece, E. 2008. Doğu Anadolu Fayı (DAF) Atlası. General Directorate of Mineral Research and Exploration. Special Publications, Ankara, Serial Number, 13, 359.

Herece, E Doğu Anadolu Fay Sisteminin Yaşı ve Atımı 62nci Türkiye Jeoloji Kurultayı, 13−17 April 2009, MTA–Ankara, Türkiye.

Jackson J., Mckenzie D.P. (1984) Active Tectonics of the Alpine-Himalayan Belt between Western Turkey and Pakistan Geophys. J. R. Astr. Soc.77 185–264.

Joyner, W. B., and Boore, D. M. 1988. Measurement, Characterization and Prediction of Strong Ground Motion. Pages 43–102 Of: Proceedings of Earthquake Engineering and Soil Dynamics II. Geotechnical Division, ASCE.

Kalafat, D., Güneş, Y., Kekovali, K., Kara, M., Deniz, P., Yilmazer, M. 2011. Bütünleştirilmiş Homojen Türkiye Deprem Kataloğu (1900-2010); M≥4.0).

Boğaziçi Üniversitesi, Kandilli Rasathanesi ve Deprem Araştırma Enstitüsü, Yayin No: 1049, 640 S., Bebek-İstanbul.

Kalkan, E., Gulkan, P., Yilmaz, N., and Celebi, M. (2009) Reassessment of Probabilistic Seismic Hazard in the Marmara Region. Bull. Seismol. Soc. Am. 99 (4), 2127-2146.

Karabacak, V., Altunel, E., Meghraoui, M. and Akyüz, H. S. 2010. Field Evidences from Northern Dead Sea Fault Zone (South Turkey): New Findings for the Initiation Age and Slip Rate. Tectonophysics, 480, 172–182

Karabacak, V., Önder, Y., Altunel, E., Yalçıner, C. C., Akyüz, H. S. and Kıyak, N. G. 2011. Doğu Anadolu Fay Zonunun Güney Batı Uzanımının Paleosismolojisi ve Ilk Kayma Hızı. Proceeding of The Aktif Tektonik Arastırma Grubu Onbesinci Çalıştayı (ATAG-15), 19–22 Ekim 2011, Çukurova Üniversitesi, Karatas¸-Adana, 17.

Karig, D.E., Kozlu, H., 1990. Late Paleogene-Neogene evolution of the triple Junction near Maraş, South-Central Turkey. J. Geol. Soc. London, 147, 1023-1034.

Kayabalı, K. (2002). Modeling of Seismic Hazard for Turkey Using the Recent Neotectonic Data, Engineering Geology, Vol. 63, 221-232.

Kempler, D., and Z. Garfunkel, Structure and Kinematics in The Northeastern Mediterranean: A Study of an Irregular Plate Boundary, Tectonophysics, 234, 19 – 32, 1994.

Koç, A., Kaymakci, N. (2013). Kinematics of Sürgü Fault Zone (Malatya, Turkey): A remote sensing study, Journal of Geodynamics, 65, 292-307.

Kozlu, H. 1987. Structural Development and Stratigraphy of Misis–Andırın Region. In Proceedings of the Seventh Turkish Petroleum Congress, Ankara, pp. 104–16.

Le Bon, M., Klinger, Y., Amrat, A.Q., Agnon, A., Dorbath, L., Baer, G., Ruegg, J.C., Charade, O., Mayyas, O., 2008. Slip Rate and Locking Depth from GPS Profiles Across the Southern Dead Sea Transform, Journal of Geophysical Research 113, 1–19.

Lovelock, P.E.R., A Review of the Tectonics of the Northern Middle East Region, Geol. Mag., 121, 577-587,1984.

Lyberis, N., T. Yürür, J. Chorowicz, E. Kasapoğlu, and N. Gündoğdu, The East Anatolian Fault: An Oblique Collisional Bel, Tectonophysics, 2041-15,1992.

Mahmoud, S., Reilinger, R., Mcclusky, S., Vernant, P., Tealeb, A., 2005. GPS Evidence for Northward Motion of the Sinai Block: Implications for E. Mediterranean Tectonics. Earth and Planetary Science Letters 238, 217–224.

Mahmoud, Y., 2012. Caractérisation Géodesique De La Deformation Active Du Point Triple d'Hatay (Syrie-Turquie) (Geodetic Characterization of the Active Deformation at the Hatay Triple Junction (Syria, Turkey)). Ph.D. Thesis, University of Strasbourg, 192 Pp.

McClusky, S., Balassanian, S., Barka, A., Demir, C., Ergintav, S. Georgiev, I., Gurkan, O., Hamburger, M., Hurst, K., Kahle, H. Kastens, K., Kekelidze, G., King, R., Kotzev, V., Lenk, O., Mahmoud, S., Mishin, A., Nadariya, M., Ouzounis, A., Paradissis, D., Peter, Y., Prilepin, M., Reilinger, R., Sanli, I., Seeger, H., Tealeb, A., Toksoz, M.N., Veis, G., 2000. Global Positioning System Constraints On Plate Kinematics and Dynamics in The Mediterranean and Caucasus. Journal of Geophysical Research 105, 5685–5719.

McGuire, R.K.: FRISK: Computer Program for Seismic Risk Analysis Using Faults as Earthquake Sources. Open File Report No 78-1007, U.S.G.S., Denver, 1978.

McGuire, R.K. (2004). Seismic Hazard and Risk Analysis, Earthquake Engineering Research Institute, MNO-10, 221 p.

McKenzie D.P. 1972 Active Tectonics of the Mediterranean Regiongeophys. J. R. Astr. Soc.30 109–185.

McKenzie, D.P. 1976. The East Anatolian Fault; A Major Structure in Eastern Turkey. Earth and Planetary Science Letters, 29, 189–193.

McKenzie D.P. 1978. Active Tectonics of the Alpine-Himalayan Belt: The Aegean Sea and Surrounding Regions (Tectonic of Aegean Region) Geophys. J. R. Astr. Soc.55 217–254.

Meghraoui, M., Bertrand, S., Karabacak, V., Ferry, M., Cakir, Z. and Altunel, E. 2006. Surface Ruptures Along the Maras Segment of the East Anatolian Fault (SE Turkey) and Kinematic Modeling from Tectonic and GPS Data. Geophysical Research Abstracts, 8, 10006. Sref-ID: 1607–7962/Gra/EGU06-A-10006.

Meghraoui,M.; Cakir,Z.; Masson,F.; Ferry, M.; Ergintav, S.; Inan, S.; Karabacak, V.; Altunel, E. Active Tectonics and Kinematic Modeling at The Triple Junction Between The East Anatolian Fault, The Dead Sea Fault and The Cyprus Arc American Geophysical Union, Fall Meeting 2009, Abstract:G33D-0669.

Meghraoui, M., Cakir, Z., Masson, F., Mahmoud, Y., Ergintav, S., Alchalbi, A., Inan, S., Daoud, M., Yonlu, O., Altunel, E., 2011. Kinematic modelling at the triple junction between the Anatolian, Arabian, African plates (NW Syria and in SE Turkey). Geophysical Research Abstracts, vol. 13, EGU2011-12599, EGU General Assembly, Vienna 2011.

Moreno G. D, A. Hubert-Ferrari, J. Moernaut, J. Fraser, M. Van Daele, M. De Batist and E. Damci Structure and Evolution of a Main Segment Boundary Alongthe East Anatolıan Fault. Eastern Turkey.Basin Research, BRE-053-2009.R3.

Moreno G, D., Hubert-Ferrari, A., Moernaut, J.G., Boes, X., Van Daele, M., Avsar, U., Çagatay, N., De Batist, M., (2011). Structure and Recent Evolution of the Hazar Basin: Strike-slip Basin on the East Anatolian Fault, Eastern Turkey Basin Research, 23, 2, 191-20.

Nalbant, S. S., Mccloskey, J., Steacy, S. and Barka, A. A. 2002. Stress Accumulation and Increased Seismic Risk in Eastern Turkey. Earth and Planetary Science Letters, 195, 291–298.

Ocak S. Probabilistic Seismic Hazard Assessment of Eastern Marmara and Evaluation of Turkish Earthquake Code Requirements, Thesis Study, 2011.

Orgülü, G., M. Aktar, N. Türkelli, E. Sandvol, And M. Barazangi, Contribution to The Seismotectonics of the Eastern Anatolian Plateau from Moderate and Small Size Events, Geophys. Res. Lett., 30/24, 8040, 2003.

Perinçek, D. and Kozlu, H., 1984, Stratigraphy and Structural Relations of the Units in the Afşin - Elbistan -Doğanşehir Region (Eastern Tauros). In: Geology of Tauros Belt (eds., O. Tekeli and M.C. Göncüoğlu). MTA, p.181-198.

Perinçek, D., Günay, Y. and Kozlu, H. 1987. New Observations On Strike–Slip Faults in East and Southeast Ana- Tolia. Proceedings of The 7th Petroleum Congress of Turkey. Turkish, 6–10 April, 1987, Ankara, Turkey, 89–103.

Perinçek, D., Çemen, I., 1990. The Structural Relationship Between the East Anatolian and Dead Sea Fault Zones in Southeastern Turkey. Tectonophysics 172, 331–340.

Poirier, J. P. And M. A. Taher, Historical Seismicity in The Near and Middle East, North Africa and Spain from Arabic Documents, Bull. Seism. Soc. Am., 70, 2185–2201, 1980.

Power, M, Chiou B, Abrahamson N, Bozorgnia Y, Shantz T, Roblee C (2008) An Overview of the NGA project. Earthquake Spectra 24(1):3–21. doi:10.1193/1.2894833

Reasenberg, P. (1985), Second-order Moment of Central California Seismicity, 1969-82, J. Geophys. Res., 90, 5479– 5495.

Reilinger, R., Mcclusky, S. Et Al. 2006. GPS Constraints on Continental Deformation in the Africa–Arabia–Eurasia Continental Collision Zone and Implications for Dynamics of Plate Interactions. Journal of Geophysical Research, 111, B05411, Doi: 10.1029/2005JB004051.

Richer, C.F. (1958): Elementary Seismology (Freeman, San Francisco, California).

Robertson, A. H. F., Unlügenç, Ü.Ç. Inan, N. and Tasli, K. 2004. The Misis–Andırın Complex: A Mid-Tertiary Melangerelatedtolate-Stagesubductionofthesouthern Neotethys in S Turkey. Journal of Asian Earth Sciences 22, 413–53.

Rojay B., Heimann A., Toprak V., Neotectonic and Volcanic Characteristics of the Karasu Fault Zone (Anatolia, Turkey): The Transition Zone Between The Dead Sea Transform And The East Anatolian Fault Zone Geodinamica Acta Volume 14, Issues 1–3, January–May 2001, Pages 197–212.

Sadigh, K., C. Y. Chang, J. A. Egan, F. Makdisi, and R. R. Youngs (1997). Attenuation Relationships for Shallow Crustal Earthquakes Based On California Strong Motion Data, Seismol. Res. Lett. 68, 180–189.

Şaroğlu, F., O. Emre, and I. Kuscu, The East Anatolian Fault Zone of Turkey, Ann. Tectonicae, VI, 99–125, 1992.

Şaroğlu, F. 1985. Doğu Anadolu'nun Neotektonik Dönemde Jeolojik ve Yapısal Evrimi. Phd Thesis, İstanbul University, Istanbul, 240 pages.

Şaroğlu, F. and Yılmaz, Y., 1990, Tectonics of the Karlıova Triple Junction, Bull. of ITU.

Şaroğlu, F. and Yılmaz, Y. 1991. Geology of Karlıova Region: Intersection of The North Anatolian and East Anatolian Transform Faults. Bulletin Technical University, Istanbul, Turkey, 44, 475–497.

Şaroğlu, F., Emre, O. and Kuşçu, I. 1992a. The East Anatolian Fault Zone of Turkey. Annalae Tectonicae, 6, 99–125.

Şaroğlu, F., Emre, Ö. and Kuşçu, I. 1992b. Tükiye Diri Fay Haritası. Maden Tetkik Ve Arama Genel Müdürlüğü Ankara, Turkey.

Scasserra, G., Stewart, J. P., Bazzurro, P. Lanzo, G. And Mollaioli, F., 2009. A Comparison of NGA Ground-Motion Prediction Equations to Italian Data, Bull. of the Seis. Soc. of Am. 99, 2961-2978.

Schwartz, D. P. And K. J. Coppersmith (1984). Fault Behavior and Characteristic Earthquakes: Examples from the Wasatch and San Andreas Faults, J. Geophys. Res. 89, 5681-5698.

Seymen, I. and Aydın, A. 1972. Bingöl Deprem Fayı Ve Bunun Kuzey Anadolu Fay Zonu Ile Ilis¸Kisi. Bulletin of the General Directorate of Mineral Research and Exploration, 79, 1–8.

Seyrek, A., Demir, T., Pringle, M. S., Yurtmen, S., Westaway, R. W. C., Beck, A. and Rowbotham, G. 2007. Kinematics of the Amanos Fault, Southern Turkey, From Ar/Ar Dating of Ofset Pleistocene Basalt Flows: Transpression between the African and Arabian Plates. In: Cunningham, W. D. and Mann, P. (Eds) Tectonics of Strike-Slip Restraining and Releasing Bends. Geological Society London Special Publications, 290, 255–284.

Shoja–Taheri, J., Naserieh, S., and Hadi, G., 2010. A Test of the Applicability of NGA Models to the Strong Ground-Motion Data in the Iranian Plateau, J. Earthquake. Engineering 14, 278–292.

Soysal, H., S. Sipahioglu, D. Kolcak, ve Y. Altinok, Turkiye Tarihsel Deprem Katalogu, TUBITAK Proje No. TBAG-341, 1981.

Stafford, P. J., F. O. Strasser, and Bommer J. J., 2008. An Evaluation of the Applicability of the NGA Models to Ground Motion Prediction in the Euro-Mediterranean Region, Bull. Earthq. Eng. 6, 149–177.

Stucchi M, Rovida A, Gomez Capera AA Et Al (2012) The SHARE European Earthquake Catalogue (SHEEC) 1000-1899. Journal of Seismology.

Tan, O., Pabuçcu, Z. Et Al. 2011. Aftershock Study and Seismotectonic Implications of the 8 March 2010 Kovancılar (Elazığ, Turkey) Earthquake ($M_W$= 6.1). Geophysical Research Letters, 38, L11304.

Tarı Ufuk, Tüysüz Okan, Ş. Can Genç, Caner İmren, Bonnie A.B. Blackwellde, Nalan Lom, Özge Tekeşin, Sibel Üsküplü, Levent Erel, Savaş Altıok and Murat Beyhan The Geology and Morphology of the Antakya Graben between the Amik Triple Junction and the Cyprus Arc, doi:10.1080/09853111.2013. 858962

Taymaz, T., Eyidoğan, H., Jackson, J., 1991. Source Parameters of Large Earthquakes in the East Anatolian Fault Zone (Turkey). Geophys. J. Int. 106, 537–550.

Türkelli, N., E. Sandvol, E. Zor, R. Gök, T. Bekler, A. Al-Lazki, H. Karabulut, S. Kuleli, T. Eken, C. Gürbüz, S. Bayraktutan, D. Seber, and M. Barazangi, Seismogenic Zones in Eastern Turkey, Geophys. Res. Lett., 30(24), 8039, doi:10.1029/2003GL018023, 2003.

Weichert, D. H. (1980), Estimation of the Earthquake Recurrence Parameters for Unequal Observation Periods for Different Magnitudes, Bull. Seismol. Soc. Am. 70, no. 4, 1337–1346.

Wells, D. L., and K. J. Coppersmith (1994). New Empirical Relationships Among Magnitude, Rupture Length, Rupture Width, Rupture Area, and Surface Displacement, Bull. Seismol. Soc. Am. 84, 974–1002.

Westaway, R. W. C., and J. Arger, The Gölbas¸I Basin, Southeastern Turkey: A Complex Discontinuity in a Major Strike-Slip Fault Zone, J. Geol. Soc. London, 153, 729 – 744, 1996.

Westaway, R. and Arger, J. 2001. Kinematics of the Malatya–Ovacik Fault Zone. Geodinamica Acta, 14, 103–131.

Westaway, R. 2003. Kinematics of The Middle East and Eastern Mediterranean Updated. Turkish Journal of Earth Sciences, 12, 5–46.

Westaway, R. 2004. Kinematic Consistency between the Dead Sea Fault Zone and The Neogene and Quaternary Left-Lateral Faulting in SE Turkey. Tectonophysics, 391, 203–237.

Westaway, R., Demir, T., Seyrek, A. and Beck, A. 2006. Kinematics of Active Left-Lateral Faulting in SE Turkey from Offset Pleistocene River Gorges: Improved Constraint on the Rate and History of Relative Motion between the Turkish and Arabian Plates, Journal of the Geological Society, London, 163, 149–164.

Wiemer S (2001) A Software Package to Analyze Seismicity: ZMAP. Seismol Res Lett 72:373–382.

Yalçın, M. N. 1979. Doğu Anadolu Yarılımının Türkoğlu-Karaağaç¸ (K. Maras) Arasındaki Kesiminin Özellikleri ve Bölgedeki Yerleşim Alanları. Türkiye Jeoloji Kurumu Altınlı Simpozyumu, Özel Sayı, 49–55.

Yaltirak, C., Alpar, B., and Yuce, H., 1998. Tectonic Elements Controlling Tthe Evolution of the Gulf of Saros (Northeastern Aegean Sea), Tectonophysics,300, 227-248.

Yarar, R., Ergunay, O., Erdick, M. and Gulkan, P., 1980. A preliminary probabilistic assessment of the seismic hazard in Turkey: Proc. 7th World Conf. Earthquake Eng., Istanbul, 309-316.

Yılmaz H., Över S., And Özden S. Kinematics of The East Anatolian Fault Zone Between Turkoglu (Kahramanmaras) And Celikhan (Adiyaman), Eastern Turkey Earth Planets Space, 58, 1463–1473, 2006.

Youngs, R. R., and K. J. Coppersmith (1985). Implications of Fault Slip Rate and Earthquake Recurrence Models to Probabilistic Seismic Hazard Estimates, Bull. Seismol. Soc. Am. 75, no. 4, 939–964.

Yurtmen, S., G. Rowbotham, F. İsler, and P. Floyd, Petrogenesis of Quaternary Alkali Volcanics, Ceyhan-Turkey, in Tectonics and Magmatism of Turkey and the Surrounding Area, Edited by E. Bozkurt, J. A. Winchester, and J. D. A. Piper, Geol. Soc. London Spec. Publ., 173, 489–512, 2000.

Zhao, J. X., Zhang, J., Asano, A., Ohno, Y., Oouchi, T., Takahashi, T., Ogawa, H., Irikura, K., Thio, H. K., Somerville, P. G., Fukushima, Y., and Fukushima, Y. 2006. Attenuation Relations of Strong Ground Motion in Japan Using Site Classification Based on Predominant Period. Bulletin of the Seismological Society of America, 96(3), 898–913.